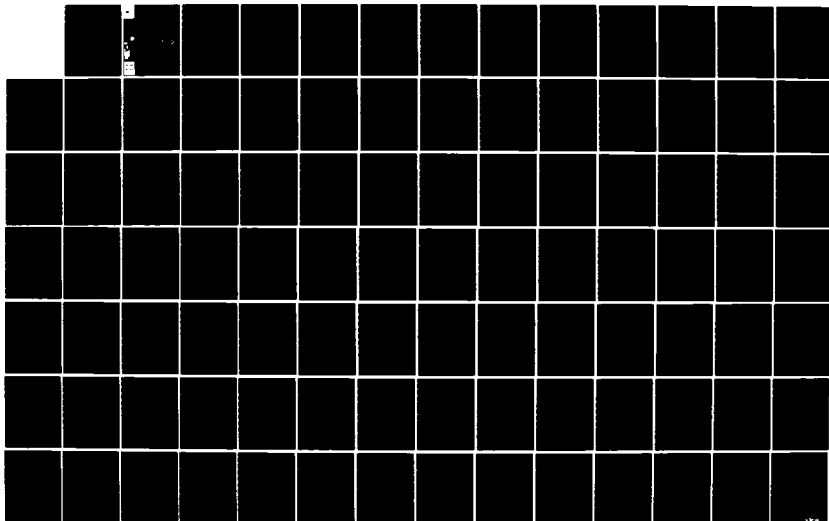
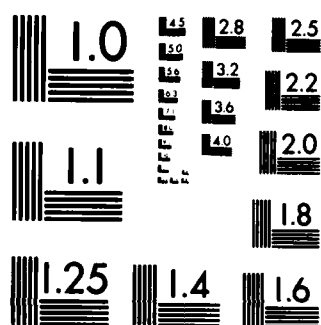


D-A152 817

THE ATCHAFALAYA RIVER DELTA REPORT 8 NUMERICAL MODELING 1/1  
OF HURRICANE-INDU. (U) ARMY ENGINEER WATERWAYS  
EXPERIMENT STATION VICKSBURG MS HYDRA. B A EBERSOLE  
JAN 85 WES/TR/HL-82-15/8 F/G 8/8 NL

UNCLASSIFIED





MICROCOPY RESOLUTION TEST CHART  
NATIONAL BUREAU OF STANDARDS-1963-A



US Army Corps  
of Engineers

AD-A152 817



HYDRAULICS  
LABORATORY

TECHNICAL REPORT HL-82-15

2

# THE ATCHAFALAYA RIVER DELTA

## Report 8

### NUMERICAL MODELING OF HURRICANE-INDUCED STORM SURGE

by

Bruce A. Ebersole

Coastal Engineering Research Center

DEPARTMENT OF THE ARMY  
Waterways Experiment Station, Corps of Engineers  
PO Box 631  
Vicksburg, Mississippi 39180-0631



DTIC  
ELECTE  
APR 25 1985  
S B D

January 1985

Report 8 of a Series

Approved For Public Release; Distribution Unlimited

DTIC FILE COPY

Prepared for US Army Engineer District, New Orleans  
New Orleans, Louisiana 70160

Monitored by Hydraulics Laboratory  
US Army Engineer Waterways Experiment Station  
PO Box 631, Vicksburg, Mississippi 39180-0631

Destroy this report when no longer needed. Do not return  
it to the originator.

The findings in this report are not to be construed as an official  
Department of the Army position unless so designated  
by other authorized documents.

The contents of this report are not to be used for  
advertising, publication, or promotional purposes.  
Citation of trade names does not constitute an  
official endorsement or approval of the use of  
such commercial products.

Unclassified

SECURITY CLASSIFICATION OF THIS PAGE (When Data Entered)

REPORT DOCUMENTATION PAGE		READ INSTRUCTIONS BEFORE COMPLETING FORM
1. REPORT NUMBER Technical Report HL-82-15	2. GOVT ACCESSION NO. <i>H152 817</i>	3. RECIPIENT'S CATALOG NUMBER
4. TITLE (and Subtitle) THE ATCHAFALAYA RIVER DELTA; Report 8, NUMERICAL MODELING OF HURRICANE-INDUCED STORM SURGE	5. TYPE OF REPORT & PERIOD COVERED Report 8 of a series	
7. AUTHOR(s) Bruce A. Ebersole	6. PERFORMING ORG. REPORT NUMBER	
9. PERFORMING ORGANIZATION NAME AND ADDRESS US Army Engineer Waterways Experiment Station Coastal Engineering Research Center PO Box 631, Vicksburg, Mississippi 39180-0631	8. CONTRACT OR GRANT NUMBER(s)	
11. CONTROLLING OFFICE NAME AND ADDRESS US Army Engineer District, New Orleans PO Box 60267 New Orleans, Louisiana 70160	10. PROGRAM ELEMENT, PROJECT, TASK AREA & WORK UNIT NUMBERS	
14. MONITORING AGENCY NAME & ADDRESS (if different from Controlling Office) US Army Engineer Waterways Experiment Station Hydraulics Laboratory PO Box 631, Vicksburg, Mississippi 39180-0631	12. REPORT DATE January 1985	
	13. NUMBER OF PAGES 94	
	15. SECURITY CLASS. (of this report) Unclassified	
	15a. DECLASSIFICATION/DOWNGRADING SCHEDULE	
16. DISTRIBUTION STATEMENT (of this Report)  Approved for public release; distribution unlimited.		
17. DISTRIBUTION STATEMENT (of the abstract entered in Block 20, if different from Report)		
18. SUPPLEMENTARY NOTES  Available from National Technical Information Service, 5285 Port Royal Road, Springfield, Virginia 22161.		
19. KEY WORDS (Continue on reverse side if necessary and identify by block number)  Atchafalaya Bay; Hurricanes; Numerical modeling; and Storm surge.		
20. ABSTRACT (Continue on reverse side if necessary and identify by block number)  This report contains a description of the US Army Engineer Waterways Experiment Station (WES) Implicit Flooding Model (WIFM) and how it was applied to the Atchafalaya River Delta Project. Input required by the model for this application is discussed. The model is verified to both tidal and hurricane conditions by comparing prototype water-surface elevations to simulated re- sults. Hurricane wind fields are generated using the standard project  (Continued)		

Unclassified

SECURITY CLASSIFICATION OF THIS PAGE (When Data Entered)

Unclassified

SECURITY CLASSIFICATION OF THIS PAGE(When Data Entered)

20. ABSTRACT (Continued)

hurricane (SPH) model. The storm surge model is used to simulate the response of the Atchafalaya Bay area for a set of 12 hypothetical hurricane events. Hurricane parameters defining this ensemble of storms were derived from historical data.

*Key words:*

*100-1003*

Unclassified

SECURITY CLASSIFICATION OF THIS PAGE(When Data Entered)

## PREFACE

This report was published to document the process by which the US Army Engineer Waterways Experiment Station (WES) Implicit Flooding Model (WIFM) was applied to the Atchafalaya River Delta Study in order to simulate the impact of hurricanes on this area.

The study was conducted under the direction of the following WES personnel: Messrs. H. B. Simmons, Chief of the Hydraulics Laboratory; F. A. Herrmann, Jr., Assistant Chief of the Hydraulics Laboratory; R. A. Sager, Chief of the Estuaries Division; W. H. McAnally, Jr., Project Manager; and J. V. Letter, Jr., Task Coordinator. This study was performed by Mr. Bruce A. Ebersole, formerly of the Wave Dynamics Division (WDD), Hydraulics Laboratory, under the direct supervision of Dr. R. W. Whalin and Mr. C. E. Chatham, Jr., former and acting Chiefs of WDD. The WDD and its personnel were transferred to the Coastal Engineering Research Center (CERC), WES, on 1 July 1983, under the direction of Dr. R. W. Whalin, Chief of the Coastal Engineering Research Center.

Commanders and Directors of WES during the study and the preparation and publication of this report were COL John L. Cannon, CE, COL Nelson P. Conover, CE, COL Tilford C. Creel, CE, and COL Robert C. Lee, CE. Technical Director was Mr. F. R. Brown.



Accession For	
NTIS	<input checked="" type="checkbox"/>
DTIC	<input type="checkbox"/>
Other	<input type="checkbox"/>
Distribution/	
Availability Codes	
Dist	Avail and/or Special
A-1	

# CONTENTS

	<u>Page</u>
PREFACE . . . . .	1
CONVERSION FACTORS, US CUSTOMARY TO METRIC (SI)	
UNITS OF MEASUREMENT . . . . .	3
PART I: INTRODUCTION . . . . .	4
PART II: MODEL DESCRIPTION . . . . .	6
PART III: MODEL INPUT . . . . .	8
Grid Generation . . . . .	8
Boundary Conditions . . . . .	10
External Forcing Functions . . . . .	12
PART IV: MODEL VERIFICATION . . . . .	15
Tidal Verification . . . . .	15
Storm Surge Verification . . . . .	17
PART V: HYPOTHETICAL STORM SIMULATIONS . . . . .	23
PART VI: SUMMARY . . . . .	26
REFERENCES . . . . .	27
TABLES 1-6	
FIGURES 1-61	



CONVERSION FACTORS, US CUSTOMARY TO METRIC (SI)  
UNITS OF MEASUREMENT

US customary units of measurement used in this report can be converted to metric (SI) units as follows:

<u>Multiply</u>	<u>By</u>	<u>To Obtain</u>
cubic feet per second	0.02831685	cubic metres per second
feet	0.3048	metres
feet per second	0.3048	metres per second
inches of mercury	3386.38	pascals
knots (international)	0.514444	metres per second
miles (US nautical)	1.852	kilometres
miles (US statute)	1.609344	kilometres

## THE ATCHAFALAYA RIVER DELTA

### NUMERICAL MODELING OF HURRICANE-INDUCED STORM SURGE

#### PART I: INTRODUCTION

1. The Atchafalaya Bay system is comprised of the following components: (a) the bay itself, (b) a portion of the Gulf of Mexico adjacent to the bay, (c) low-lying marshlands surrounding the bay, and (d) the Lower Atchafalaya River and Wax Lake Outlet, which are the dominant sources of fresh water and sediment into the system. Hydrodynamics within the bay system, and associated sedimentation processes, are driven primarily by three mechanisms: astronomical forcing, meteorological forcing, and river discharges. Most of the time this system is well behaved, i.e., the flooding and ebbing of the astronomical tide and the resulting current patterns are fairly predictable. These currents rework sediment carried into the bay by rivers into other parts of the system.

2. A few times each year freshwater inflows and their sediment content increase substantially and force the response of the system to change. Lowlands adjacent to the rivers become inundated and sediments are deposited over the marshes. As a result, tidal current patterns change, and not only is more sediment deposited in other parts of the bay but more is jetted into the Gulf. These events play a very significant role in the evolution of the bay system.

3. A still rarer event that can drastically alter the behavior of the bay area is a nearby passage of an intense tropical storm or hurricane. Such events can cause large variations in water-surface elevation, called storm surge, and may result in large-scale flooding of lowlands and reshaping of the marshes and deltaic deposits. This storm surge is caused by both wind and atmospheric pressure. The wind exerts a surface stress on the water column that is inversely proportional to the water depth; and for this reason, in the Atchafalaya Bay one can expect substantial changes in water level due to effects of high wind over shallow depths. Gradients in surface atmospheric pressure also exert forces on the water but to a somewhat lesser degree than wind. Water is, in effect, pushed from regions of high pressure to regions

of low pressure, and it is common to find a bulge of water about 1 to 3 ft\* high under the "eye" of a hurricane due to this effect. The combined effect of these two phenomena is a wave of water that travels along with the storm which in extreme cases can be as high as 15 ft and extend for tens of miles. The impact of this wave of water on geographical regions such as the Atchafalaya Bay area is obvious.

4. The purpose of this task of the Atchafalaya Bay investigation is the development of a numerical model to simulate the hydrodynamics, within the bay system, resulting from astronomical and/or meteorological forcing. Response of the bay system to long waves is verified for two types of conditions. The ability of the model to predict the hydrodynamics resulting from astronomical tide forcing alone is verified by comparing simulated free-surface elevation time-histories with measured prototype data. Response of the bay for the case of meteorological forcing due to hurricanes is verified using comparisons between high-water marks recorded during two historical storms, Hurricanes Audrey (1957) and Hilda (1964), and model results.

5. A set of hypothetical hurricanes, which are typical of this geographical area, is simulated in the numerical model. Characteristics of these storms are determined by studying the track, intensity, and extent of storms that have influenced this region in the past and whose relevant storm parameters have been documented. Hydrodynamics resulting from these storms will be used in other tasks to predict the evolution of the Atchafalaya River delta--in particular, how the occurrence of one or several of these extreme events can alter the delta growth process during the next 50 years.

---

\* A table of factors for converting US customary units of measurements to metric (SI) units is presented on page 3.

## PART II: MODEL DESCRIPTION

6. A numerical model is an algorithm used to solve a system of equations that approximate the physics of some natural process, within some domain of interest, and subject to certain constraints. In our particular case, we want to solve the equations that govern the hydrodynamics within the Atchafalaya Bay system in response to both astronomical and meteorological forcing.

7. The equations that govern fluid flow are a series of three-dimensional, partial differential equations which represent the conservation of both mass and momentum. Those equations can be greatly simplified by making several assumptions. The water is assumed to be incompressible and homogeneous and any vertical accelerations of the water are considered negligible. By integrating the equations from the seabed up to the free surface, assuming the velocity is constant with depth, and neglecting any effects of lateral diffusion and convective accelerations, the following set of long-wave equations can be derived for two horizontal dimensions.

### Conservation of Momentum:

$$\frac{\partial U}{\partial t} - fV + g \frac{\partial}{\partial x} (\eta - \eta_a) + \frac{gU}{C^2 D} (U^2 + V^2)^{1/2} + F_x = 0 \quad (1)$$

$$\frac{\partial V}{\partial t} + fU + g \frac{\partial}{\partial y} (\eta - \eta_a) + \frac{gV}{C^2 D} (U^2 + V^2)^{1/2} + F_y = 0 \quad (2)$$

### Conservation of Mass:

$$\frac{\partial \eta}{\partial t} + \frac{\partial}{\partial x} (UD) + \frac{\partial}{\partial y} (VD) = 0 \quad (3)$$

The variable  $\eta$  is the water-surface elevation defined in Figure 1;  $U$  and  $V$  are vertically integrated velocities at time  $t$  in the  $x$ - and  $y$ -directions, respectively;  $D = \eta - h$  is the total water depth;  $h$  is the still-water depth;  $\eta_a$  is the hydrostatic elevation reflecting the atmospheric pressure deficit from ambient pressure;  $f$  is the Coriolis parameter that accounts for the rotational effects of the earth on fluid flow;  $C$  is the Chezy frictional coefficient;  $g$  is the acceleration due to gravity; and  $F_x$  and  $F_y$  are

external forcing terms, which in this model are effective wind stresses.

8. The computer program used to solve this set of equations is the US Army Engineer Waterways Experiment Station (WES) Implicit Flooding Model (WIFM) (see Butler 1978a, 1978b, 1978c, 1980, 1981). This model solves finite difference approximations of the governing equations on a grid mesh of fixed spatial extent for a finite number of constant time increments, utilizing an alternating-direction, implicit solution scheme. For a more detailed description of the scheme itself as well as information on the kinds of model input required, the reader is referred to the above references. Some aspects of model input, as they relate to the Atchafalaya Bay applications, are discussed in more detail in the sections to follow. This discussion will concentrate on various kinds of boundary conditions used, information on grid generation and grid input, and specification of the external forcing functions defined in Equations 1 and 2.

## PART III: MODEL INPUT

### Grid Generation

9. Equations 1, 2, and 3 and the solution scheme used in the WIFM require that a two-dimensional spatial domain of interest be discretized using a number of finite-sized increments called grid cells. Cell size determines the accuracy of the numerical solution to the governing equations. Therefore, in areas of great interest, finer resolution is desired in order to increase the accuracy of results. There is, of course, a trade-off between a high degree of accuracy and the cost associated with computing the solution for a large number of cells. In addition, the grid mesh must extend to some point such that boundary conditions at this point accurately reflect the influence of the far field on the domain of interest; and again, there is a cost trade-off associated with the selection of the location of these outer boundaries.

10. The grid generation technique utilized in WIFM (Butler 1978, 1980) is based on a telescoping principle in which the modeler can increase or decrease grid spacings in both coordinate directions, resulting in a mesh that is variable and rectilinear. Advantages of such a grid system are: (a) great detail can be created in specific areas of interest; (b) the grid can be extended into the far field by using expanding grid cells--this is desirable for certain types of boundary conditions; and (c) the orthogonality of the grid system simplifies the solution scheme at grid cell interfaces and can be advantageous for certain boundary conditions. Basically, this variable grid spacing is achieved by dividing each direction into several regions and for each region replacing the real space coordinates  $x$  and  $y$  in the governing equations with the computational coordinates  $\alpha_1$  and  $\alpha_2$  such that

$$x_i = a_{1i} + b_{1i} + \alpha_1^{c_{1i}} \quad \text{where } i = 1 \text{ to } M \quad (4)$$

$$y_j = a_{2j} + b_{2j} + \alpha_2^{c_{2j}} \quad \text{where } j = 1 \text{ to } N \quad (5)$$

and where  $a$ ,  $b$ , and  $c$  are constants and  $M$  and  $N$  represent the number of mapping regions in each coordinate direction. The constants are determined

by requiring that both the function, whether it be  $x$  or  $y$ , and its first derivative be continuous at region interfaces.

11. The grid used in the model is shown in Figure 2 and was constructed with the following criteria in mind. A large degree of resolution was desired in the Atchafalaya River mouth, the navigation channel, Wax Lake Outlet, and Southwest Pass into Vermilion Bay in order that the hydrodynamics in these areas could be accurately modeled. Model boundaries were placed sufficiently distant from the Atchafalaya Bay that the boundary conditions used properly describe the far-field hydrodynamics. In addition, distant boundaries assure that if the boundary conditions used are not completely correct, the solution in the areas of interest will not be greatly affected by any errors generated at the boundary. Finally, some degree of resolution was desired in the above-water portions of the grid so that any inland flooding experienced during tropical storms could be accurately simulated.

12. Once a two-dimensional grid is generated, segmenting the area of interest into a large number of grid cells ( $48 \times 115 = 5,520$  in this application), information required by the model must be defined on the grid mesh. The information includes: (a) depth of water or elevation of dry land at each cell, (b) estimate of the frictional influence of the bathymetry or topography at each cell, and (c) dimensions of all natural and man-made barriers that could influence the flow within the grid system (such as levees, dikes, roadbeds, dunes, and ridges). Water depths in the western Atchafalaya Bay and the northern Gulf of Mexico were obtained from National Ocean Survey bathymetric charts. These were increased by 1 ft in order to transform the depths from the chart datum, which is mean low water, to the model mean sea level datum. Depths in the eastern part of the bay were obtained from a more recent 1977 survey, conducted by the US Army Engineer District, New Orleans. Above-water elevations were taken from United States Geological Survey (USGS) charts that reflect topographic conditions prior to 1957. Much of the above-water topography surrounding Atchafalaya Bay is marshland and because accurate estimates of the elevations of these areas are unavailable, elevations were assumed to vary from 1.5 to 2.0 ft. Information on barrier elevations within the modeled region also came from the USGS charts, as well as Corps of Engineer reports showing man-made construction in the area.

13. Another input variable to the model is the frictional influence of the land surface and sea floor on the hydrodynamics within the system. In the

equations of motion, frictional effects are described by the Chezy friction law using Manning's roughness coefficient,  $n$ . For the Atchafalaya Bay applications, the Manning's  $n$  for areas below mean sea level was chosen to vary between 0.018 and 0.025 depending on water depth, with lower values used for very shallow depths. For above-water elevations, which are predominantly marshlands, a Manning's  $n$  of 0.035 was used.

#### Boundary Conditions

14. The next aspects of the model input to be discussed are the particular boundary conditions employed by the solution scheme. These conditions describe the hydrodynamics at both the outer edges of the grid and within the grid interior. Three variables to be solved at each grid cell are  $U$  and  $V$ , the depth-averaged velocities, and  $\eta$ , the free-surface displacement. The orientation of  $U$  and  $V$  are shown in Figure 1. In place of  $U$  and  $V$ , the mass transport per unit width  $Q_x$  and  $Q_y$ , in the  $x$ - and  $y$ -direction, respectively, could be used where

$$Q_x = UD \quad (6)$$

$$Q_y = VD \quad (7)$$

and  $D$  is the total water depth. To completely describe the flow field at the boundary, the two components of velocity, or transport, must be defined as a function of the free surface. Since data were not available to completely define the flow field at the boundary, assumptions were made to simplify the problem. In this model, only the free surface, the velocity or transport, or the gradient of the velocity or transport is specified at the boundaries.

15. For grid cells through which no water can pass, a "no-flow" condition is imposed. This requires that the velocity, or transport, normal to the boundary be zero. When a certain flow is to be prescribed at a boundary, as in the case of river discharge, the magnitude of the flow is assigned at the desired cell face in the appropriate coordinate direction. This flow specification can be constant or vary with time. Another example of describing the flow at a boundary is during overtopping or flooding. These two instances are treated through the use of a broad-crested weir equation to define flow normal to a cell face,  $Q_n$ , by



$$Q_n = \pm C_o d_h \sqrt{d_h} \quad (8)$$

In Equation 8,  $d_h$  is either the elevation of water above a barrier to be overtopped or the depth of water above that in an adjacent cell to be flooded, and  $C_o$  is an empirically determined admittance coefficient that controls the volume of water allowed to overtop or flood.

16. A final example of a boundary condition that involves the transport is a "zero-gradient" condition. This condition assumes that there is no change in the flow in some coordinate direction. For example, if transport in the x-direction at a boundary is assumed to vary negligibly from one cell to the next, the condition

$$\frac{\partial Q_x}{\partial x} = 0 \quad (9)$$

can be specified at the cell interface.

17. An alternative to specifying the flow at a boundary is to define the free surface. In all Atchafalaya Bay model applications described herein, along a majority of the offshore boundaries, the time variation of the free surface was defined. This free surface is that due to either the astronomical tide alone or to the tide in combination with a free surface anomaly caused by an atmospheric pressure deficit. The time-varying tidal functions were obtained from results of the Gulf of Mexico Tide Model (GOMT) which was developed by Reid and Whitaker (1981).

18. The GOMT was developed to predict amplitudes and phases of the dominant constituents of the astronomical tide in the Gulf of Mexico. A finite difference, time marching, implicit solution scheme was used to solve the linearized, depth-integrated tidal equations. Grid resolution of 15 min  $\times$  15 min in latitude and longitude was used over the entire Gulf resulting in the 50  $\times$  70 grid mesh shown in Figure 3. No-flow conditions were employed along the entire Gulf coastline, and at the Florida Straits and Yucatan Channel an admittance boundary condition was employed that allowed both inflow and outflow. Flux potential at these two ports (both amplitude and phase) as well as the amplitude and phase of direct astronomical forcing was determined by a tuning procedure in which differences between the simulated and observed tide at eighteen coastal stations and two interior Gulf stations were minimized in a least squares sense. This tuning was carried out individually for the five

largest tidal constituents ( $K_1, O_1, P_1, M_2, S_2$ ). A more thorough documentation of the GOMT and the tuning process is described by Reid and Whitaker (1981).

19. To increase the accuracy of the GOMT results in the north central Gulf region, three changes were made to the model and tuning process. Linear friction in the tidal equations was reduced by 50 percent in water depths of 40 m or less. Five more stations in the Atchafalaya Bay and Mississippi Sound were added to the original twenty used in the tuning procedure. In the least squares analysis, these additional stations were weighted more heavily than those far away from the region of interest.

20. Figures 4-7 show comparisons between observed and modeled amplitudes and phases for both a semidiurnal ( $M_2$ ) and a diurnal ( $O_1$ ) constituent. Results for both the original (balanced) and revised (project) tuning are shown for all stations in order to illustrate the spatial variability of both amplitude and phase around the Gulf. Some of the stations are listed as a spatial reference. Root-mean-square errors for both tunings are listed at the top of each figure.

21. Cotidal lines for both the  $M_2$  and  $O_1$  constituents are shown in Figures 8 and 9 and they indicate that the astronomical tide in Atchafalaya Bay is in a quasi-steady, resonant condition. This creates a problem when GOMT model results are used to drive a model whose water boundaries extend beyond the resonant zone. Without a boundary condition, which couples the velocity fields to the free surface at the open boundaries, this resonance cannot be exactly reproduced by forcing with the free-surface elevation alone. Therefore, in the Atchafalaya Bay model, constituent amplitudes were increased in order to generate the proper tidal signal at the bay entrance.

#### External Forcing Functions

22. The final model inputs are the external forcing functions  $\eta_a$ ,  $F_x$ , and  $F_y$ , in Equations 1 and 2, which are due to meteorological phenomena. The term  $\eta_a$  is simply the difference between the surface atmospheric pressure at some point of interest in the computational grid and that in the far field. The pressure difference is converted to feet of water. This effect, called the inverted barometric effect, is significant during hurricanes that are characterized by very low pressure centers. The forcing terms  $F_x$  and  $F_y$  represent the effects of horizontal wind stress:

$$F_x = \frac{1}{\rho D} \tau_{sx} \quad (10)$$

$$F_y = \frac{1}{\rho D} \tau_{sy} \quad (11)$$

where

$$\frac{\tau_{sx}}{\rho} = k |\vec{W}| W_x \quad (12)$$

$$\frac{\tau_{sy}}{\rho} = k |\vec{W}| W_y \quad (13)$$

In this system of equations,  $\rho$  is the density of water,  $D$  is the total water depth,  $\tau_{sx}$  and  $\tau_{sy}$  are horizontal components of wind stress,  $k$  is a dimensionless surface friction coefficient,  $|\vec{W}|$  is the magnitude of the wind speed (in knots), and  $W_x$  and  $W_y$  are the  $x$  and  $y$  wind speed components. The wind stress coefficient  $k$  is based on the form given by Van Dorn (1953) and is assumed to be a function of wind speed such that

$$k = k_1 \quad \text{for} \quad |\vec{W}| \leq W_c \quad (14)$$

$$k = k_1 + k_2 \left(1 - \frac{W_c}{|\vec{W}|}\right)^2 \quad \text{for} \quad |\vec{W}| > W_c \quad (15)$$

where  $k_1 = 1.1 \times 10^{-6}$ ,  $k_2 = 2.5 \times 10^{-6}$ , and  $W_c$  is a critical wind speed defined to be 14 knots.

23. In the simulation of hurricane storm surges, the wind speed components  $W_x$  and  $W_y$ , and the pressure-induced free-surface anomaly  $\eta_a$ , are computed using the Standard Project Hurricane (SPH) model developed by the Hydrometeorological Branch (Hydromet) within the Office of Hydrology of the National Weather Service. Essentially, the model generates a time-history of the surface atmospheric pressure and wind speed (measured at a 10-m elevation) at each point of a uniformly spaced grid mesh which is superimposed on the Atchafalaya Bay grid. This weather information is computed using nomograms developed from historical hurricane data and the following hurricane parameter input: (a) a far-field surface atmospheric pressure, (b) an effective radius which controls the decrease in wind speed radially outward from the eye of the storm (this parameter will be referred to later as RMAXE), (c) a digitization

of the coastline, and (d) a time-history of the following variables,

- a. x and y coordinates of the hurricane center relative to the computational grid origin.
- b. Radius to maximum winds.
- c. Maximum wind speed.
- d. Central pressure.
- e. Inflow angle of the radial winds.
- f. Angle between the storm heading and a line passing through the center of the band of maximum winds.

For more information concerning the SPH, the reader is referred to information published by the National Weather Service (1972, 1979).

## PART IV: MODEL VERIFICATION

### Tidal Verification

24. As part of the overall Atchafalaya Bay study an extensive data-gathering effort was undertaken during 1981-82, which included installation of a fairly dense network of tide gages throughout the bay system. Since a large amount of tidal stage data was available, the Atchafalaya Bay model was applied to see how well it could simulate the astronomical tide. Accuracy of the simulation would be based on a comparison between observed and computed hydrographs for as many gage locations throughout the system as possible.

25. Three criteria were evaluated in selecting the time period considered for simulation. Those times were considered during which a majority of the tide gages in the bay system were operational and yielded good data. This criterion ensured good spatial coverage throughout the area for which comparisons could be made. Wind conditions during these time periods were examined and those times characterized by high wind were removed from consideration. Consequently, prototype tide elevation data were relatively free of any meteorologically induced anomalies. The third criterion was to examine the river discharges from the two major sources of freshwater inflow during the time periods considered and select only those periods of time when discharges were relatively low. The reason for this is that the complicated network of branching channels and deltaic deposits of the Atchafalaya River delta could only be represented accurately at a scale which would make the cost of any simulation prohibitive. At the grid scales selected and during periods of low outflow, errors in simulated flow patterns in the rest of the bay due to an inaccurate delta representation would be minimized since the low velocities would not significantly affect the propagation speed of the tide. The effect of the delta was calibrated by adjusting the frictional influence of the bottom in this vicinity. During large river discharges, much of the marshland surrounding the river channel becomes flooded. The extent of this flooding, the resulting flow patterns, and effects of the flooding on the flow distribution at the mouth of the Atchafalaya River and Wax Lake Outlet make simulations during high outflow very difficult.

26. Subjecting all available tide gage data to these three criteria resulted in the time period of 13-16 January 1981 being chosen for verification.

A constant discharge into the bay of 53,000 cfs was assumed to be divided between two sources with 65 percent coming from the Atchafalaya River and 35 percent from the Wax Lake Outlet. This very small discharge was assumed constant throughout the simulation but in fact varied from 47,000 to 56,000 cfs between 12 January and 17 January. These discharges were computed from the observed river stages at Simmesport, shown below, and the stage-discharge relation shown in Figure 10.

<u>Date</u>	<u>River Stage ft</u>	<u>Discharge cfs</u>
12 Jan 1981	1.7	50,000
13 Jan 1981	1.9	52,500
14 Jan 1981	2.2	56,000
15 Jan 1981	2.2	55,000
16 Jan 1981	2.1	53,000
17 Jan 1981	1.4	47,000

Wind effects were neglected during this simulation. Actual wind speeds and directions recorded during this time are shown in Figure 11 and the location of the anemometer (WS-E, whose recording elevation was at 5.8 m) is shown in Figure 12.

27. The remaining input required by the model for the tidal simulation is a specification of the offshore boundary conditions. Along the deepwater grid boundaries, the free surface was specified to be the astronomical tide elevation predicted using amplitudes and phases for the five major constituents computed from GOMT results. As mentioned earlier, to compensate for the inability of any boundary condition to properly include the resonant effect of the tide, diurnal amplitudes were increased by 35 percent and the semi-diurnal amplitudes by 25 percent along the boundary. A zero flux gradient boundary condition was employed along the open boundaries where water depths were shallow.

28. The tidal simulation was run for a total of 78 hr of real-time. During the first 10 hr both the boundary tide specification and the river discharges were increased from zero up to their full values. This virtually eliminated any "shocking" of the system, thereby minimizing the effects of spuriously introduced oscillations on the solution. Computed hydrographs at the 12 locations shown in Figure 12 were compared with their prototype

counterparts (Figures 13-16). Since vertical control of the observed data is unknown in terms of the model mean sea level, the two sets of hydrographs were compared by adjusting the vertical axis of the computed hydrographs so that discrepancies between the crests and troughs were of approximately the same magnitude. Model results compare quite well with observed data at all locations throughout the bay system. A majority of the amplitude errors are between 0.1 and 0.3 ft, while the phase errors range from 10 to 30 min. These differences are quite acceptable for this area where the tide range is 1.5 to 2.5 ft.

29. A series of vector plots (Figures 17-26) are included to illustrate the general circulation patterns during a "typical" tidal cycle that occurred at the end of the tidal simulation. These figures show the time variation (one plot every 3 hr) of mass transport per unit width for the immediate Atchafalaya Bay vicinity.

#### Storm Surge Verification

30. The remaining task of the model verification phase is the simulation of selected hurricanes and a comparison between computed results and the previously observed response of the Atchafalaya Bay system to these extreme events. Many factors make such a comparison difficult. Hurricanes occur infrequently, and of the ones that have occurred in the Gulf of Mexico and have been well documented, few have had a serious impact on the immediate area around Atchafalaya Bay. In order to make comparisons, an accurate representation of meteorology during the storm must be available; but due to the intensity of these storms, very little data are collected during the time the storm has its greatest impact on the coastal area, which is just prior to landfall. Another problem in verifying the model to hurricane conditions is the lack of data describing the hydrodynamics (usually free-surface hydrographs) that existed during the storm. This problem is prevalent in this geographical area where the number of tide gages is very few due to the lack of suitable structures on which to install gages and difficulties in servicing them once they are installed.

31. In light of these problems, three storms were considered for verification, Hurricanes Audrey (1957), Hilda (1964), and Carmen (1974). Carmen had the most hydrograph and high-water-mark data, but very little

documentation on storm wind fields was available. The other two storms had some water-level data available (mostly in terms of high-water marks); however, each had fairly detailed information on weather patterns associated with the storm as well as information on the parameters required by the SPH model to generate wind fields. The storm information was prepared by the Hydromet Office of the US Weather Bureau. A decision was made to verify the model to those two storms for which more accurate storm meteorology was known. It was believed that by using the limited water-level data available along with an accurate account of the wind and pressure fields, one could better judge the accuracy of the model's ability to simulate the storms. The other alternative, in the case of Carmen, would have been to try to reproduce hydrographs measured during the storm while knowing little about the atmospheric forcing that caused those water-level fluctuations.

32. The following is the process by which the simulations for both storms were carried out. The model was run for 54 hr prior to the start of the surge run with astronomical tide forcing only. Hydrodynamics at the end of this run were saved and used as start-up conditions for the storm simulation. A duration was selected for the surge simulation in which enough time was allowed for the bay system to respond to the wind fields while the storm was some distance from the coast and was continued until 9 or 12 hr after landfall or until the storm had passed out of the model grid system. During the storm surge run, the model was driven by wind and pressure fields generated by the SPH model and boundary conditions were specified by one of two types. In deep water, greater than 200 ft, the free surface at the boundary was defined to be that resulting from the sum of the astronomical tide and inverted barometric pressure head due to the storm. In shallow water, the zero-gradient condition of transport normal to the boundary was used.

33. In the January 1983 tidal verification, topography at the outer edge of Atchafalaya Bay decreased gradually into the northern Gulf of Mexico. During the time of occurrence of both storms, Hilda and Audrey, a shell reef existed at the bay entrance. A vertical barrier, representing the reef, was added to the model topography and extended vertically 1.5 to 2.0 ft above model mean sea level in areas where the reef was believed to have existed. No discharges were included in the surge simulations, since little information on their magnitudes during the storm was available. Research indicated that the monthly average discharges during these times were very small, in the range of



70,000 to 90,000 cfs. In light of the amount of inundation experienced during these storms, neglecting the discharges does not appreciably affect the hydrodynamic response in the majority of the bay system.

34. The first storm to be simulated was Hurricane Hilda which passed just southwest of Eugene Island in a northerly direction during 3-5 October 1964 (Figure 27). Many sources of data were researched in order to estimate the meteorology associated with this storm both prior to and after landfall (Hawkins and Rubsam 1968; Leipper 1965; US Weather Bureau 1964, 1965; USAED, New Orleans 1966; and Wanstrath 1978). From this information, a time-history of the various parameters required by the SPH model was formulated and subsequently used to generate wind and pressure fields for the simulation. Simulated wind fields were then compared with those constructed by the Hydromet Branch of the US Weather Bureau as part of their development of the storm data.

35. Storm parameters for Hurricane Hilda are shown in Table 1. The wind fields computed by the SPH model (Figures 28-37), are shown every 6 hr with hour zero being the starting time of the storm surge simulation, 0600 hours on 2 October 1964 GMT. Wind speed contours are plotted in 5-knot increments. The value of  $R_{MAXE}$  was selected by matching the simulated winds in the far field with the values given in Hydromet analysis. Results of their work, which are shown in Figures 38-41, can be compared with the SPH results using the following comparisons:

<u>SPH Time</u>	<u>Hydromet Time, GMT</u>
Hour 12	1800 2 Oct
Hour 24	0600 3 Oct
Hour 36	1800 3 Oct
Hour 48	0600 4 Oct

The offshore boundary of the model grid system is shown on these figures as a frame of reference.

36. Two major shortcomings of the SPH model are evident in these wind-field comparisons. Nomograms used to generate hurricane wind distributions were developed using an average distribution derived from a set of selected storms. Wind-field accuracy for any single simulated storm is really a function of how well the shape of that storm fits the shapes of storms considered in the nomogram formulation, especially in the far field. The SPH model does

not represent the effects of land on the wind fields in a totally correct manner; it employs no physics in estimating interaction between overland and over-water winds but instead uses empirically determined wind reduction factors determined from historical data. Any effect on the wind direction as a result of this land influence, called storm "filling," is also neglected by the SPH model.

37. Using the SPH-generated forcing functions and initial conditions from the tidal "hot start," the storm surge simulation was run for 51 hr. "Shocking" of the existing tidal conditions with an instantaneous wind stress and inverted barometric effect did introduce some transients into the solution in the early part of the simulation; however, by the time the storm wave had entered the model grid region, the oscillations were damped out by frictional dissipation.

38. Without extensive hydrograph data, comparisons between the simulated and actual response of the Atchafalaya Bay system to Hurricane Hilda had to be done using available high-water-mark information as well as estimates of the extent of inland flooding. The average absolute error of all comparisons was 0.75 ft. The tide gage at Eugene Island is the only point of comparison in the prime area of interest, the eastern portion of the Atchafalaya Bay. Absolute error at this location was 0.2 ft. Additional water-level data were available at a few points along the Atchafalaya River and waterways branching from it; but since the simulation did not include river discharges, these comparisons were not presented. The difference in time of arrival of peak water level between observed and simulated results at Eugene Island was about 25 min. Table 2 lists both the simulated and observed high-water marks and the times of their occurrence, when known, for Hurricane Hilda.

39. In Figure 42, the stippled region shows the documented extent of flooding that occurred during Hilda. This information also was used to measure the success of the model simulation. Figure 42 also shows the contours of high-water marks (in feet) resulting from the model run. Flooding extent is fairly well reproduced by the model (approximately given by the 2-ft contour) with the exception of the western portion of the bay. This is misleading because peak water levels computed during the early stages of the storm simulation did reach about 1.6 ft in Vermilion Bay. The marshlands surrounding the bay were at an elevation of 1.5 ft and the model disallowed any flooding until the water level adjacent to a land cell exceeded the land elevation

by 0.2 ft. Also any marshlands with elevations less than 1.5 ft would have been flooded which would not have been indicated by the model results since all the marshlands are prescribed to have elevations greater than 1.5 ft.

40. The other storm used to verify the model was Hurricane Audrey, which occurred during June 1957 and which made landfall far to the west of the Atchafalaya Bay yet produced the largest amount of flooding in this area in recent years. The path of this storm is shown in Figure 27. Wind fields and atmospheric pressure distributions were computed in the same fashion as was done for Hurricane Hilda using the storm parameter input shown in Table 3. These parameters were determined from information presented in Sumner (1957), Ross and Blum (1957), Moore et al. (1957), US Weather Bureau (1957, 1958). Wind fields computed from the SPH model are shown in Figures 43-49. The plots start with hour zero, which corresponds to hour 1200 on 26 June 1957, and are shown every 6 hr. Figures 50 and 51 show the wind fields generated in the Hydromet analysis; and as in the analogous Hilda figures, the grid boundary is shown for reference. Wind speeds are in miles per hours instead of knots and the time reference is central standard time. In comparing these wind fields with the SPH-generated wind fields, the following information is helpful:

<u>SPH Time</u>	<u>Hydromet Time, CST</u>
Hour 18	0000 27 June
Hour 24	0600 27 June

41. The shape of this storm, namely the extreme eccentricity of the wind fields, is not a common feature among tropical storms; therefore the SPH model could not exactly reproduce the Audrey wind fields everywhere within the bounds of the computational grid. An  $R_{MAXE}$  value of 10 was chosen for the final Audrey wind fields because it reproduced the far fields more accurately than larger values, with some loss of accuracy in the immediate vicinity of the bay itself. Still, the comparison in wind fields is quite good.

42. As with Hurricane Hilda, hot-start conditions were established by running the model for 54 hr with tidal forcing alone. The actual surge simulation was carried out for only 36 hr because the forward speed of Hurricane Audrey was twice as fast as that of Hurricane Hilda.

43. Information on observed water levels during Audrey came from a report on the storm tide by Harris (1958). Since vertical control is missing from the tide elevation time series used to compute peak water elevations

during this storm, documented high-water marks do not necessarily reflect the true water-level rise relative to model mean sea level. To better account for these discrepancies, the rise of the peak surge relative to the water level recorded during the initial stages of the hydrograph was taken as the high-water mark. Comparisons of these adjusted, observed values and simulated high-water marks are shown in Table 4. The error at Eugene Island is very small, 0.1 ft, and the overall average absolute error is slightly less than 1.0 ft. If the comparison for Cameron, which is located along the western boundary of the grid, is neglected the absolute average error decreases to about 0.5 ft. Additional data along the Atchafalaya River were available but were not used since the simulation neglected discharge.

44. Figure 52 shows the documented extent of flooding due to Hurricane Audrey and also illustrates the simulated flooding as shown by contours of high-water marks. As with Hurricane Hilda, the model simulates the inundation quite well.

## PART V: HYPOTHETICAL STORM SIMULATIONS

45. The initial phase of the storm surge task of the Atchafalaya Bay study was the generation and verification of a numerical model to predict hydrodynamics within the bay area resulting from tidal and/or meteorological forcing. A second aspect of the study task involves the simulation of a set of hypothetical hurricanes with dynamical characteristics that are representative of severe storms which have affected this area in the past. The variation in the free surface and associated velocity patterns accompanying these events will be used to investigate future response of the Atchafalaya River delta growth process to hurricane influence.

46. A decision was made to simulate an ensemble of 12 storms with each storm characterized by a unique set of parameters. These parameters, which dictate wind-field and barometric characteristics for a particular storm, were defined to be storm track, forward speed, central pressure deficit, and radius to maximum winds. Three storm tracks were considered with each producing a different hydrodynamic response in the bay, in a qualitative sense.

47. The first track involved a hurricane with a landfall point approximately 60 miles west of the Atchafalaya Bay main navigation channel at a location just south of White Lake, La., and with a track heading of 20 deg east of north. This storm path results in a continual influx of water into the bay until the storm moves well inland. In terms of surface elevation, this event can result in substantial flooding. Hurricane Audrey took this type of path. A second track considered was one which was directed due north and made landfall a few miles to the west of the Atchafalaya River mouth. The hydrodynamics during this type of event are dominated by a steady outflow of water out of the bay while the storm is offshore. With the arrival of the storm surge wave, the direction of flow in the bay is rapidly reversed and subsequent flooding can occur. Qualitatively, Hurricane Hilda behaved in this manner. The final track considers a storm moving in a direction 20 deg west of north with a landfall point approximately 40 miles east of the bay near Pelican Lake, La. This type of event results in a steady draining of water from the bay since wind fields have a southerly component most of the time.

48. For each track, four storms were simulated with each having one of two different central pressures and one of two radii to maximum winds.

Identical values of forward speed and ambient atmospheric pressure were used in all the simulations. Table 5 shows the storm parameters used for each hurricane. A constant forward speed of 11 knots was adopted since this is the value used by the New Orleans District for their design storms. Ambient pressure was chosen to be 29.77 in. Hg since this is the value recommended by the National Weather Service for all standard project hurricanes in this area. Values of the other parameters, including track heading, were selected as being typical of hurricanes that occur in the Gulf and in this particular area. Figures 53-56 illustrate the frequency of occurrence of each of these parameters, track direction, forward speed, central pressure, and radius to maximum winds for the entire population of Gulf hurricanes that have occurred in the last 80 years as well as for those storms that have affected the region close to the Atchafalaya Bay (within 100 miles to either side).

49. Each of the hurricane simulations was carried out for 33 hr, 24 prior to landfall and 9 afterward. No river discharges were considered in the simulations and the boundary conditions offshore were either zero-flux in shallow water or a specification of the inverted barometric free surface in deeper water. The entire bay system was started at rest (i.e. no tidal hot-start conditions). No shell reef was considered in the bottom bathymetry specification. To illustrate the effect of each storm, the free-surface time-history as well as some computed velocities is shown in Figures 57-60 for a location near the navigation channel adjacent to Eugene Island. As previously mentioned, the track determines the shape of the surge profile and the resulting currents. The central pressure and the radius to maximum winds determine the storm intensity, and for a given track, the larger radius to maximum winds and the smaller central pressure result in a larger magnitude of water-level variation. This fact is substantiated by the figures.

50. Table 6 illustrates the extent and variability of flooding and/or ebbing during these hypothetical storms. It shows the maximum water-surface elevations at five locations throughout the bay area: (a) the center of Fourleague Bay, (b) Atchafalaya River mouth, (c) off the tip of Point Chevreuil, (d) the center of West Cote Blanche Bay, and (e) the center of Vermilion Bay. These locations are shown in Figure 61. Only positive maxima are shown for the first four storms since Track 1 resulted in predominantly flooding conditions prior to landfall. Likewise, for the last four storms, only negative peak surges are shown. For the middle four storms, substantial ebbing and

flooding occurred and both peaks are listed. The most noticeable aspect of this table is the extreme impact a storm with a central pressure of 27.5 in. Hg, a radius to maximum winds of 30 n.m., and any of the tracks considered would have on this area. The hydrodynamics from each of these storms were saved for later use.

## PART VI: SUMMARY

51. A model was formulated to simulate hydrodynamics within the Atchafalaya Bay system. Input required by the model including boundary conditions and external forcing functions were presented as they applied to this particular model application. Response of the model was verified to both astronomical tide forcing alone and to a combination of astronomical tide and meteorological forcing due to hurricanes. In both cases, the measure of accuracy of the model results was a comparison of observed and simulated water elevations.

52. Comparisons showed that the model can accurately simulate the response of the system to the astronomical tide and hurricanes. In the case of tides alone, the amplitude errors were on the order of tenths of feet and the phase errors were very small, on the order of tens of minutes. Errors in the storm surge applications were larger, about 1 ft, but the natural phenomena in this area produced elevations up to 8 ft. Again, the phase errors were small, although they were based on a limited amount of data. Spatial extent of flooding caused by both Hurricanes Hilda and Audrey were modeled quite accurately. Considering the accuracy of the prototype data used to verify the storm effects and the accuracy of the wind and pressure forcing functions, the model simulated the storm effects quite well.

53. Using the verified model, a set of hypothetical storms was simulated. Dynamical characteristics of these storms reflect hurricanes that have occurred in this area in the past. Hydrodynamics from these storms will be used in other tasks to investigate the response of the Atchafalaya River delta growth to extreme meteorological events.



## REFERENCES

- Butler, H. L. 1978a. "Coastal Flood Simulation in Stretched Coordinates," Sixteenth International Conference on Coastal Engineering, American Society of Civil Engineers.
- \_\_\_\_\_. 1978b (Jun). "Numerical Simulation of Tidal Hydrodynamics, Great Egg Harbor and Corson Inlets, New Jersey," Technical Report H-78-11, US Army Engineer Waterways Experiment Station, Vicksburg, Miss.
- \_\_\_\_\_. 1978c (Dec). "Numerical Simulation of the Coos Bay, South Slough Complex," Technical Report H-78-22, US Army Engineer Waterways Experiment Station, Vicksburg, Miss.
- \_\_\_\_\_. 1980. "Evolution of a Numerical Model for Simulating Long-Period Wave Behavior in Ocean-Estuarine Systems," Estuarine and Wetland Processes with Emphasis on Modeling, Marine Science Series, Vol II.
- \_\_\_\_\_. 1981. "Finite Difference Numerical Model for Long-Period Wave Behavior: With Emphasis on Storm Surge Modeling," Proceedings, First National US Army Corps of Engineers Sponsored Seminar on Two-Dimensional Flow Modeling.
- Harris, D. L. 1958 (Oct). "Hurricane Audrey Storm Tide," National Hurricane Research Project Report No. 23, US Weather Bureau, Washington, DC.
- Hawkins, H. F., and Rubsam, D. T. 1968 (Jul). "Hurricane Hilda, 1964," Monthly Weather Review, Vol 96, No. 7, pp 426-452.
- Leipper, D. F. 1965 (Apr). "The Gulf of Mexico After Hurricane Hilda (Preliminary Results)," Texas A&M University, College Station, Tex.
- Moore, P. L., et al. 1957 (Dec). "The Hurricane Season of 1957," Monthly Weather Bureau, pp 401-46.
- National Weather Service. 1972 (Jun). "Preliminary Revised Standard Project Hurricane Criteria for the Atlantic and Gulf Coasts of the United States," Memorandum HUR 7-120, Office of Hydrology, Silver Spring, Md.
- \_\_\_\_\_. 1979 (Sep). "Meteorological Criteria for Standard Project Hurricane and Probable Maximum Hurricane Windfields, Gulf and East Coasts of the United States," NOAA Technical Report NWS 23, US Department of Commerce, Washington, DC.
- Reid, R. O., and Whitaker, R. E. 1981 (Nov). "Numerical Model for Astronomical Tides in the Gulf of Mexico," Vol I, Texas A&M University, College Station, Tex.
- Ross, R. B., and Blum, M. D. 1957 (Jun). "Hurricane Audrey, 1957," Monthly Weather Review, pp 221-227.
- Sumner, H. C. 1957. "Tropical Storms, Jun 1957," US Weather Bureau, Washington, DC.
- US Army Engineer District, New Orleans. 1966 (May). "Hurricane Hilda, 3-5 October 1964," New Orleans, La.
- US Weather Bureau. 1957 (Jan). "Climatological Data, National Summary," Vol 8, No. 1, US Department of Commerce, Ashville, N. C.

US Weather Bureau. 1958 (Mar). "Pressures, Wind Speeds and Directions in Hurricane Audrey near the Louisiana Coast, 27 June 1957," Memorandum HUR 7-51, US Department of Commerce, Washington, DC.

\_\_\_\_\_. 1964 (Oct). "Storm Data," Vol 6, No. 10, US Department of Commerce, Washington, DC.

\_\_\_\_\_. 1965 (Jun). "Preliminary Analysis of Surface Winds in Hurricane Hilda, 2-4 October 1964," Memorandum HUR 7-32, Office of Hydrology, Washington, DC.

Van Dorn, W. G. 1953. "Wind Stress on an Artificial Pond," Journal of Marine Research, Vol 12, pp 249-276.

Wanstrath, J. J. 1978 (Feb). "An Open-Coast Mathematical Storm Surge Model with Coastal Flooding for Louisiana," Miscellaneous Paper H-78-5, US Army Engineer Waterways Experiment Station, Vicksburg, Miss.

Table 1  
Standard Project Hurricane (SPH) Parameters for Hurricane Hilda

$P_{AMB} = 29.95$  (in. Hg)

$R_{MAXE} = 21.0$  (n.m.)

<u>Time, GMT</u>	<u><math>W_{MAX}</math></u> knots	<u><math>\theta_I</math></u> deg	<u><math>\theta_W</math></u> deg	<u><math>R_{MAX}</math></u> n.m.	<u><math>P_o</math></u> in. Hg
October					
2 0600	92	0.0	23.0	21.0	27.95
0900	↓	0.0	18.0	↓	28.00
1200		0.0	18.0		28.06
1500		0.0	5.0		28.11
1800		5.0	359.0		28.16
2100		5.0	10.0		28.20
3 0000		10.0	14.0		28.24
0300	↓	10.0	25.0	↓	28.27
0600		15.0	22.0		28.29
0900	91	15.0	23.0		28.31
1200	90	20.0	23.0		28.33
1500	87	20.0	23.0		28.35
1800	85	25.0	25.0		28.37
2100	83	25.0	29.0		28.38
4 0000	82	25.0	9.0	23.0	28.40
0300	71	25.0	351.0	31.5	28.53
0600	60	25.0	312.0	40.0	28.66
0800	65	25.0	281.0	32.5	28.88
1200	70	25.0	281.0	25.0	29.10

Note:  $P_{AMB}$  = Ambient pressure  
 $R_{MAXE}$  = Effective radius for far-field winds  
 $W_{MAX}$  = Maximum wind speed  
 $\theta_I$  = Inflow angle of radial winds  
 $\theta_W$  = Angle between storm heading and bank of maximum winds  
 $R_{MAX}$  = Radius to maximum winds  
 $P_o$  = Central pressure

Table 2  
High-Water-Mark Comparisons for Hurricane Hilda

<u>Location</u>	<u>Observed Elevation ft</u>	<u>Simulated Elevation ft</u>	<u>Error ft</u>
Eugene Island*	3.3	3.1	+0.2
Schooner Bayou	2.6	2.6	0.0
East Cote Blanche Bay	4.4	1.2	+3.2
Vermilion Lock**	2.2	1.8	+0.4
Charenton Drainage Canal	3.0	1.1	+1.9
Lake Pelto	7.4	7.8	-0.4
Little Caillou Bayou Mouth	9.8	9.5	+0.3
Little Caillou Bayou	6.9	6.2	+0.7
Leeville	5.5	5.6	-0.1
Dulac	6.6	7.7	-1.1
Bayou Terrebonne	7.0	7.3	-0.3
Caillou Bayou	5.4	5.8	-0.4

Note: Average absolute error = 0.75 ft

\* The observed time of peak elevation was 2200 hr (CST) on 3 Oct and the simulated time was 2136 hr on 3 Oct.

\*\* The observed time of peak elevation was 1345 hr (CST) on 2 Oct and the simulated time was 1206 hr on 2 Oct.

Table 3

## Standard Project Hurricane (SPH) Parameters for Hurricane Audrey

 $P_{AMB} = 29.75$  (in. Hg) $R_{MAXE} = 10.0$  (n.m.)

Time, GMT	$W_{MAX}$ knots	$\theta_I$ deg	$\theta_W$ deg	$R_{MAX}$ n.m.	$P_o$ in. Hg
June					
26 1200	88	20.0	38.0	19.0	27.95
1500	86		19.0		
1800	88		359.0		
2100	88		3.0		
27 0000	88		33.0		
0300	88		27.0		
0600	86		20.0		
0900	88		15.0		
1200	88		7.0		
1500	86		3.0		
1800	75		6.0		
2100	60		5.0		
28 0000	45		347.0		

Note:  $P_{AMB}$  = Ambient pressure $R_{MAXE}$  = Effective radius for far-field winds $W_{MAX}$  = Maximum wind speed $\theta_I$  = Inflow angle of radial winds $\theta_W$  = Angle between storm heading and bank of maximum winds $R_{MAX}$  = Radius to maximum winds $P_o$  = Central pressure

Table 4  
High-Water-Mark Comparisons for Hurricane Audrey

<u>Location</u>	<u>Observed Elevation ft</u>	<u>Simulated Elevation ft</u>	<u>Error ft</u>
Eugene Island	5.2	5.1	+0.1
Schooner Bayou	5.5	5.2	+0.3
East Cote Blanche Bay	6.0	6.8	-0.8
Vermilion Lock	8.1	7.1	+1.0
Timbalier Island	2.5	2.9	-0.4
Pecan Island	5.6	4.6	1.0
Grand Lake	3.7	3.9	-0.2
Cameron	12.1	16.4	-4.3
Hackberry	4.9	5.2	-0.3

Note: Average absolute error - 0.93 ft.

Table 5  
Characteristics of the Hypothetical Hurricanes



<u>Storm</u>	<u>Track</u>	<u>Central Pressure in. Hg</u>	<u>Radius to Maximum Winds n.m.</u>	<u>Forward Speed knots</u>	<u>Ambient Pressure in. Hg</u>
1	1	27.5	18.0	11.0	29.77
2	1	28.5	18.0		
3	1	27.5	30.0		
4	1	28.5	30.0		
5	2	27.5	18.0		
6	2	28.5	18.0		
7	2	27.5	30.0		
8	2	28.5	30.0		
9	3	27.5	18.0		
10	3	28.5	18.0		
11	3	27.5	30.0		
12	3	28.5	30.0		

Table 6  
Extreme Storm Surge Elevations Throughout the Atchafalaya Bay Area  
Resulting from the Hypothetical Hurricanes

<u>Storm Number</u>	<u>Vermilion Bay</u>	<u>West Cote Blanche Bay</u>	<u>Point Chevreuil</u>	<u>Atchafalaya River Mouth</u>	<u>Fourleague Bay</u>
1	10.9	13.0	11.1	9.3	8.1
2	6.3	8.4	7.2	5.3	4.5
3	12.8	15.6	14.1	12.5	11.0
4	7.7	10.1	9.2	7.4	6.4
5	-8.0/0.2	-6.5/0.2	-7.9/3.7	-4.0/8.5	-5.7/9.3
6	-3.5/0.1	-3.0/0.7	-4.6/2.8	-1.3/4.7	-4.0/5.1
7	-10.0/0.3	-7.0/0.3	-7.8/4.9	-4.1/10.2	-4.8/10.9
8	-4.0/0.2	-3.4/1.0	-7.0/3.6	-1.8/5.9	-4.8/6.2
9	-8.1	-6.5	-6.7	-2.9	-3.9
10	-3.9	-3.7	-4.8	-1.1	-1.9
11	-10.0	-7.0	-7.9	-2.5	-4.4
12	-5.7	-4.8	-6.3	-1.3	-2.6

---

Note: All elevations are in feet.

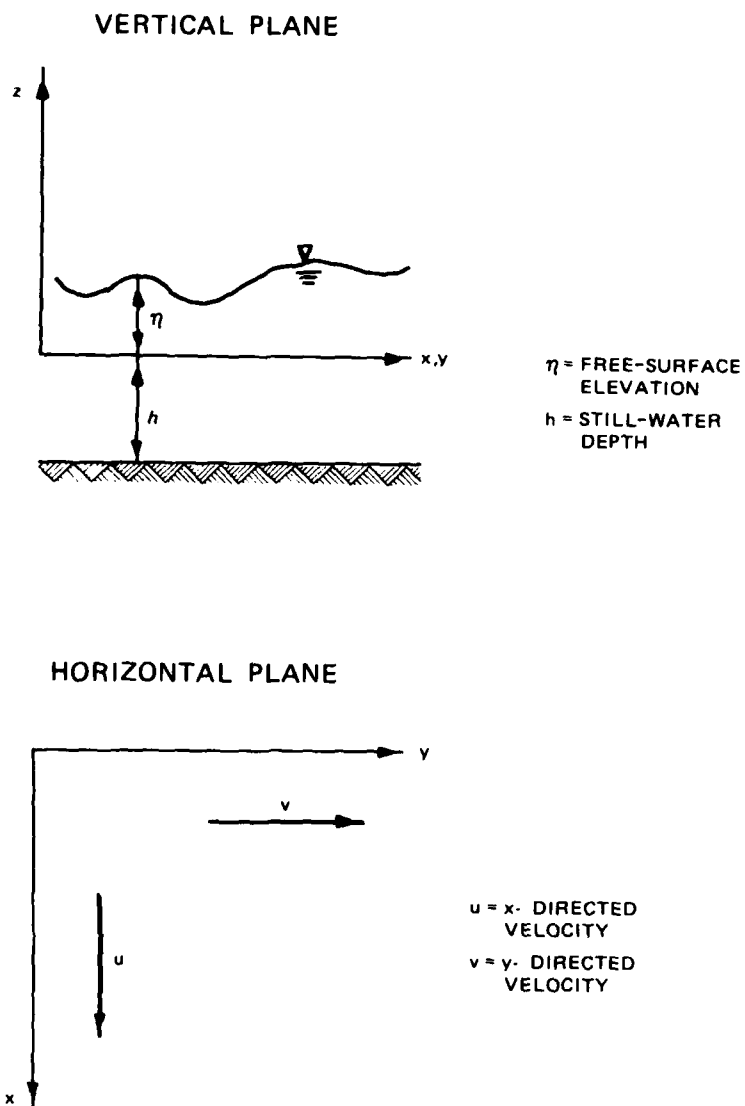


Figure 1. Definition of WIFM coordinate system and primary dependent variables



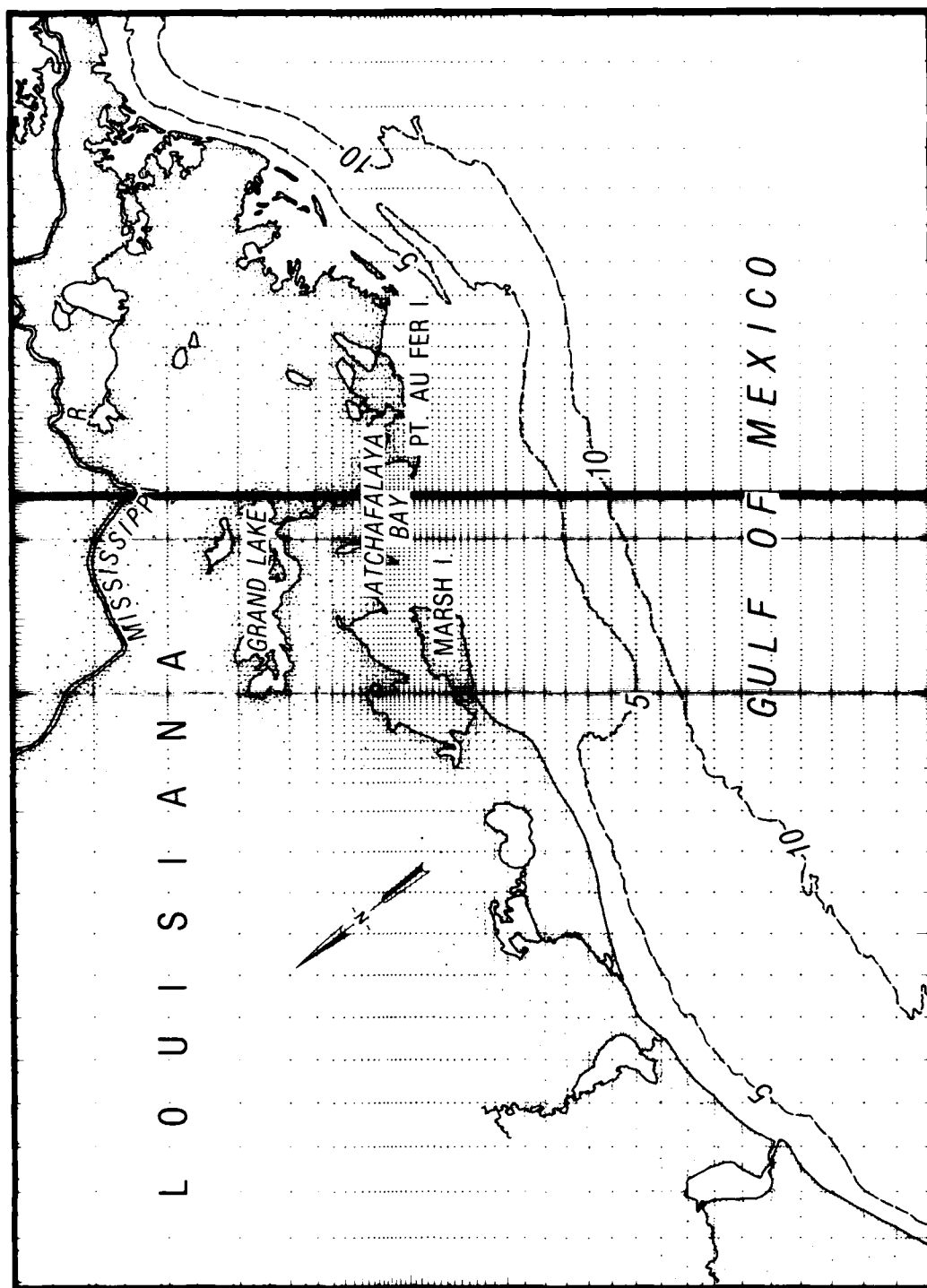


Figure 2. WIFM computation grid

## GULF OF MEXICO COMPUTATION GRID

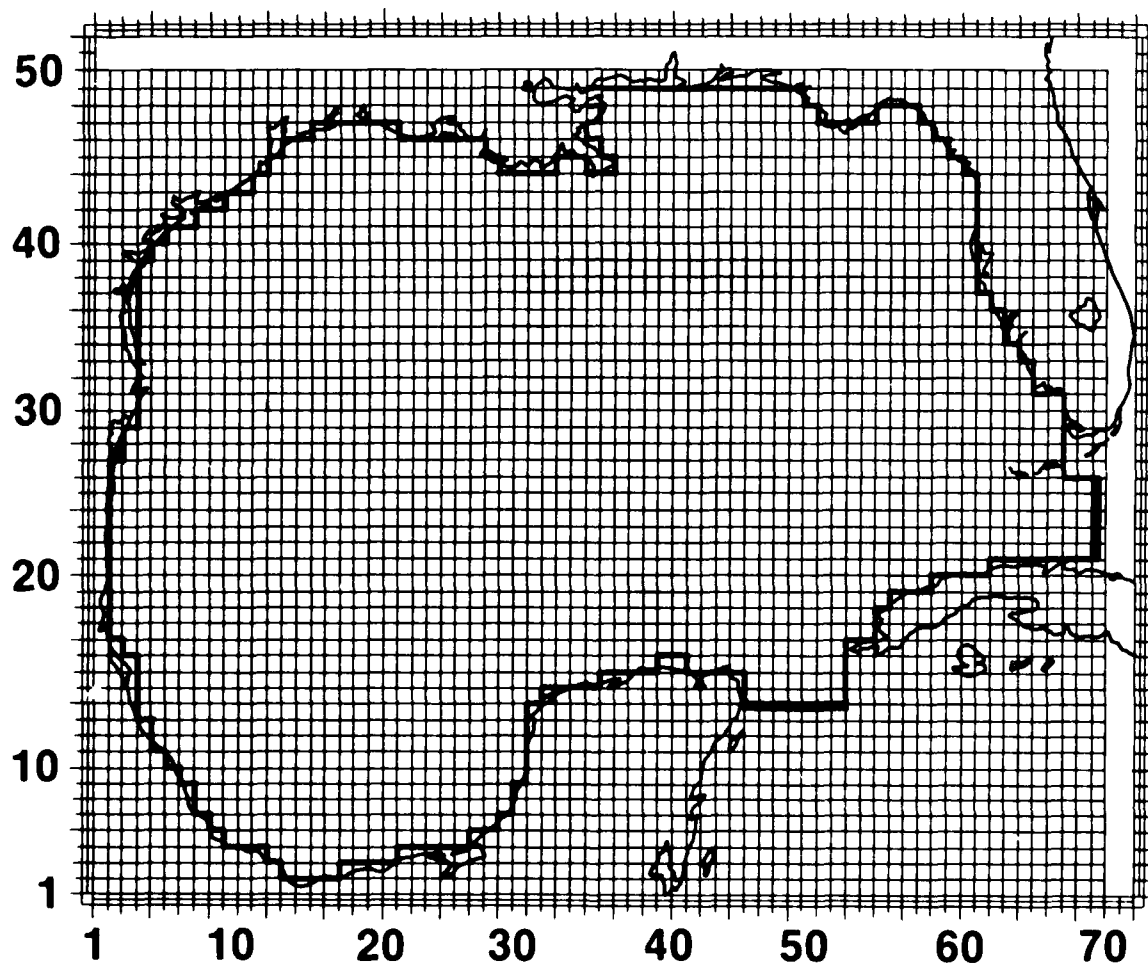


Figure 3. Gulf of Mexico (G.O.M.) computational grid

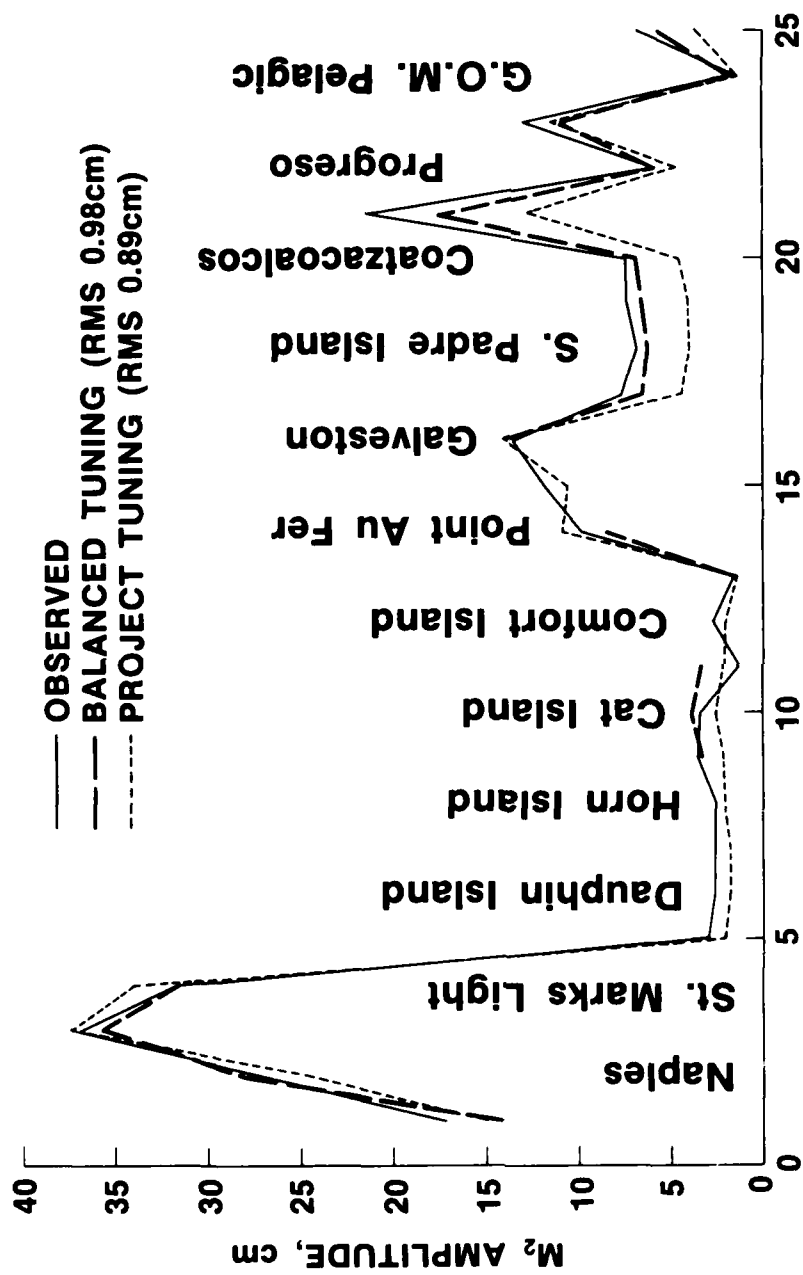


Figure 4. Observed and simulated variation of the  $M_2$  constituent amplitude in the G.O.M.

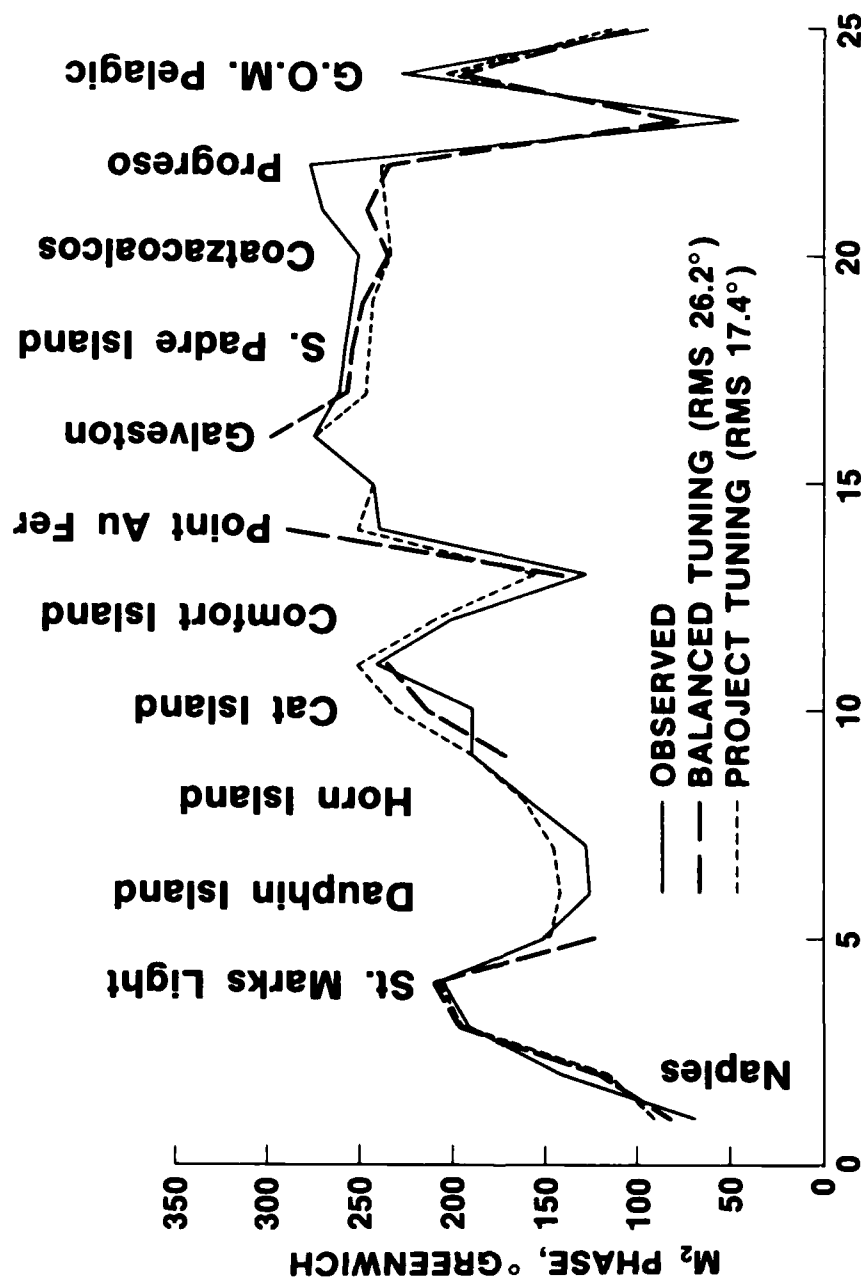


Figure 5. Observed and simulated variation of the  $M_2$  constituent phase in the G.O.M.

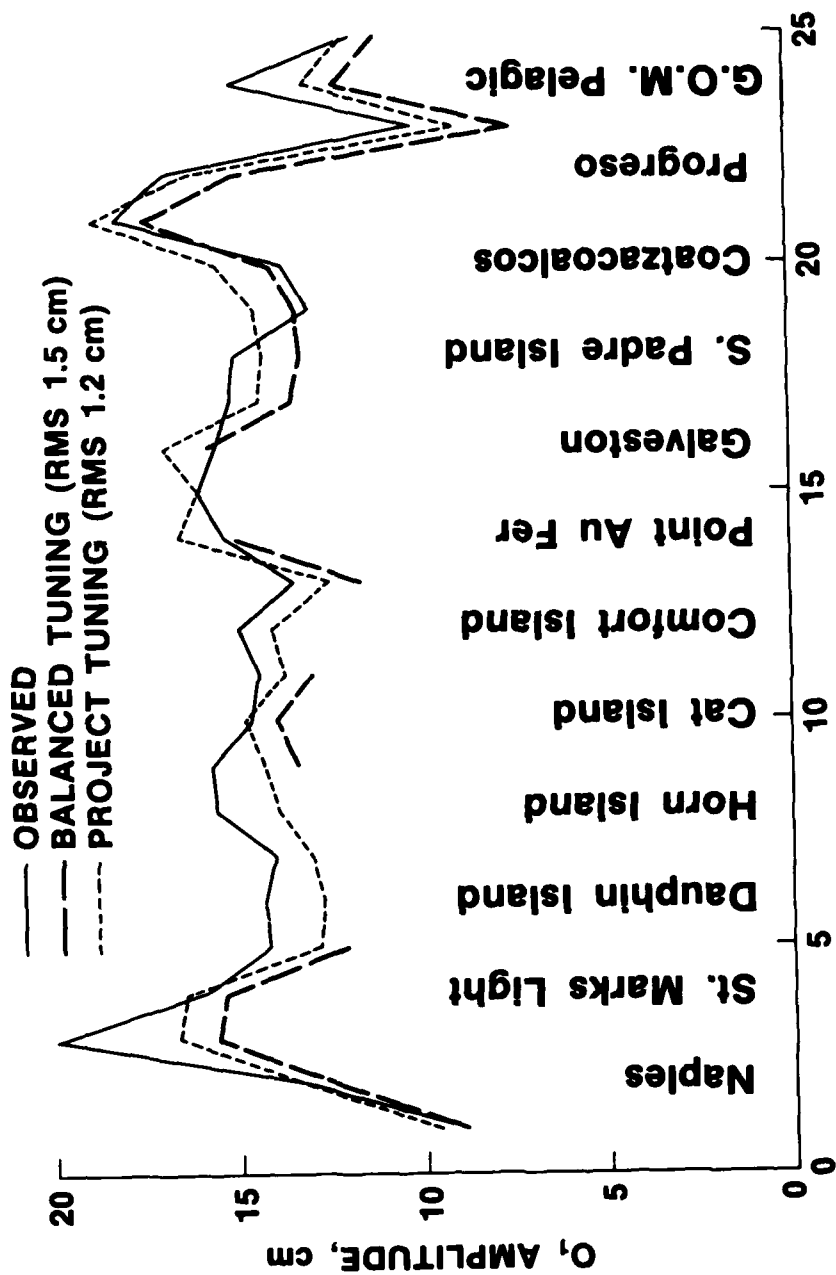


Figure 6. Observed and simulated variation of the  $O_1$  constituent amplitude in the G.O.M.

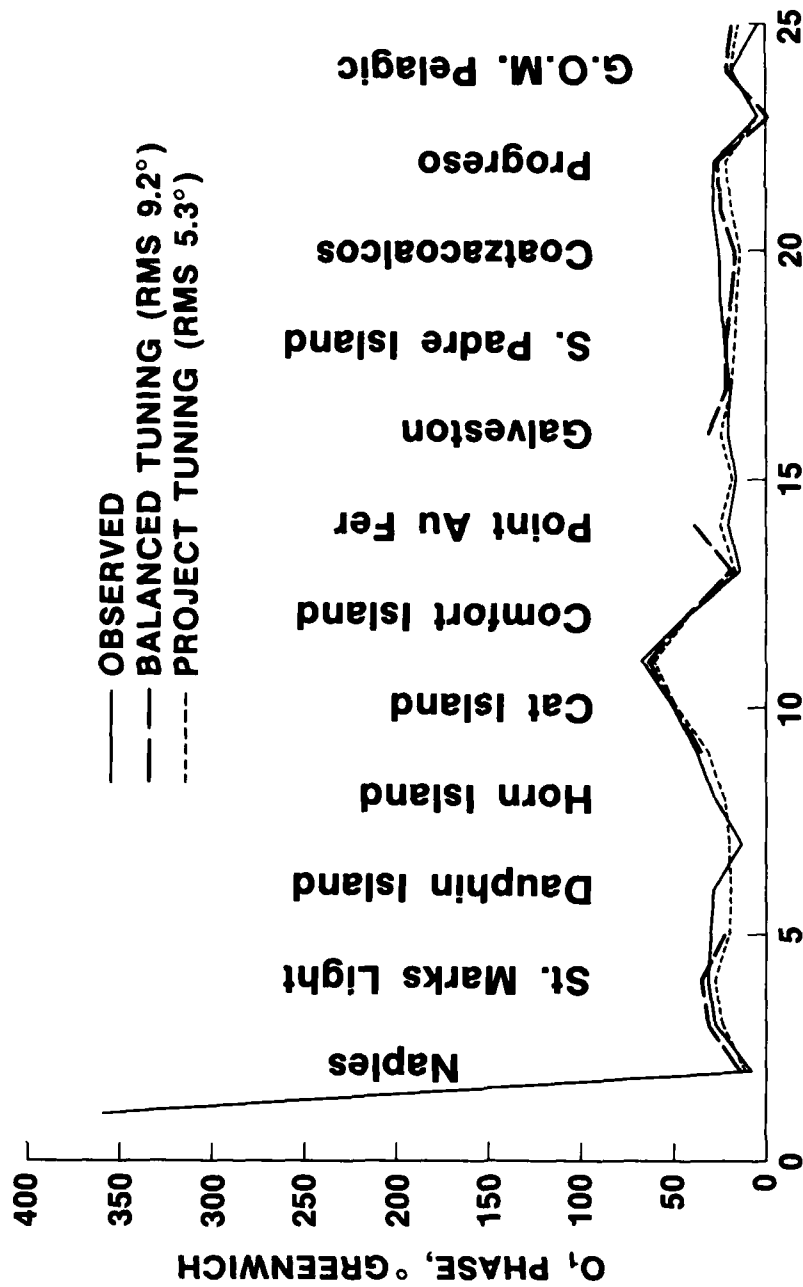


Figure 7. Observed and simulated variation of the  $O_1$  constituent phase in the G.O.M.

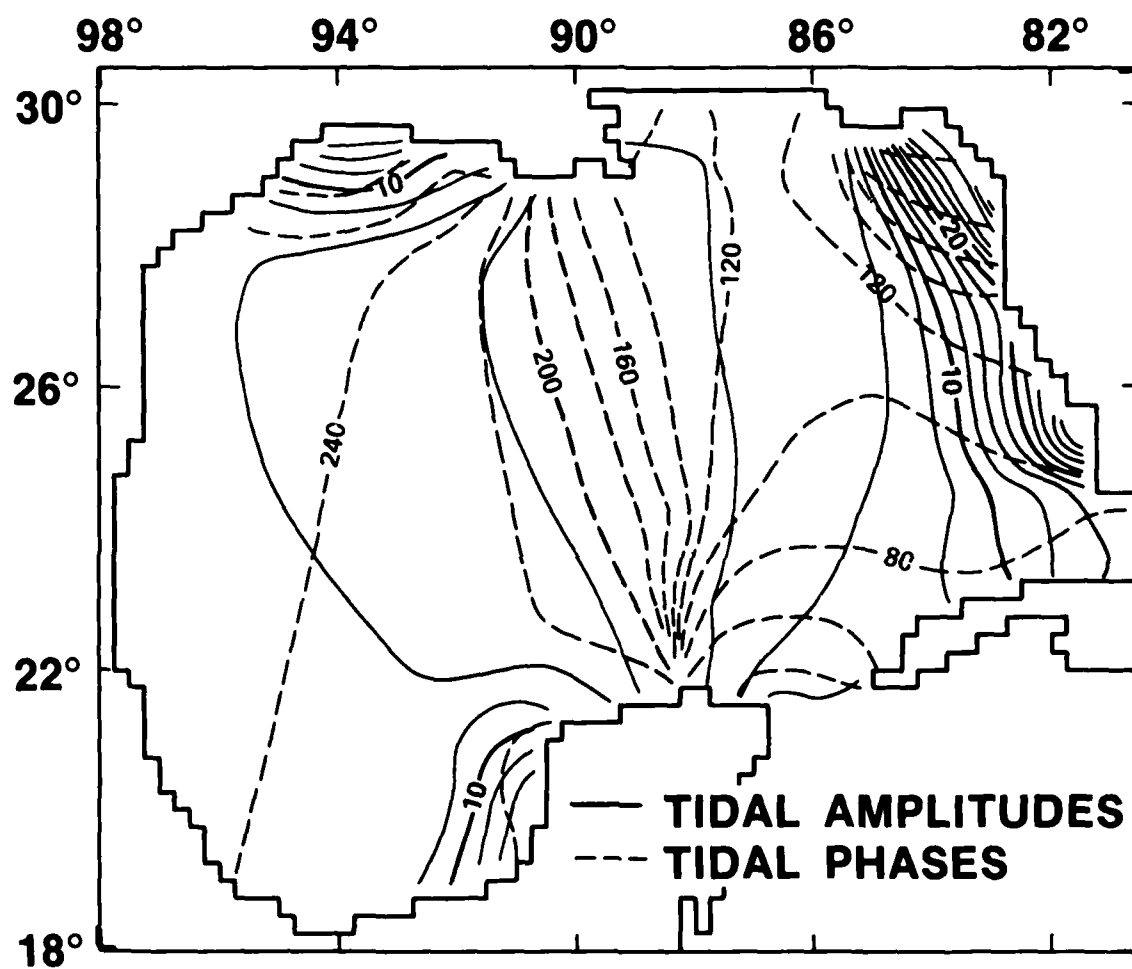


Figure 8. Simulated cotidal lines for the  $M_2$  constituent using the GOMT

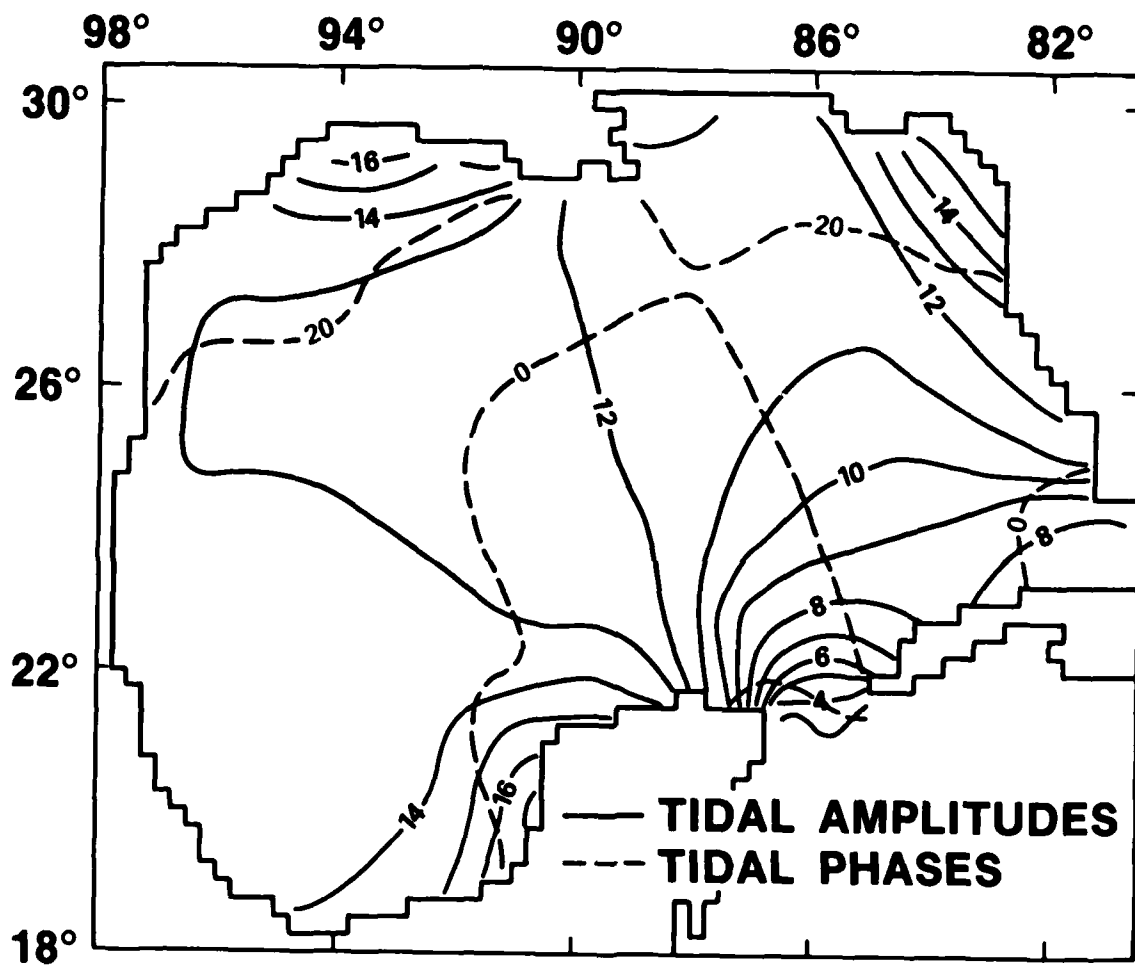


Figure 9. Simulated cotidal lines for the  $O_1$  constituent using the GOMT



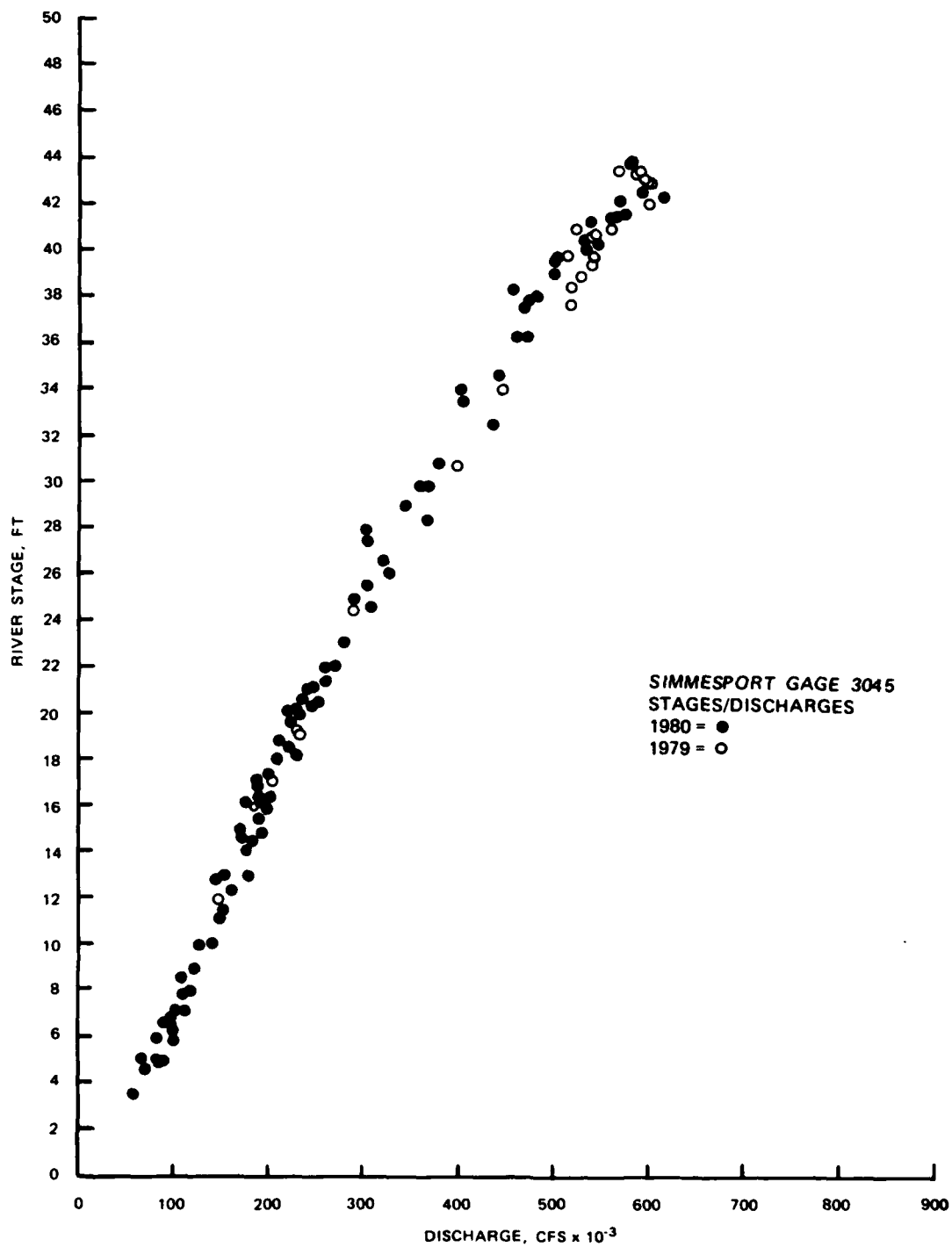


Figure 10. Stage-discharge relation at Simmesport, Louisiana

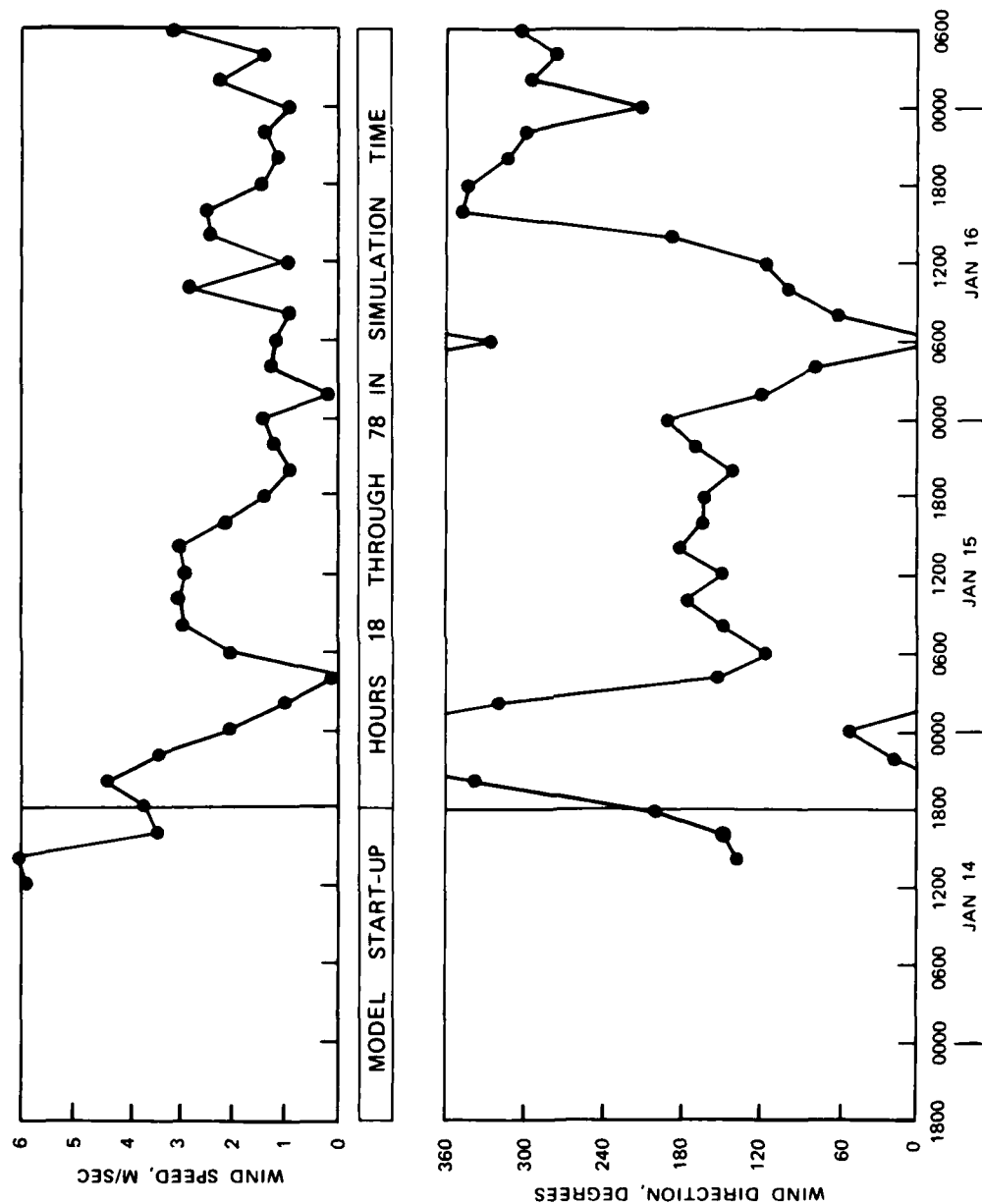


Figure 11. Prototype wind measurements during tidal verification

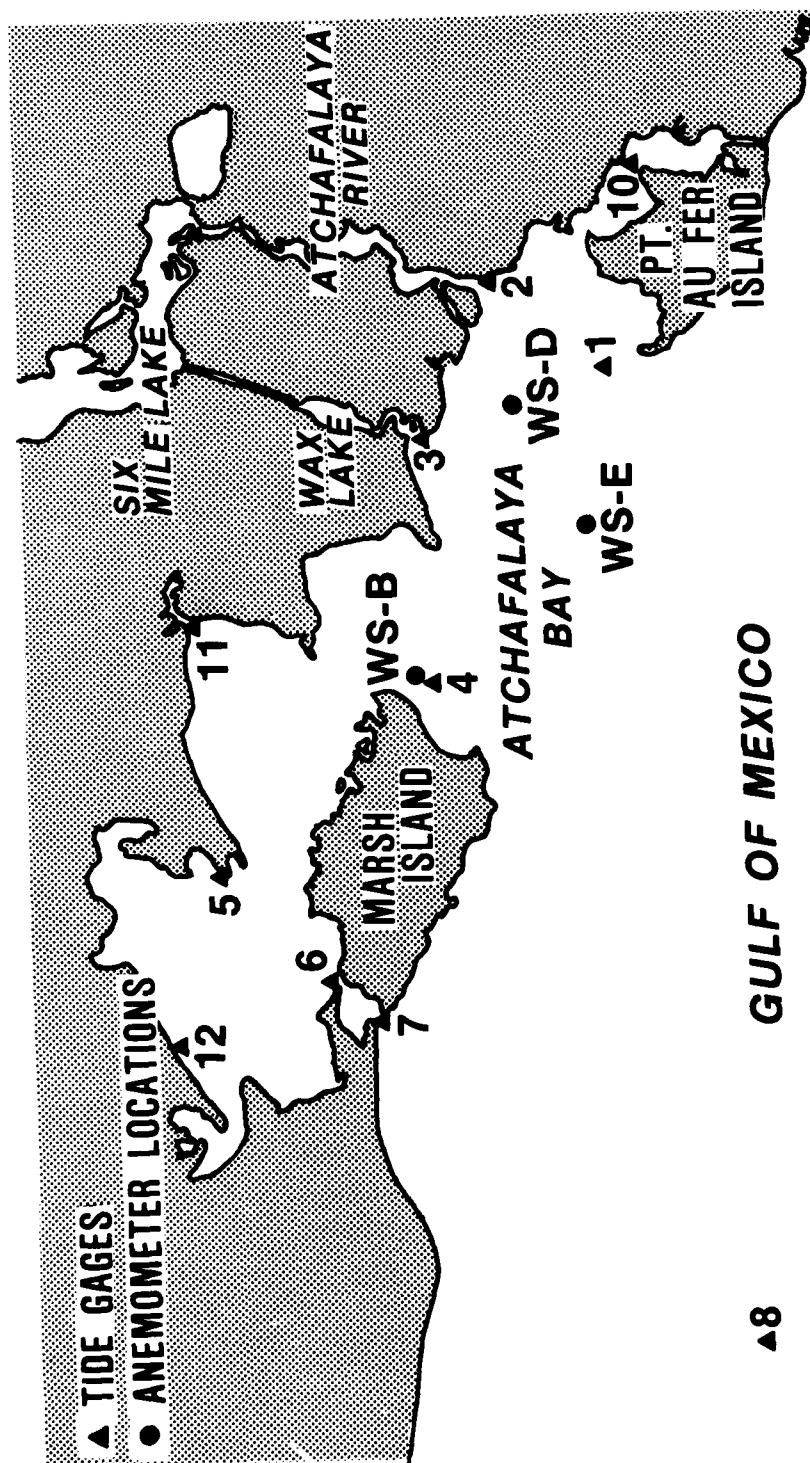


Figure 12. Prototype tide gage locations

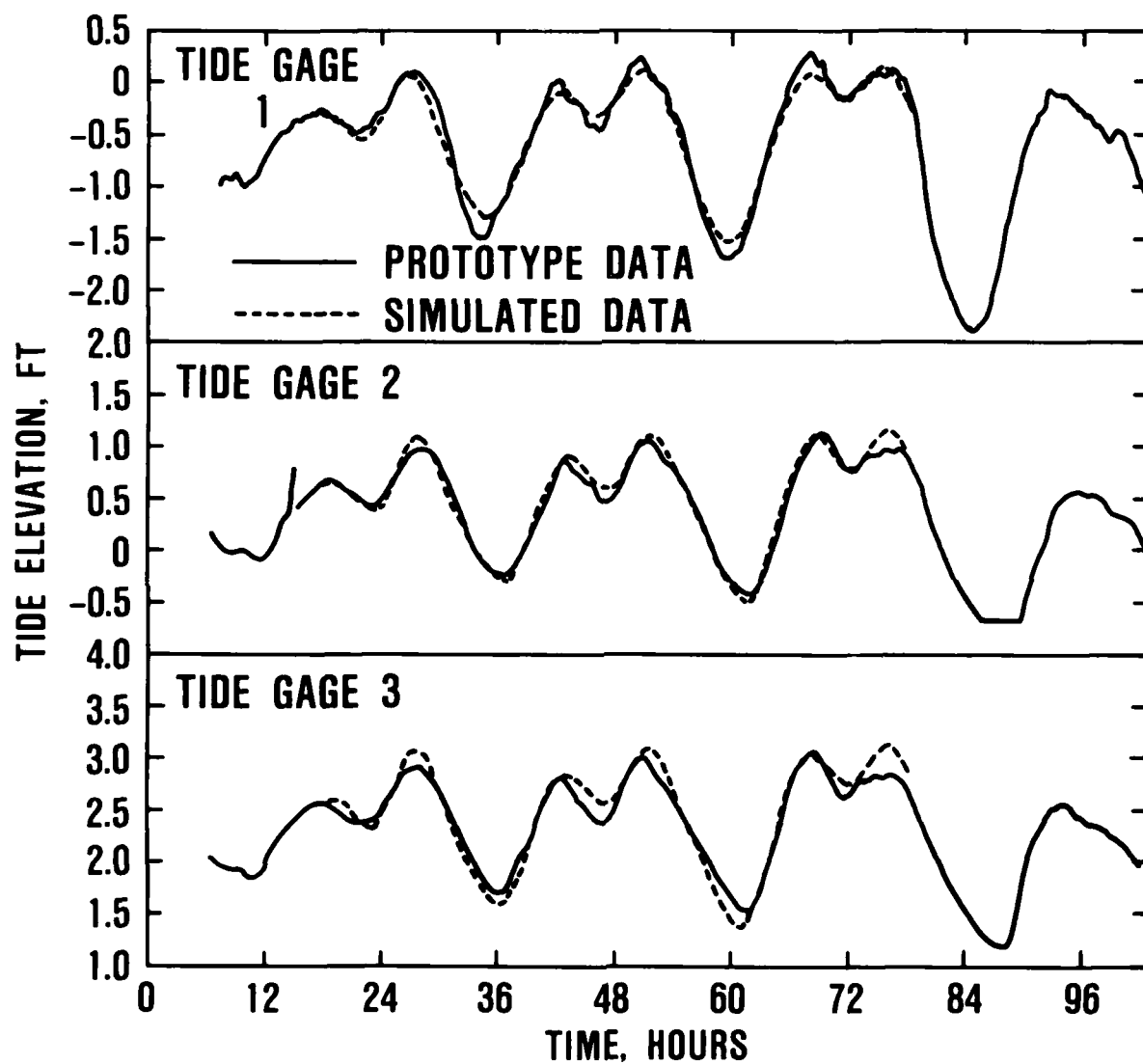


Figure 13. Observed and simulated tidal elevations (gages 1-3)

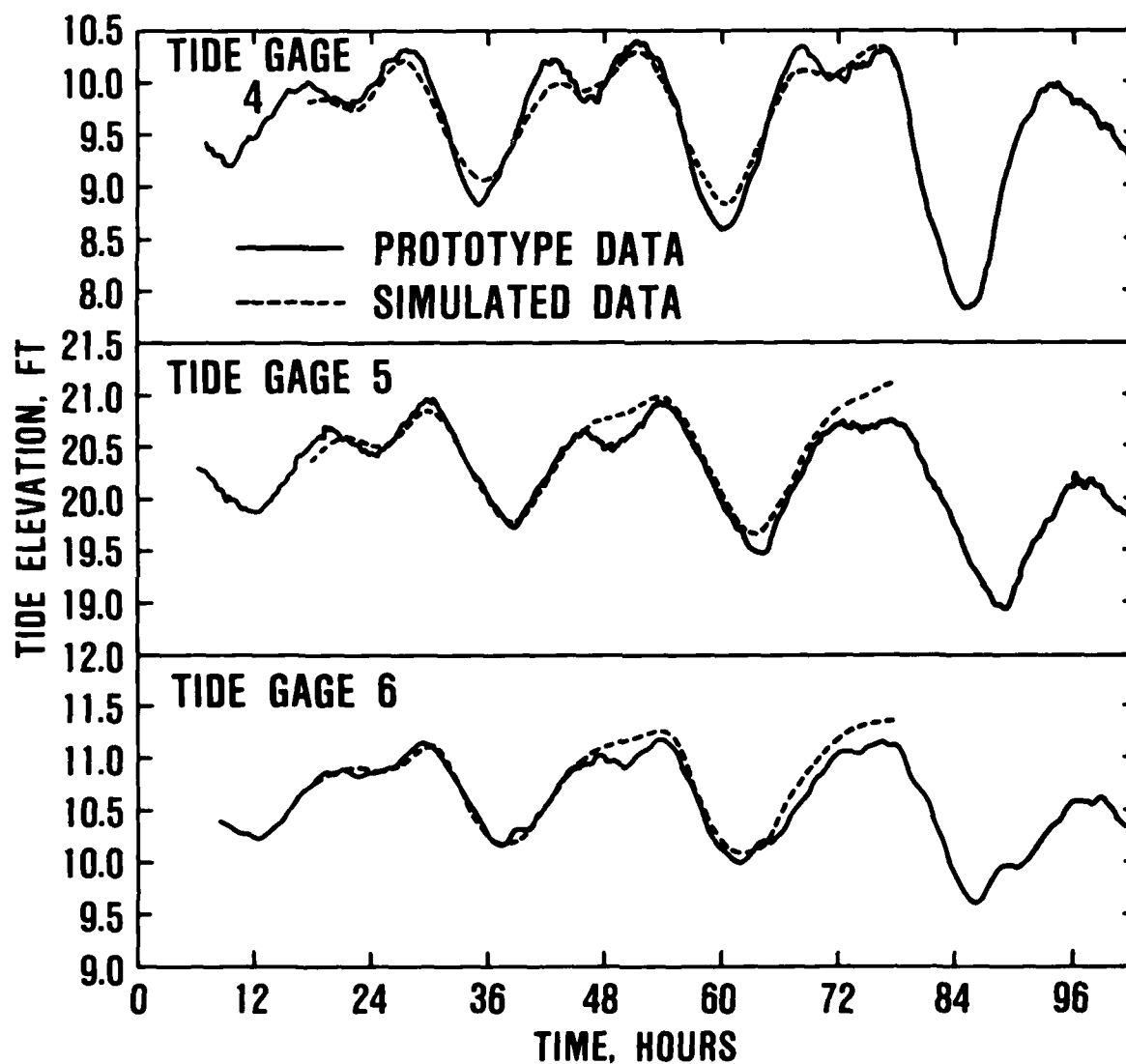


Figure 14. Observed and simulated tidal elevations (gages 4-6)

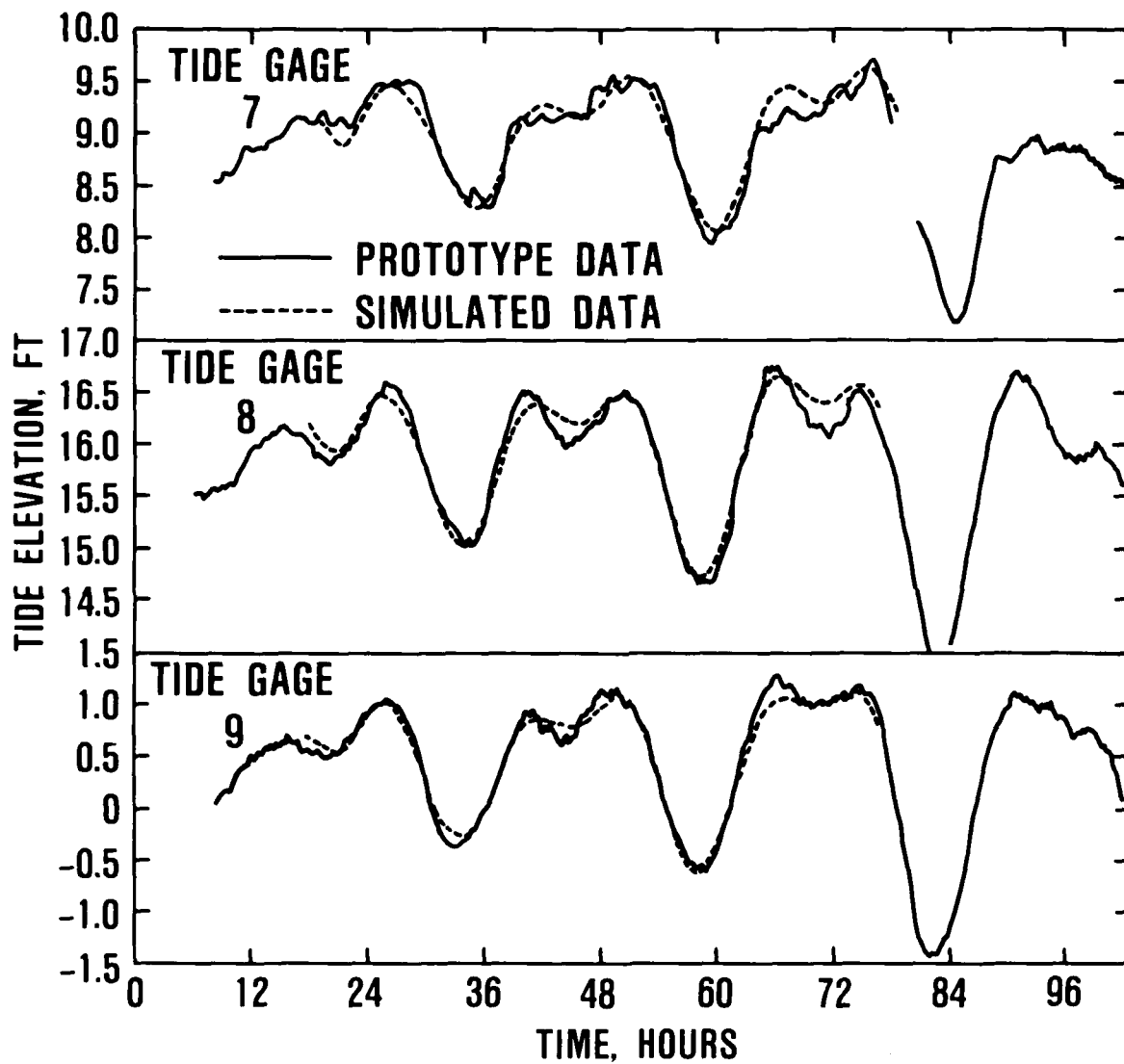


Figure 15. Observed and simulated tidal elevations (gages 7-9)

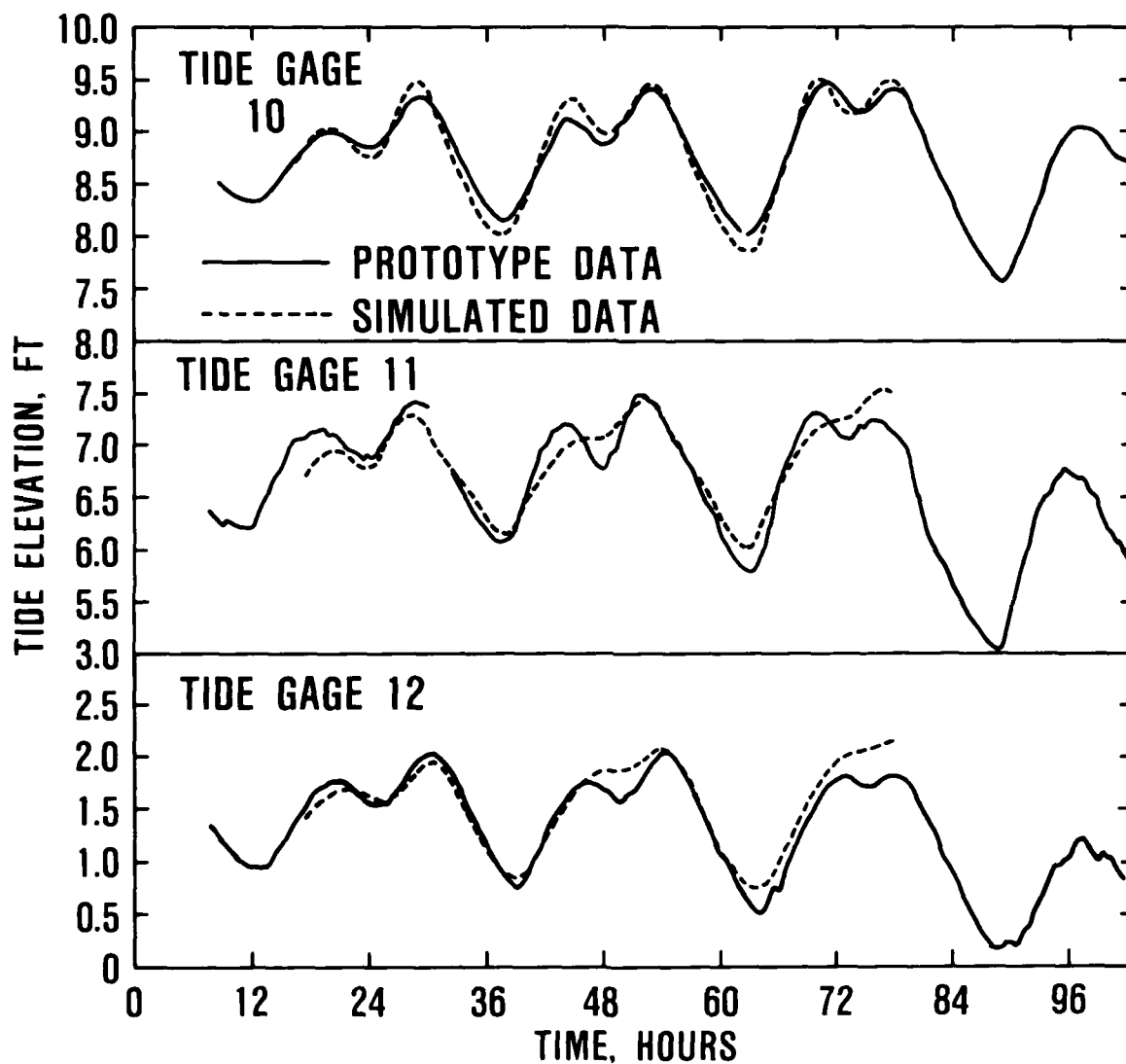


Figure 16. Observed and simulated tidal elevations (gages 10-12)

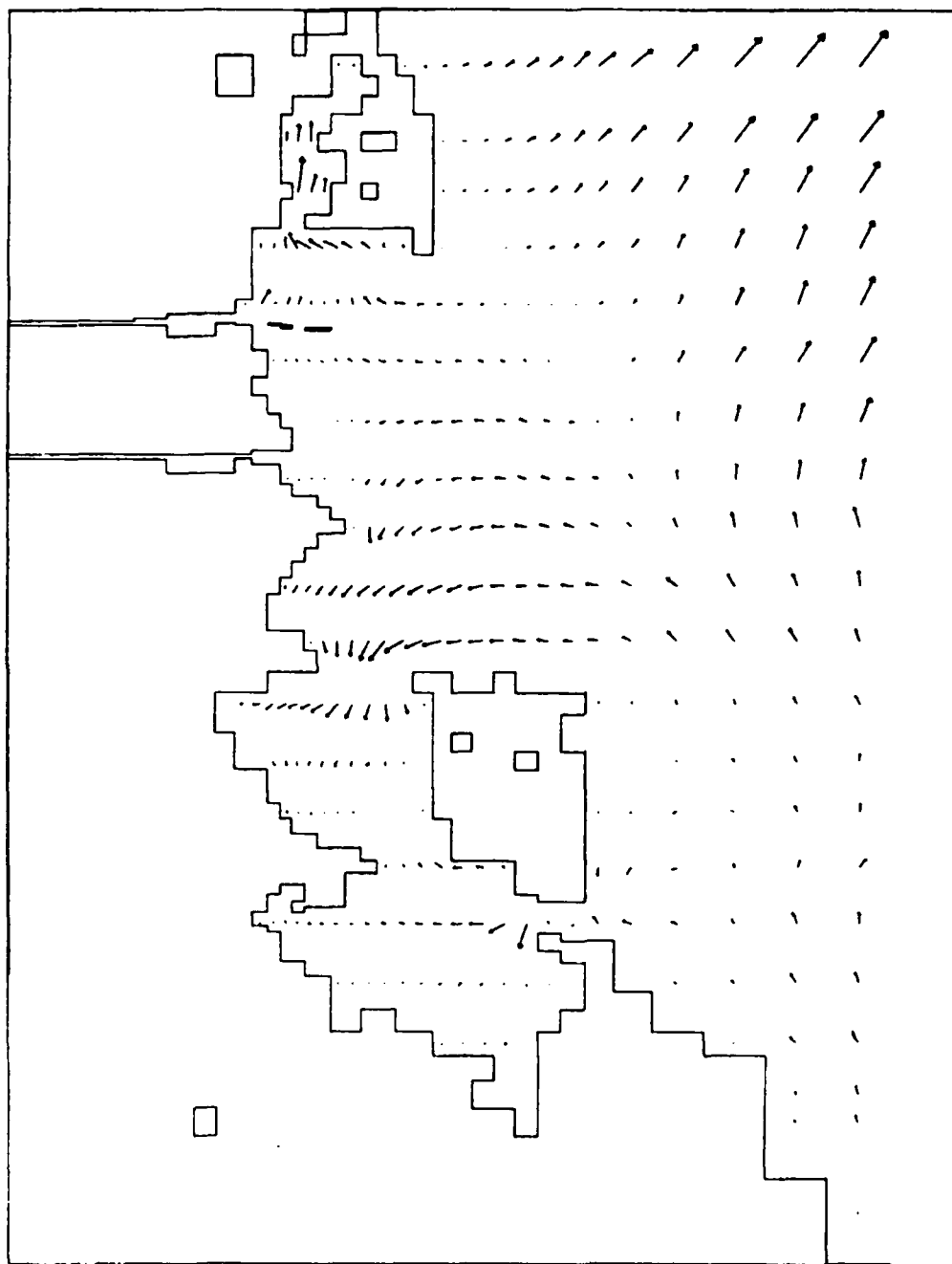


Figure 17. Simulated tidal flow field at hour 51



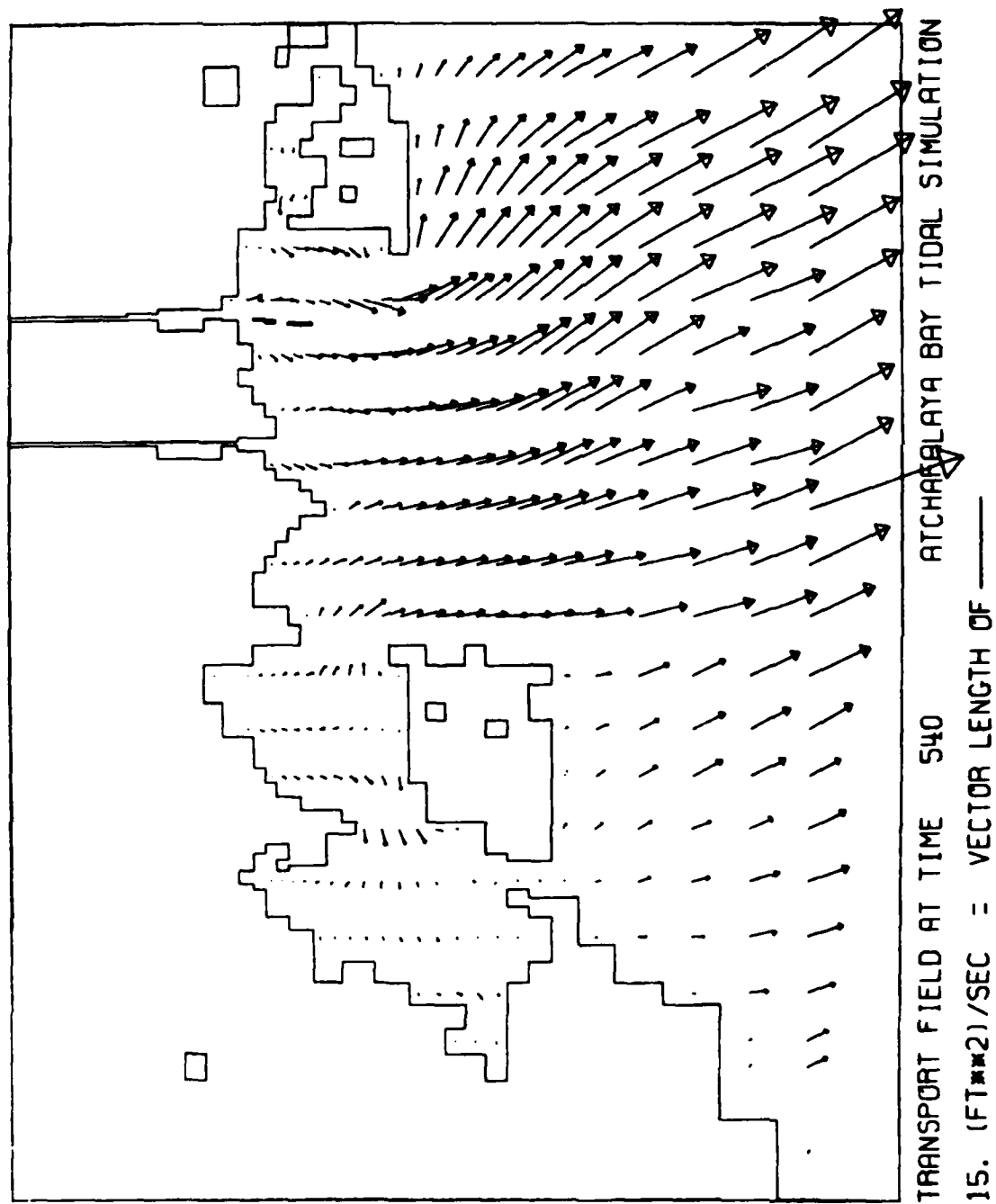
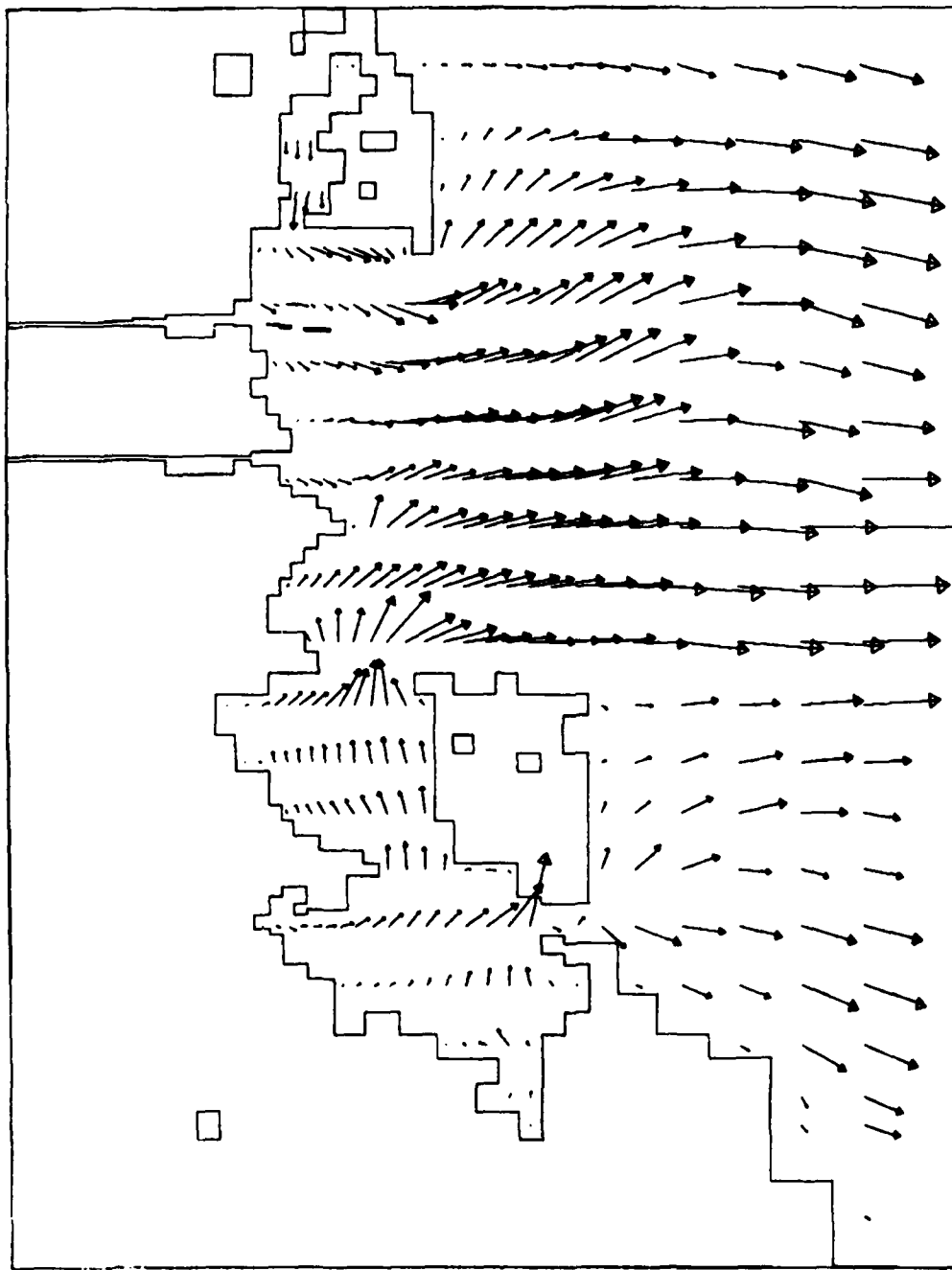


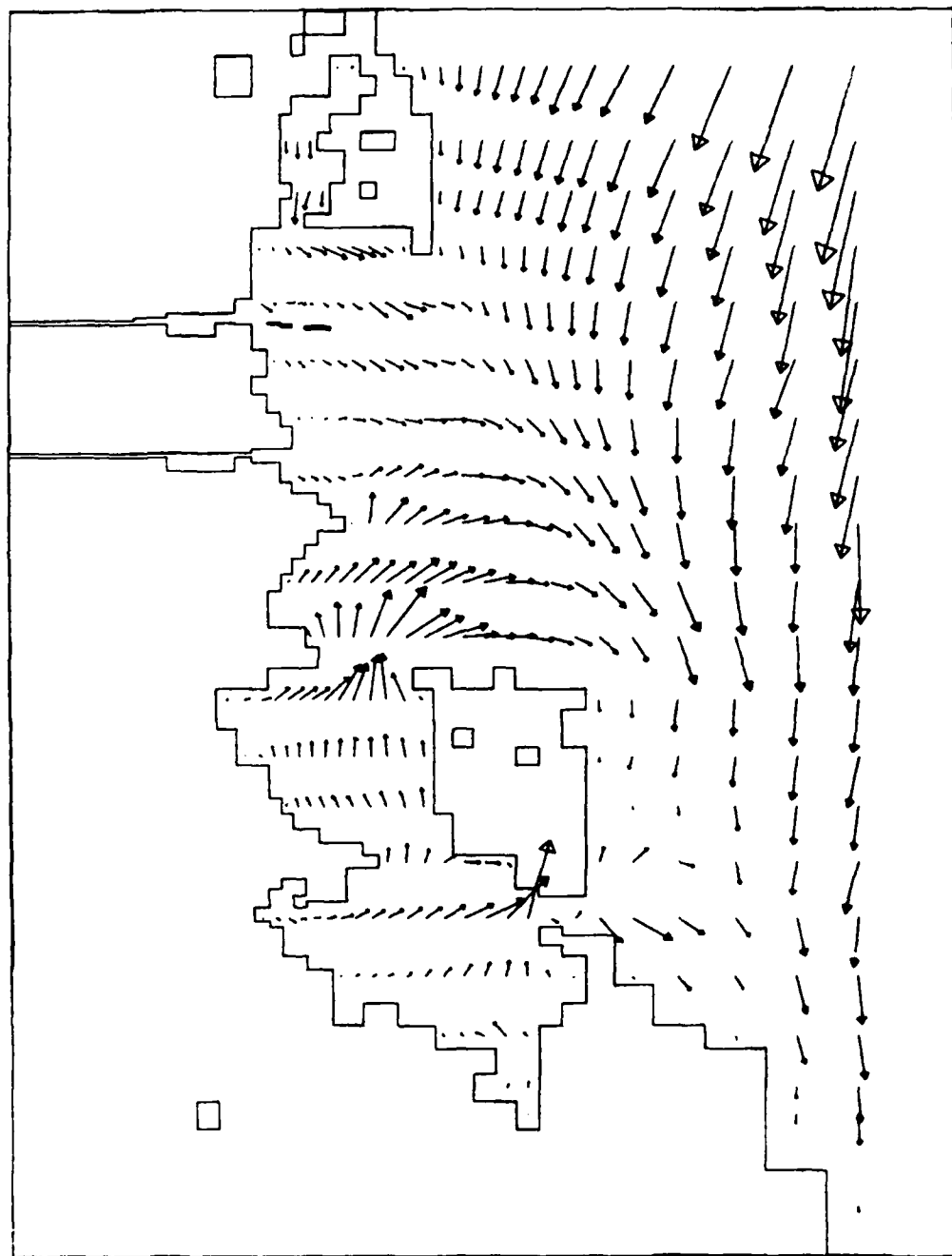
Figure 18. Simulated tidal flow field at hour 54



TRANSPORT FIELD AT TIME 570 ATCHAFALAYA BAY TIDAL SIMULATION

15. (FT\*\*2)/SEC = VECTOR LENGTH OF ▽

Figure 19. Simulated tidal flow field at hour 57



TRANSPORT FIELD AT TIME 600 ATCHAFALAYA BAY TIDAL SIMULATION

15.  $(F1^{**2})/SEC =$  VECTOR LENGTH OF —

Figure 20. Simulated tidal flow field at hour 60

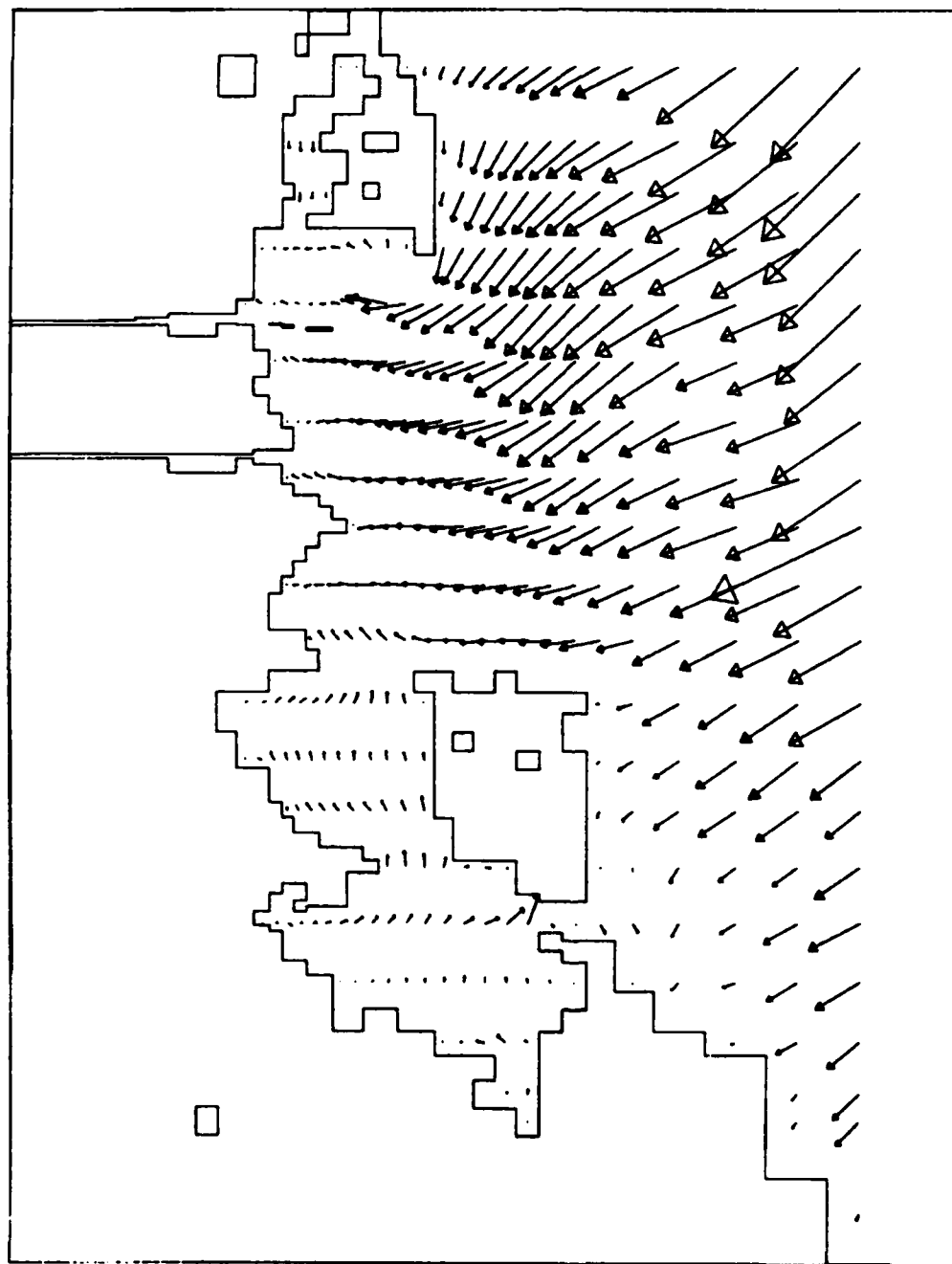


Figure 21. Simulated tidal flow field at hour 63

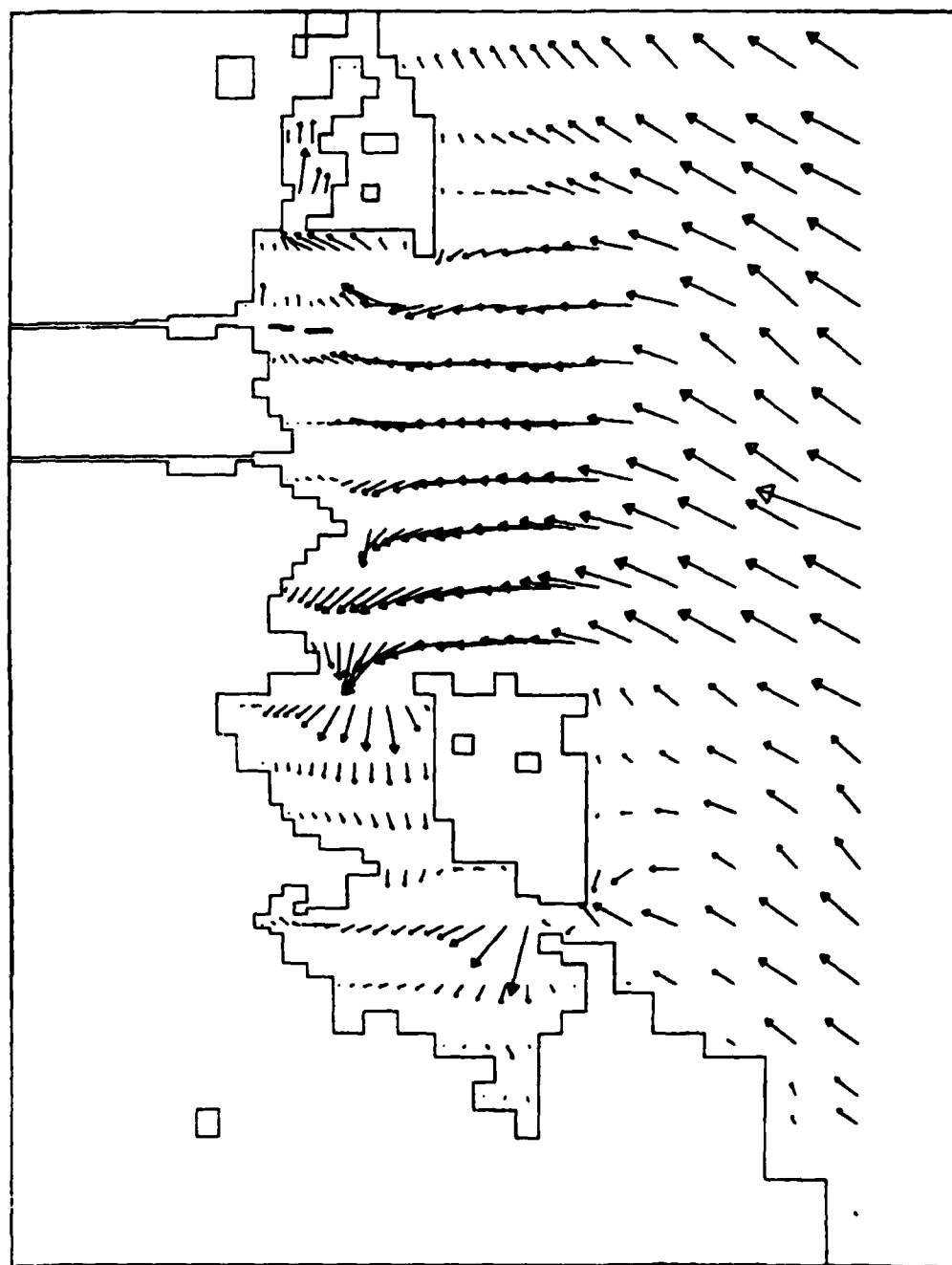


Figure 22. Simulated tidal flow field at hour 66

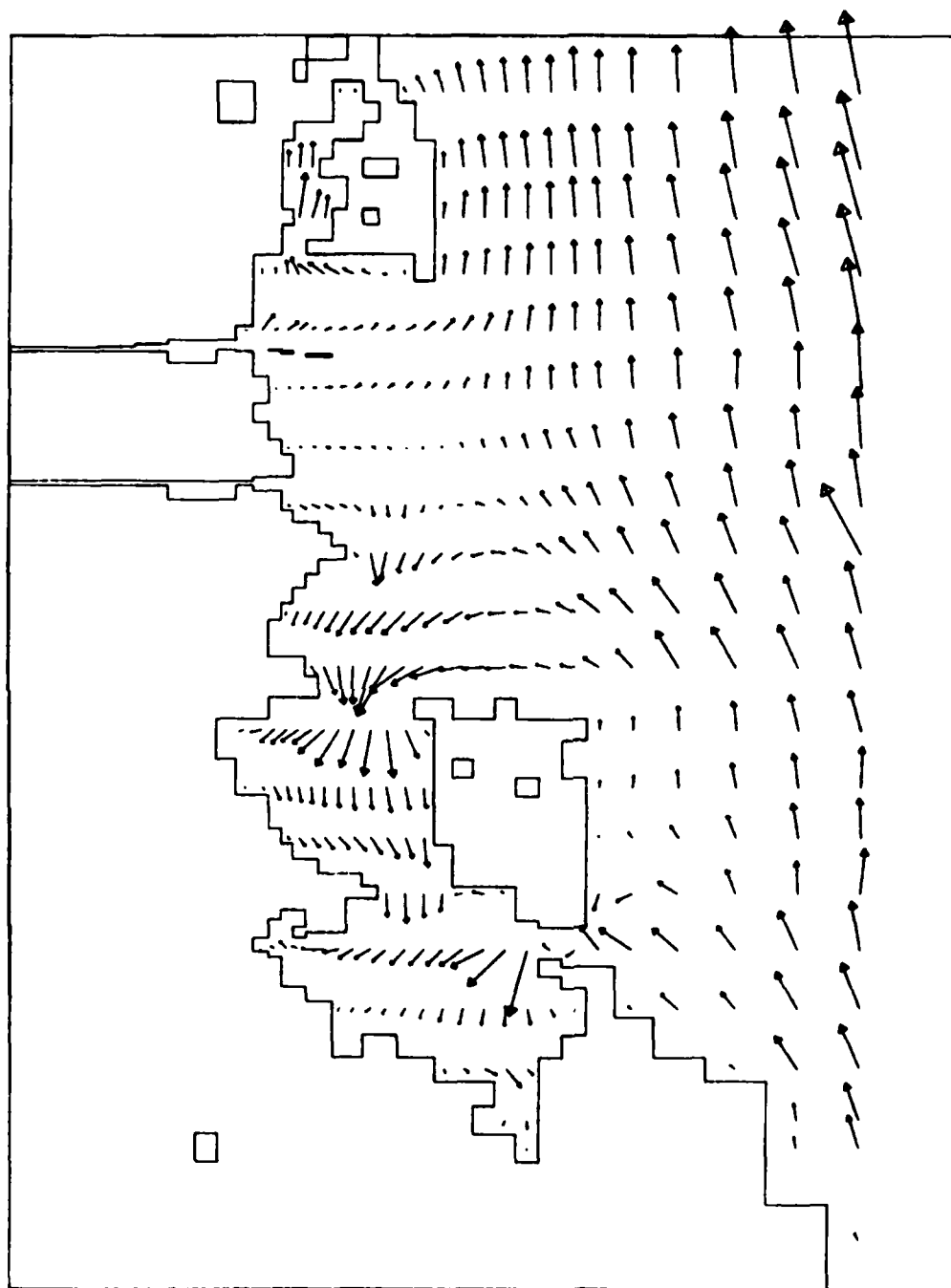
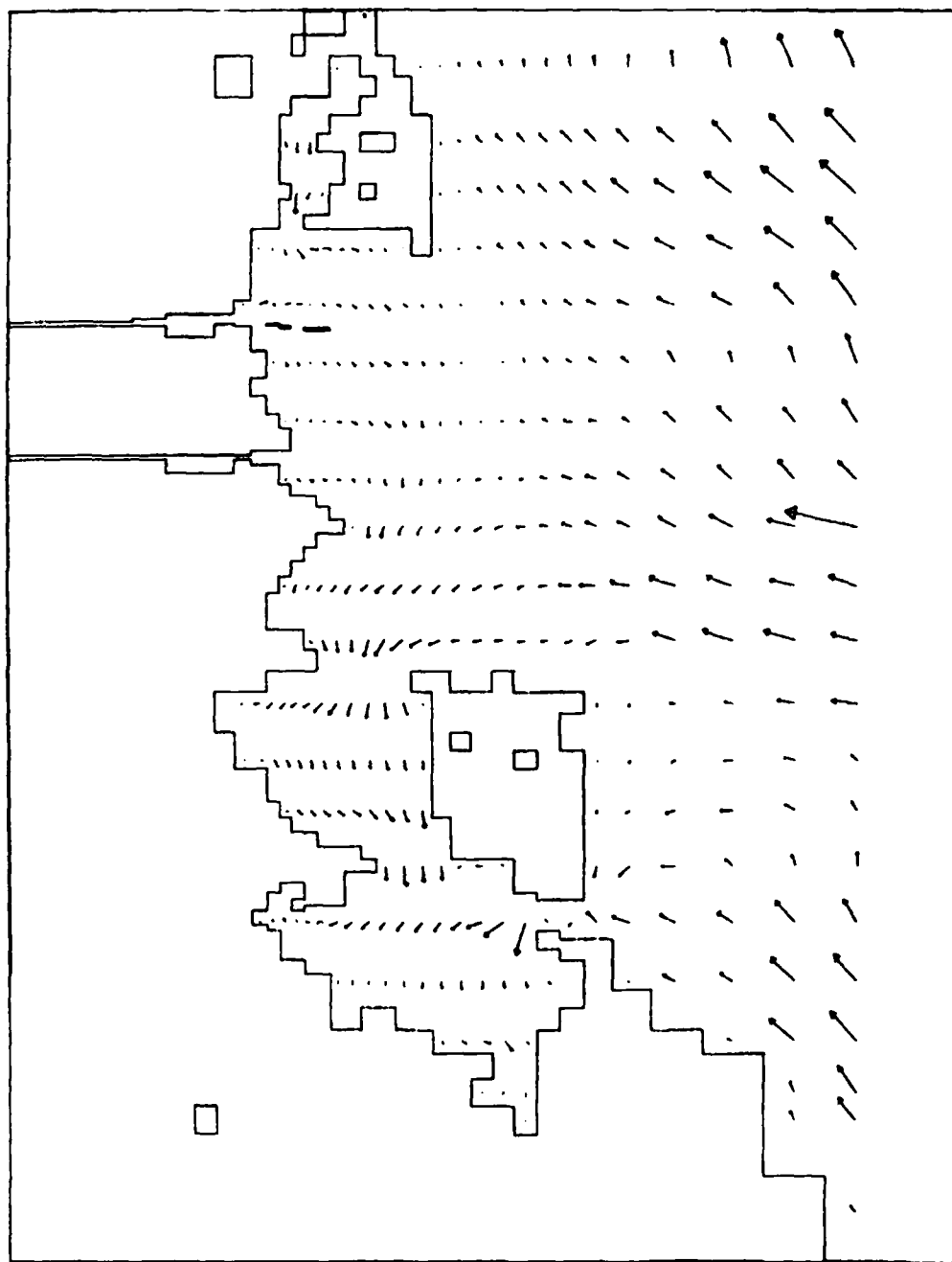


Figure 23. Simulated tidal flow field at hour 69



TRANSPORT FIELD AT TIME 720 ATCHAFALAYA BAY TIDAL SIMULATION

15. (FT\*\*2)/SEC = VECTOR LENGTH OF —

Figure 24. Simulated tidal flow field at hour 72

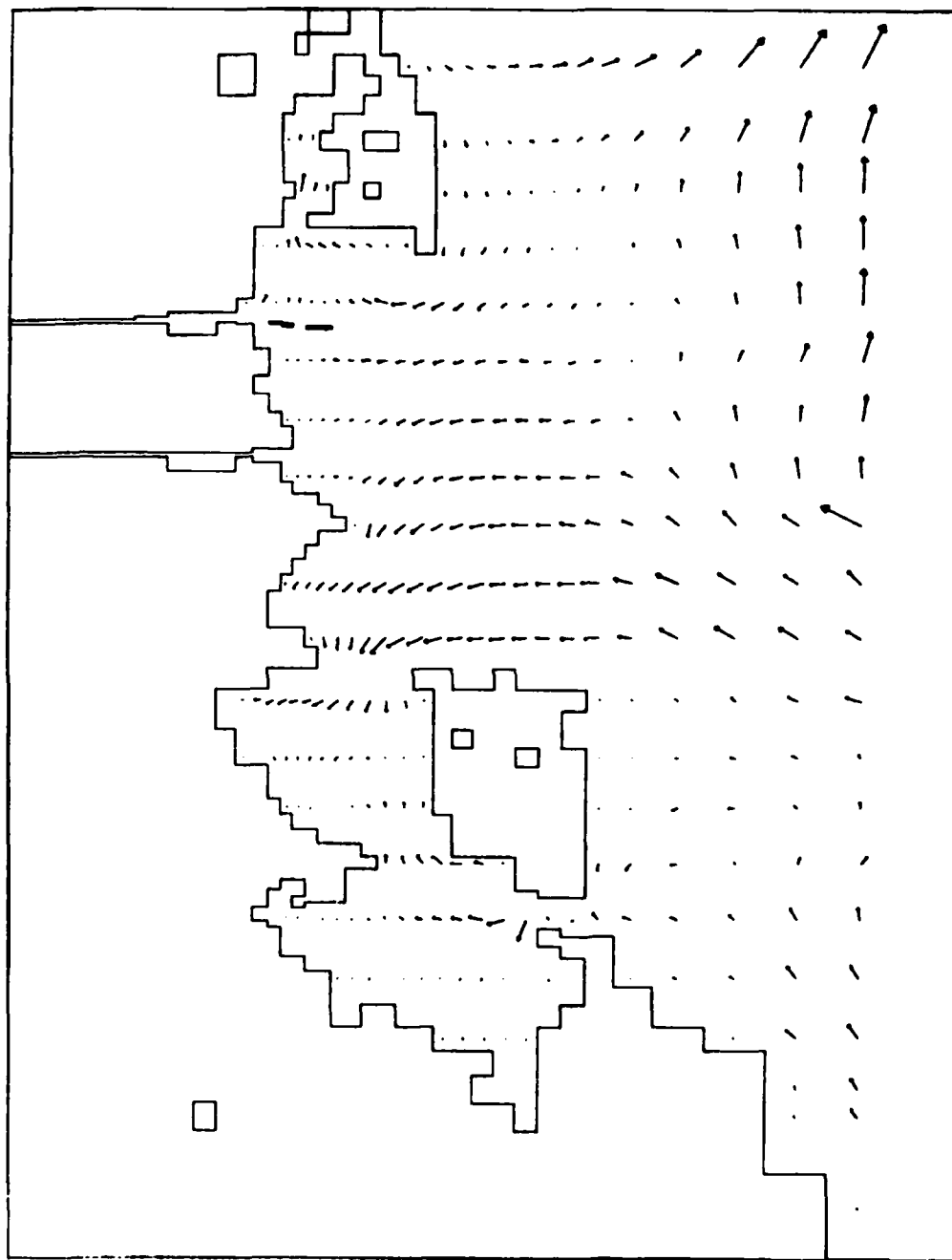


Figure 25. Simulated tidal flow field at hour 75



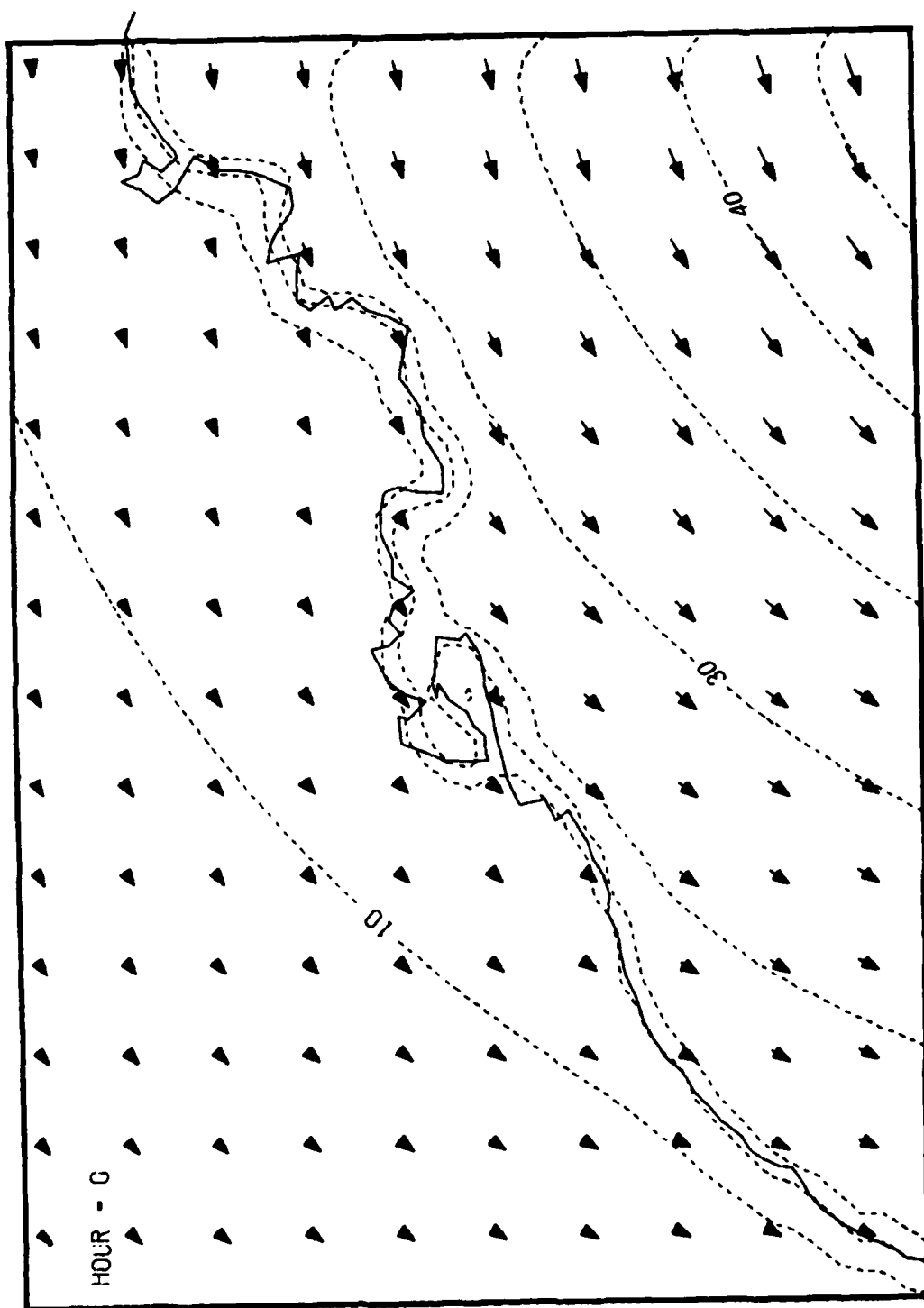


Figure 28. Simulated Hilda wind field at hour 0

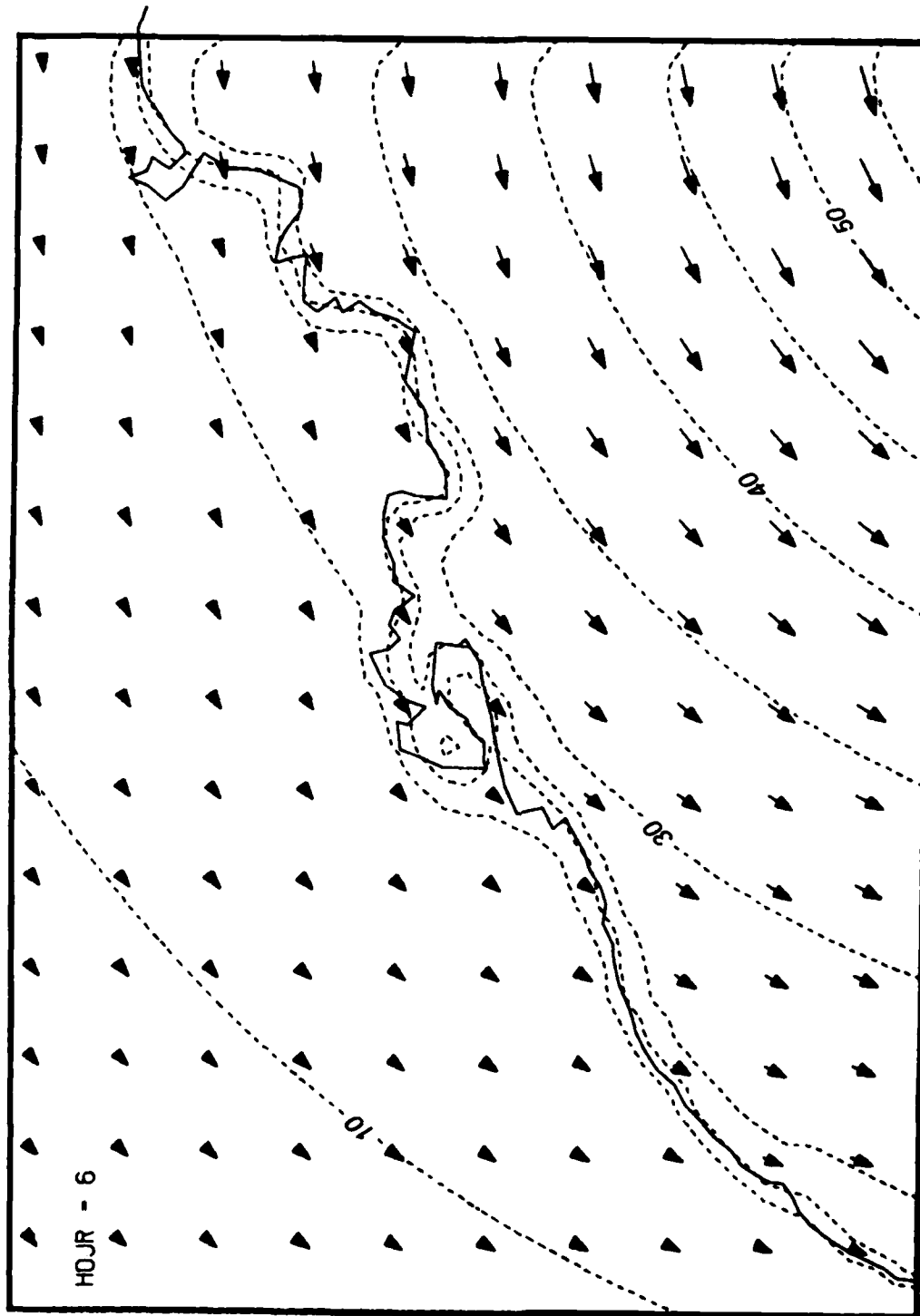


Figure 29. Simulated Hilda wind field at hour 6

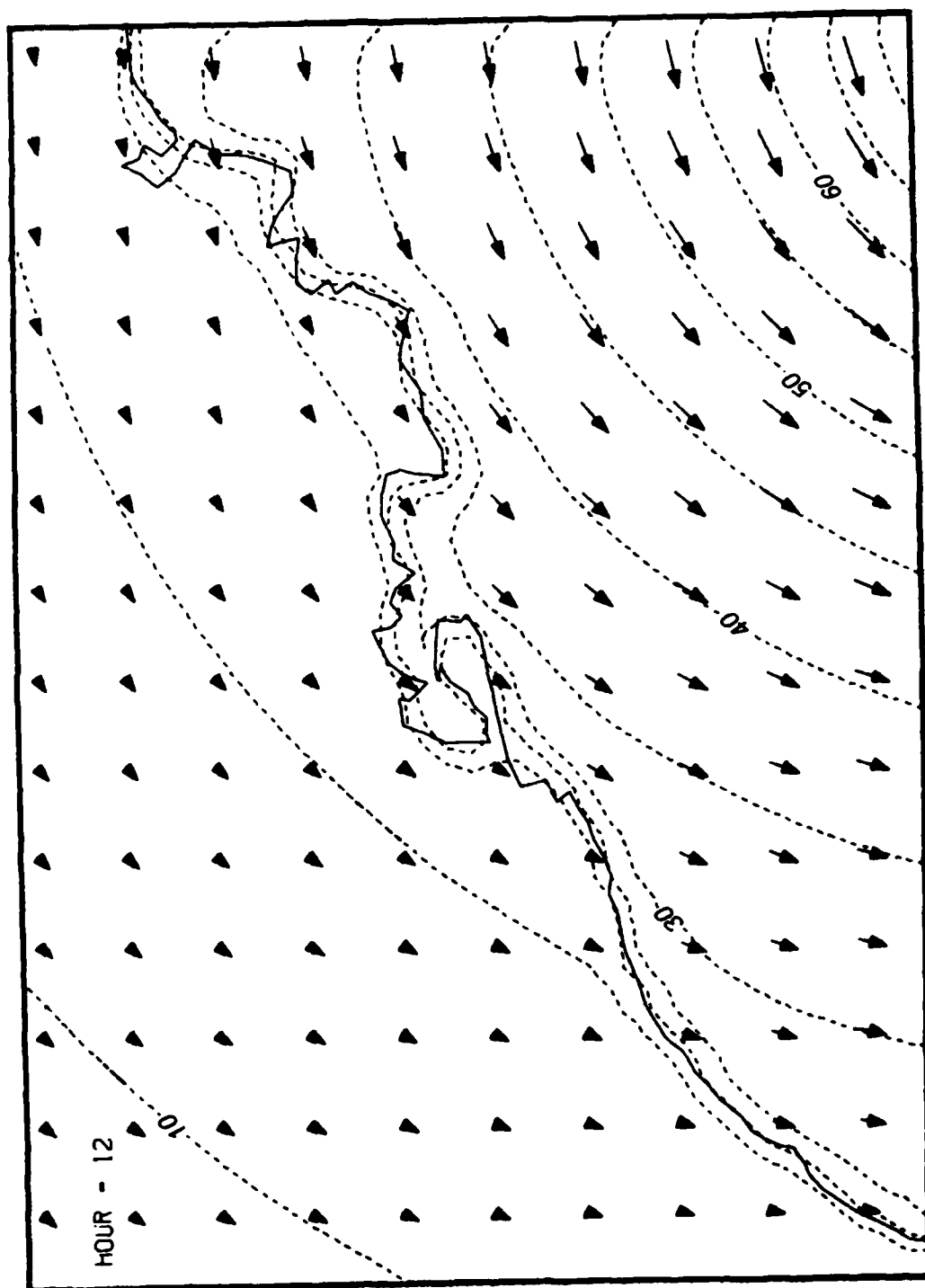


Figure 30. Simulated Hilda wind field at hour 12

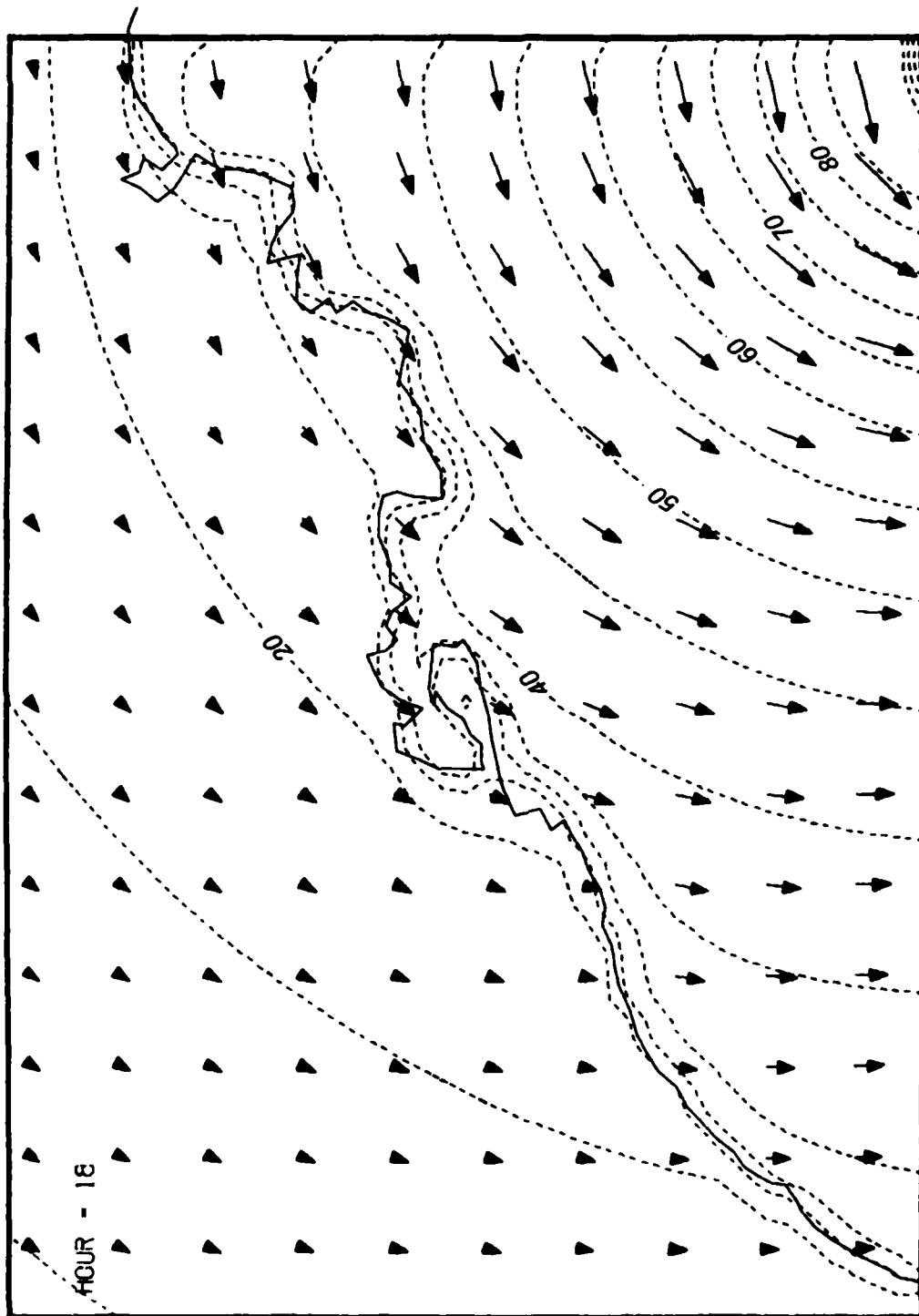


Figure 31. Simulated Hilda wind field at hour 18

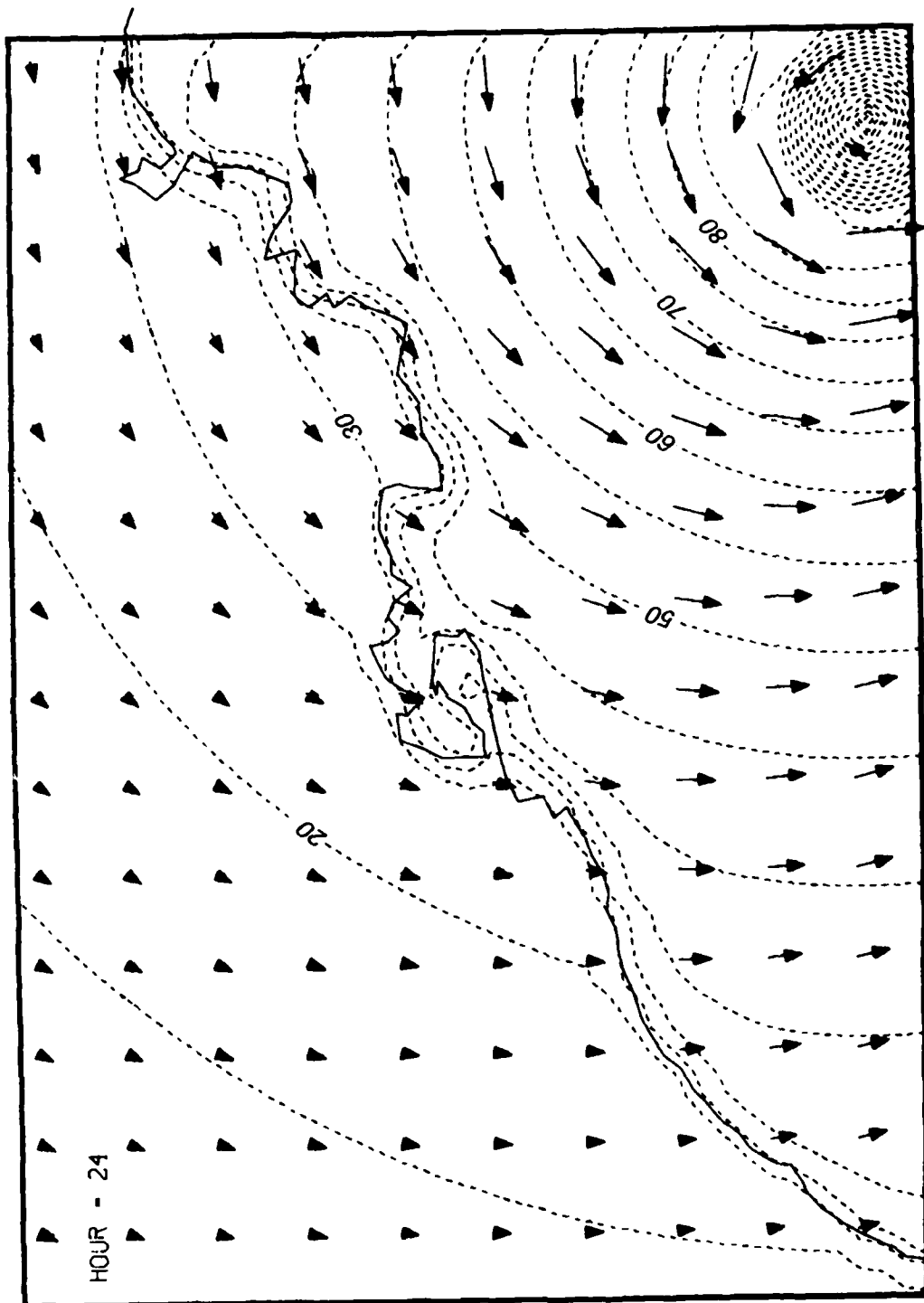


Figure 32. Simulated Hilda wind field at hour 24

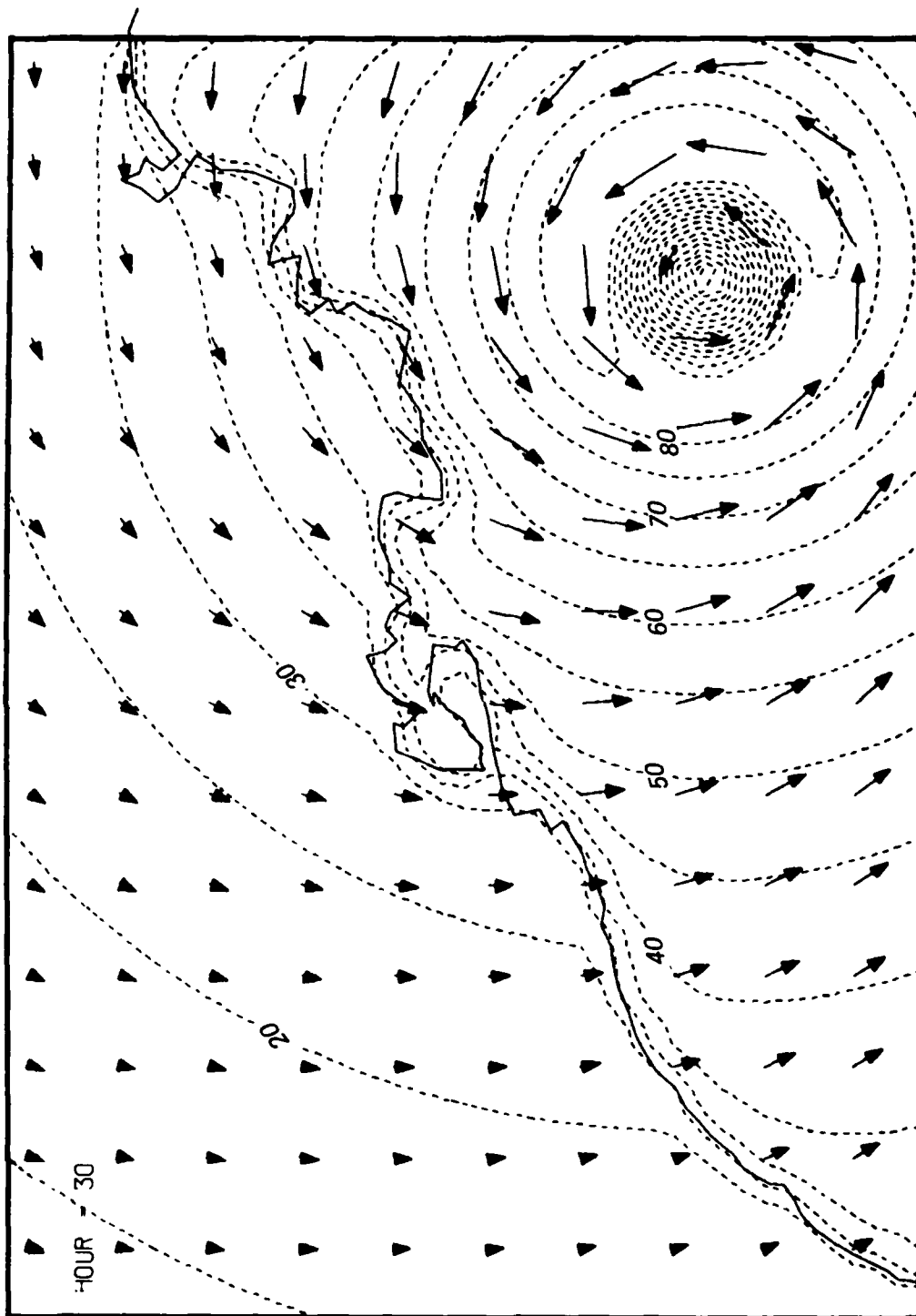


Figure 33. Simulated Hilda wind field at hour 30

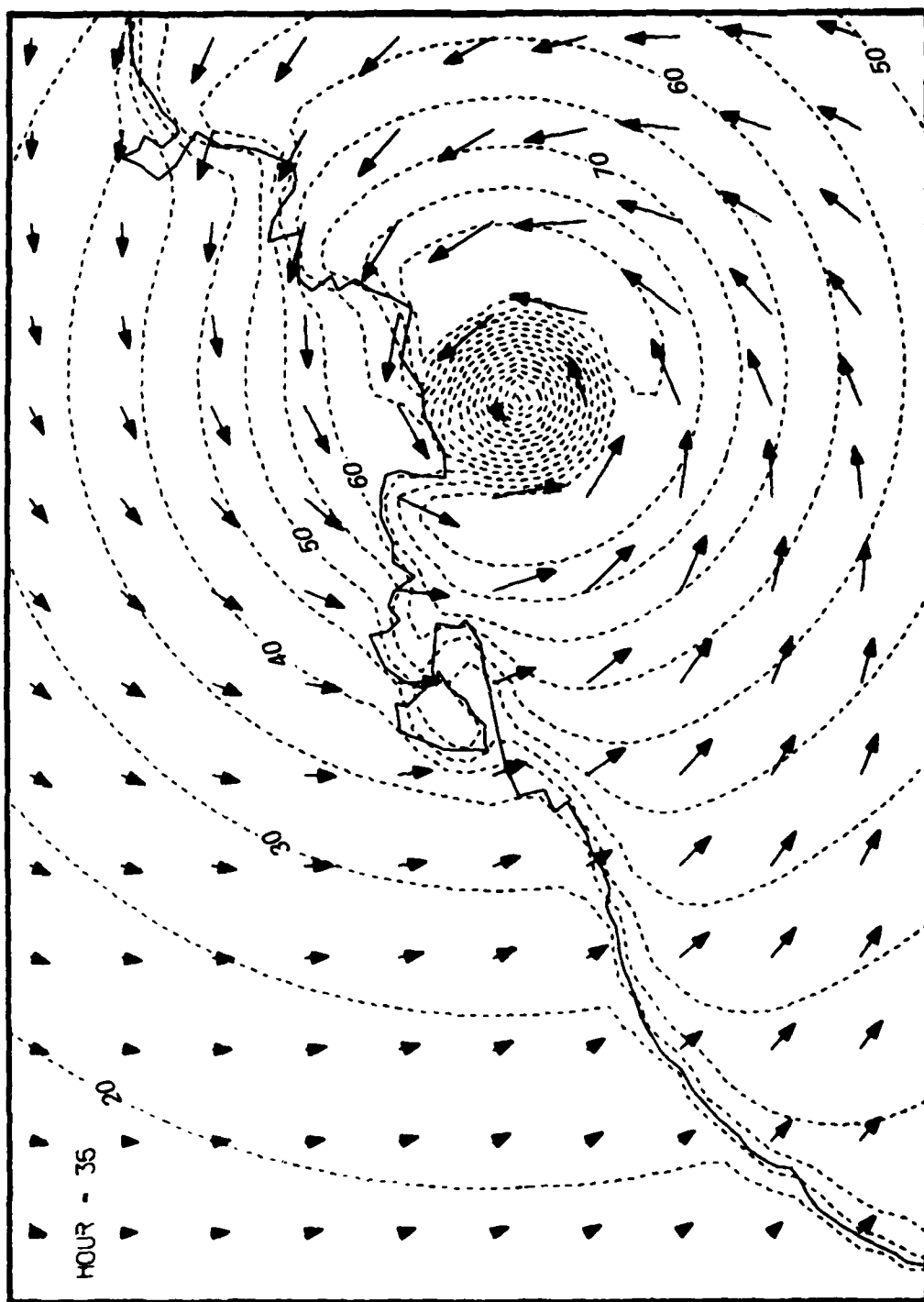


Figure 34. Simulated Hilda wind field at hour 36

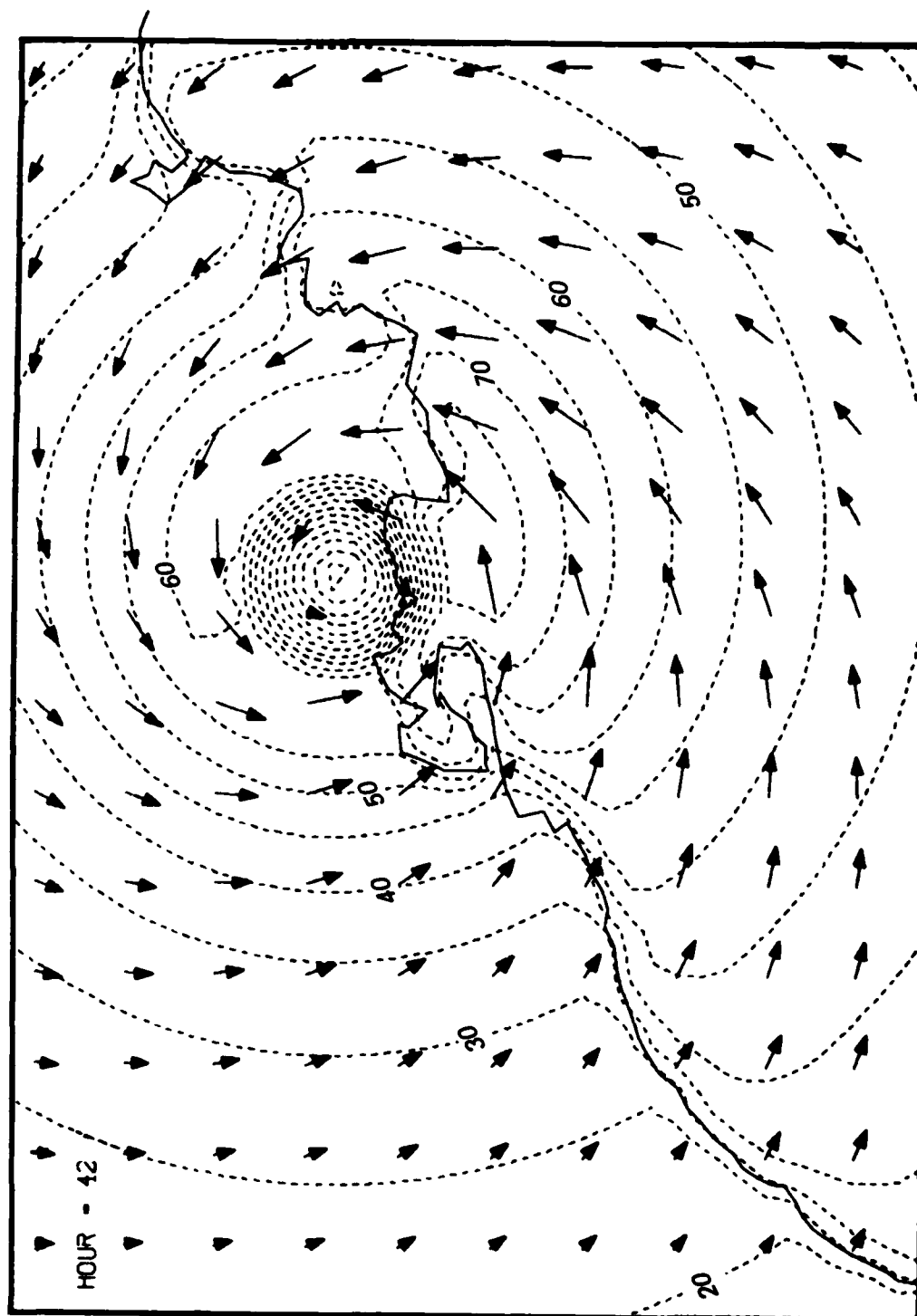


Figure 35. Simulated Hilda wind field at hour 42



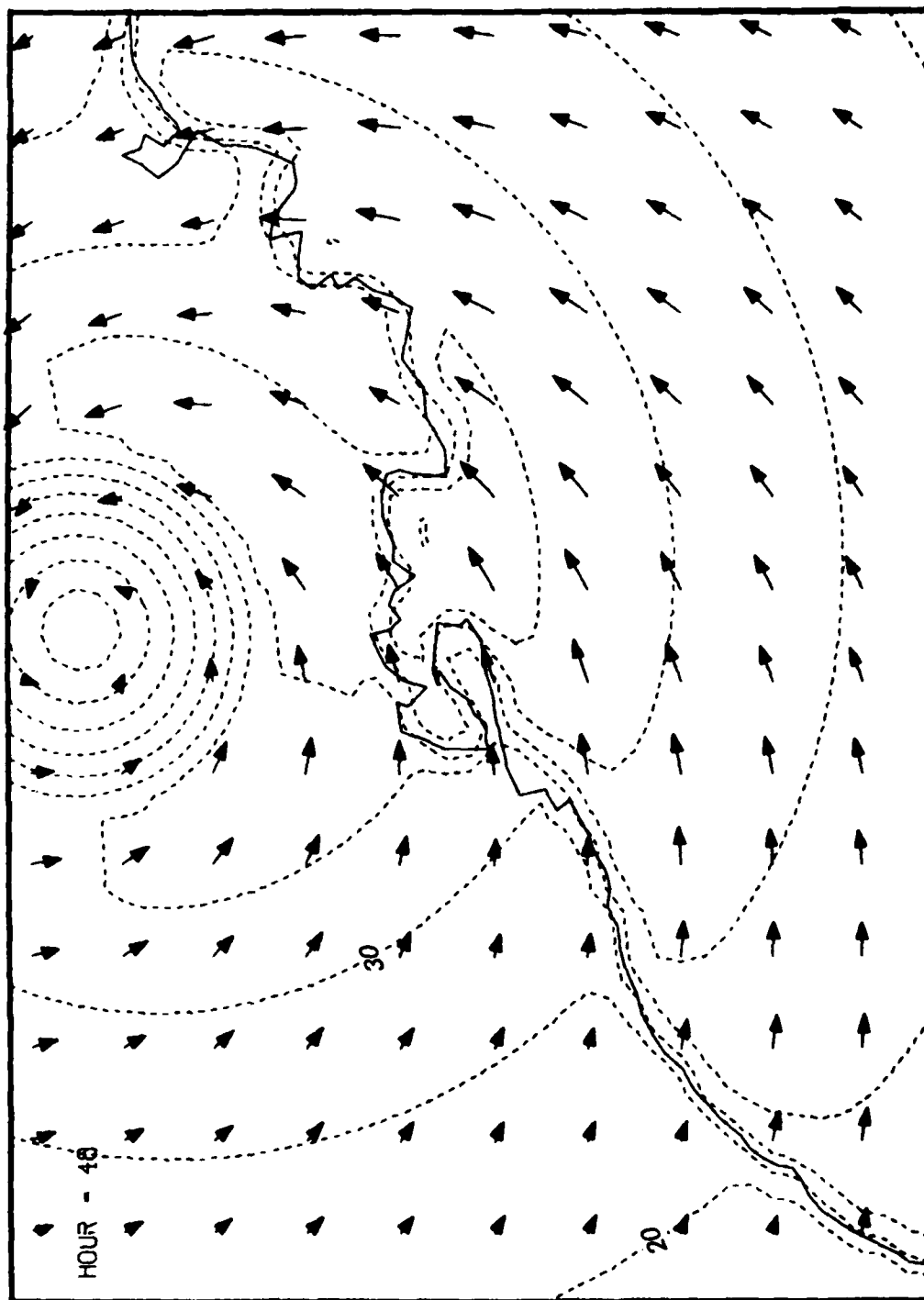


Figure 36. Simulated Hilda wind field at hour 48

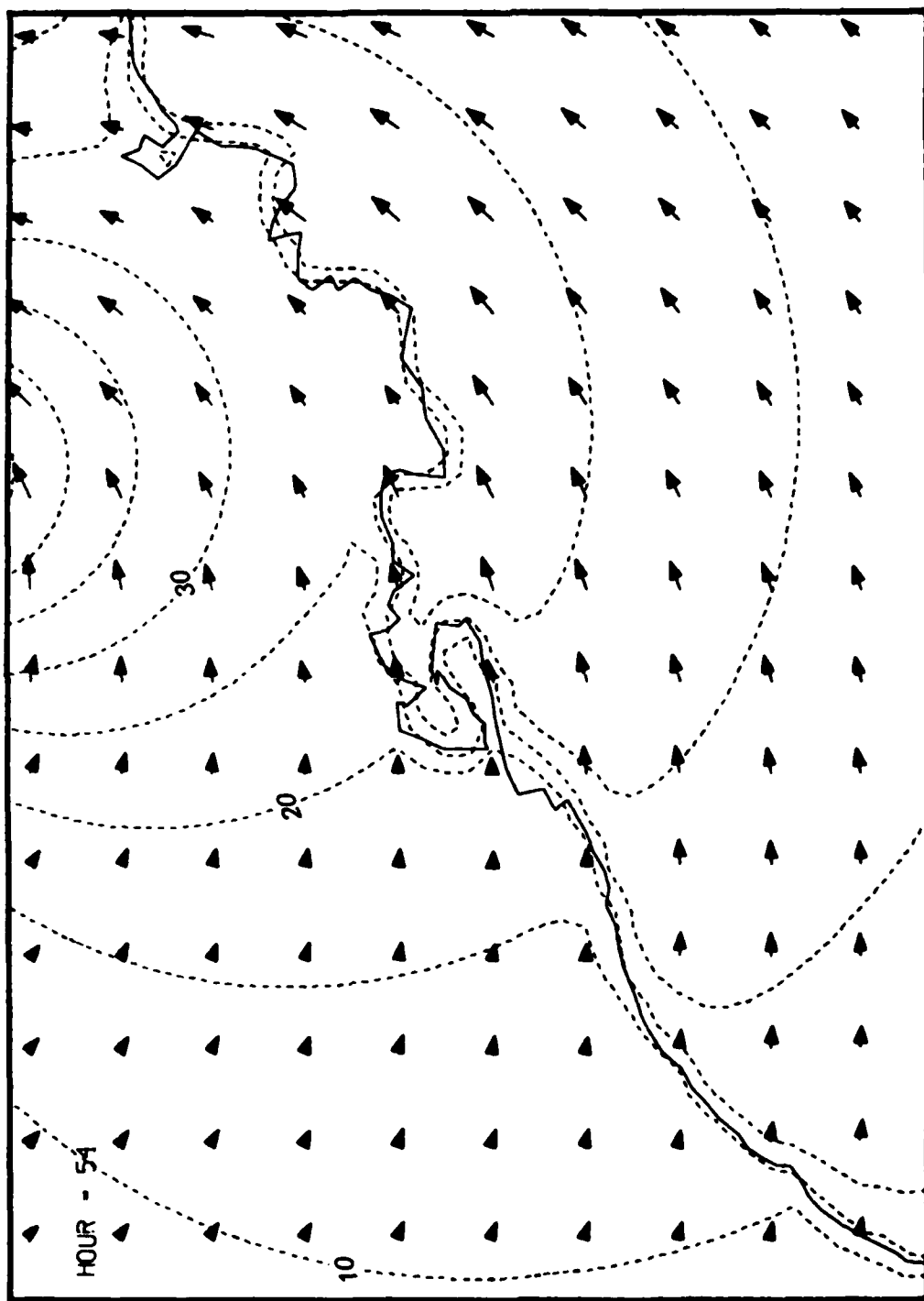


Figure 37. Simulated Hilda wind field at hour 54

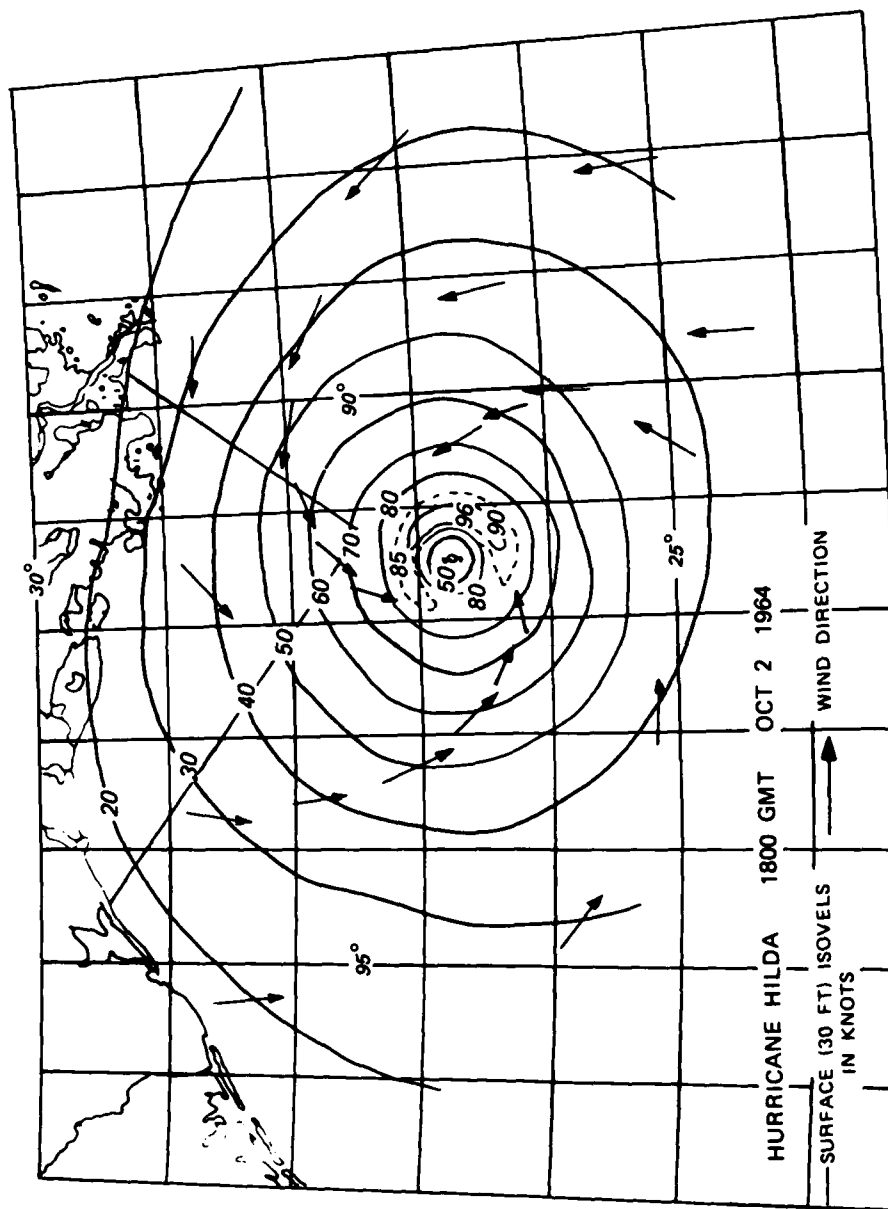


Figure 38. Observed Hilda wind field at hour 12

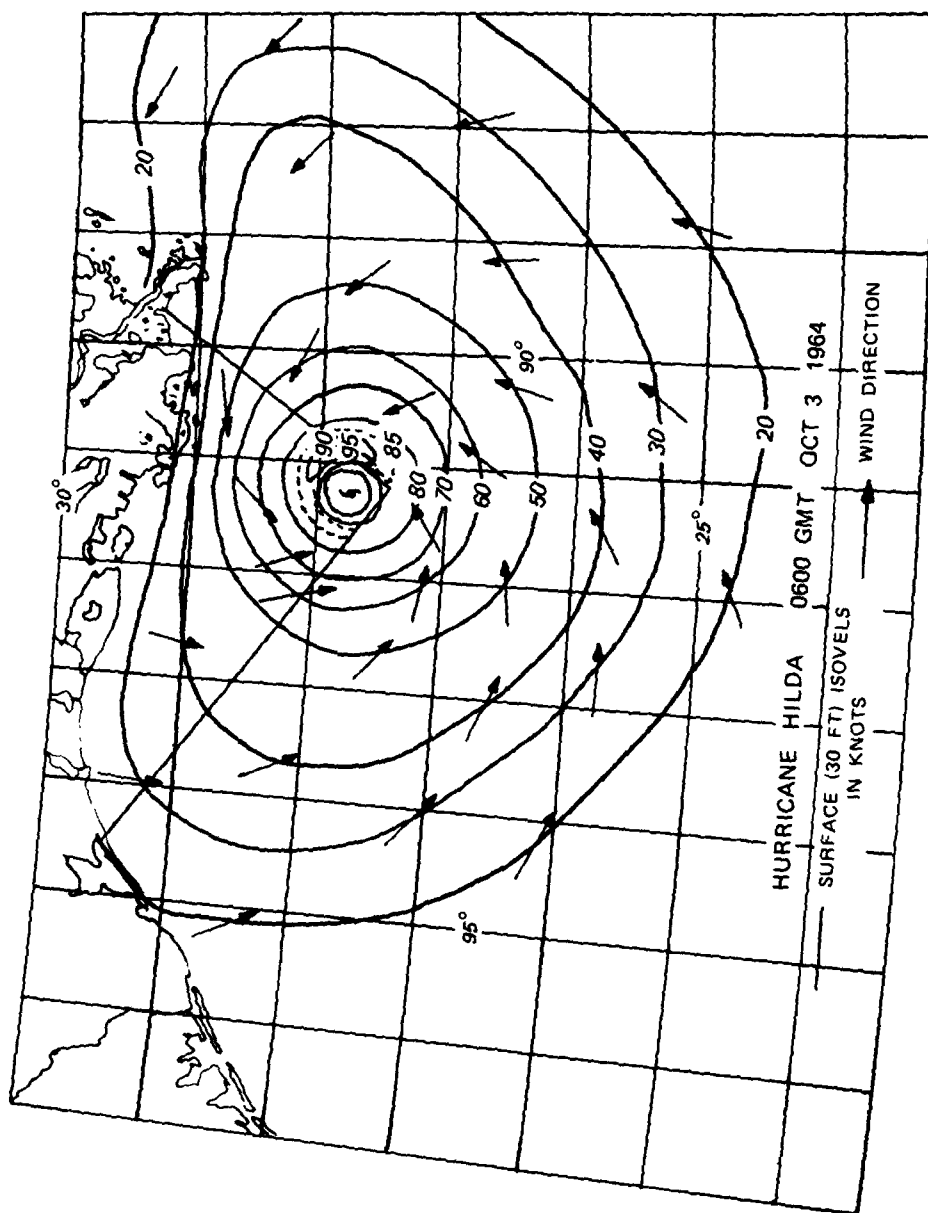


Figure 39. Observed Hilda wind field at hour 24

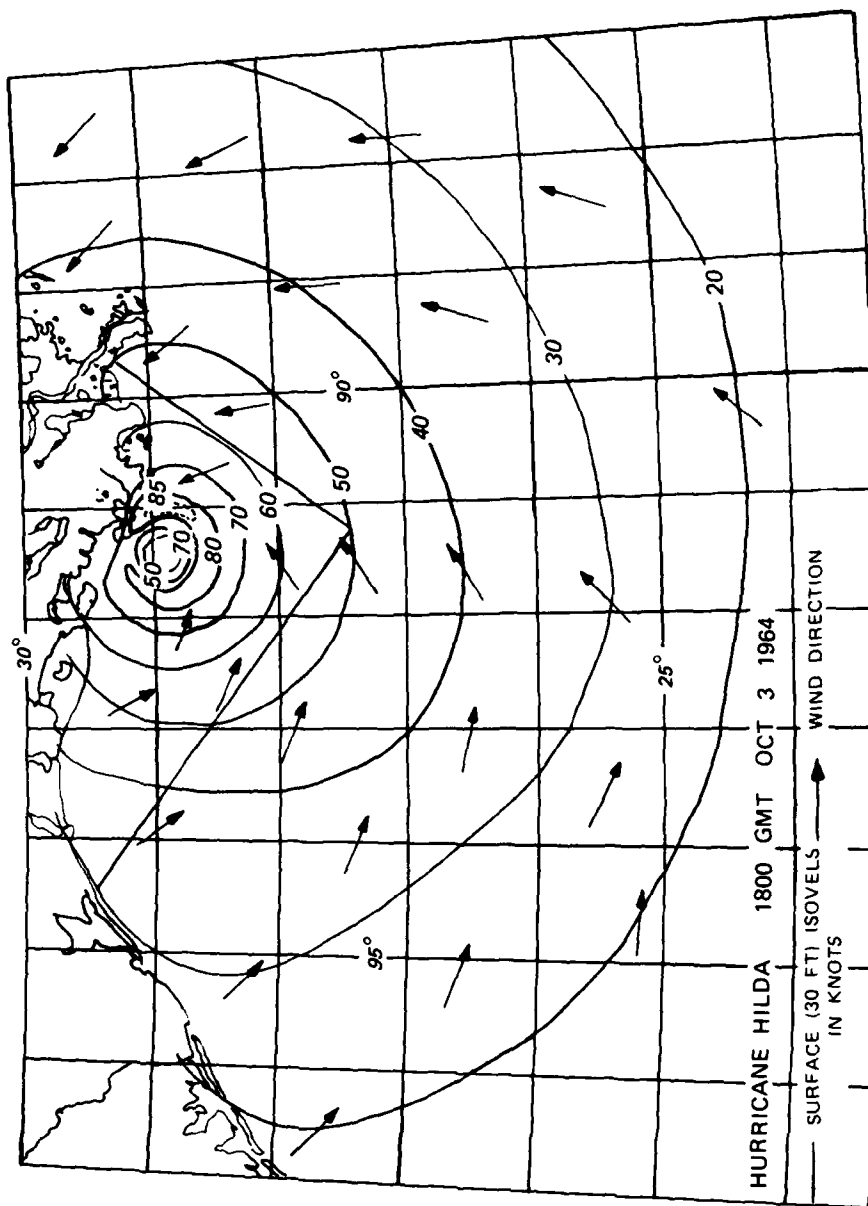


Figure 40. Observed Hilda wind field at hour 36

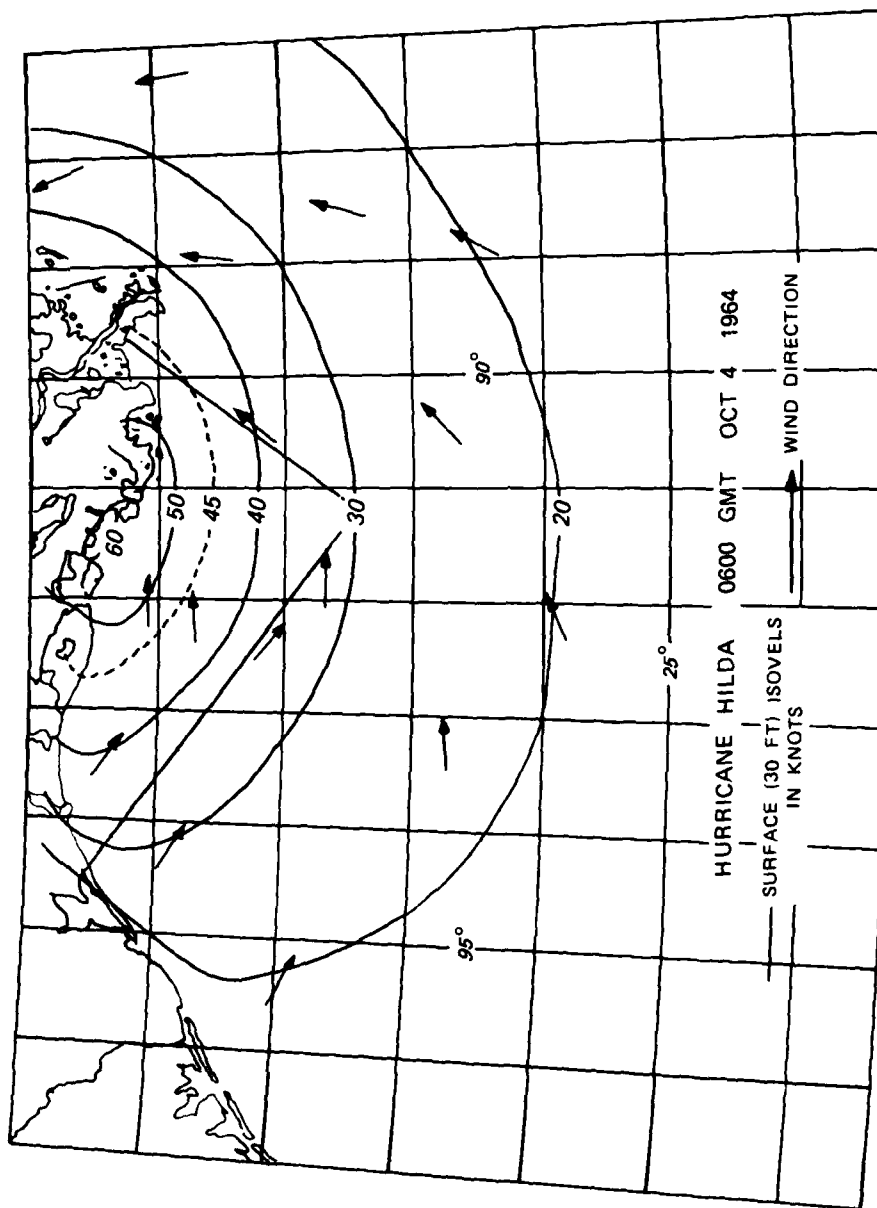
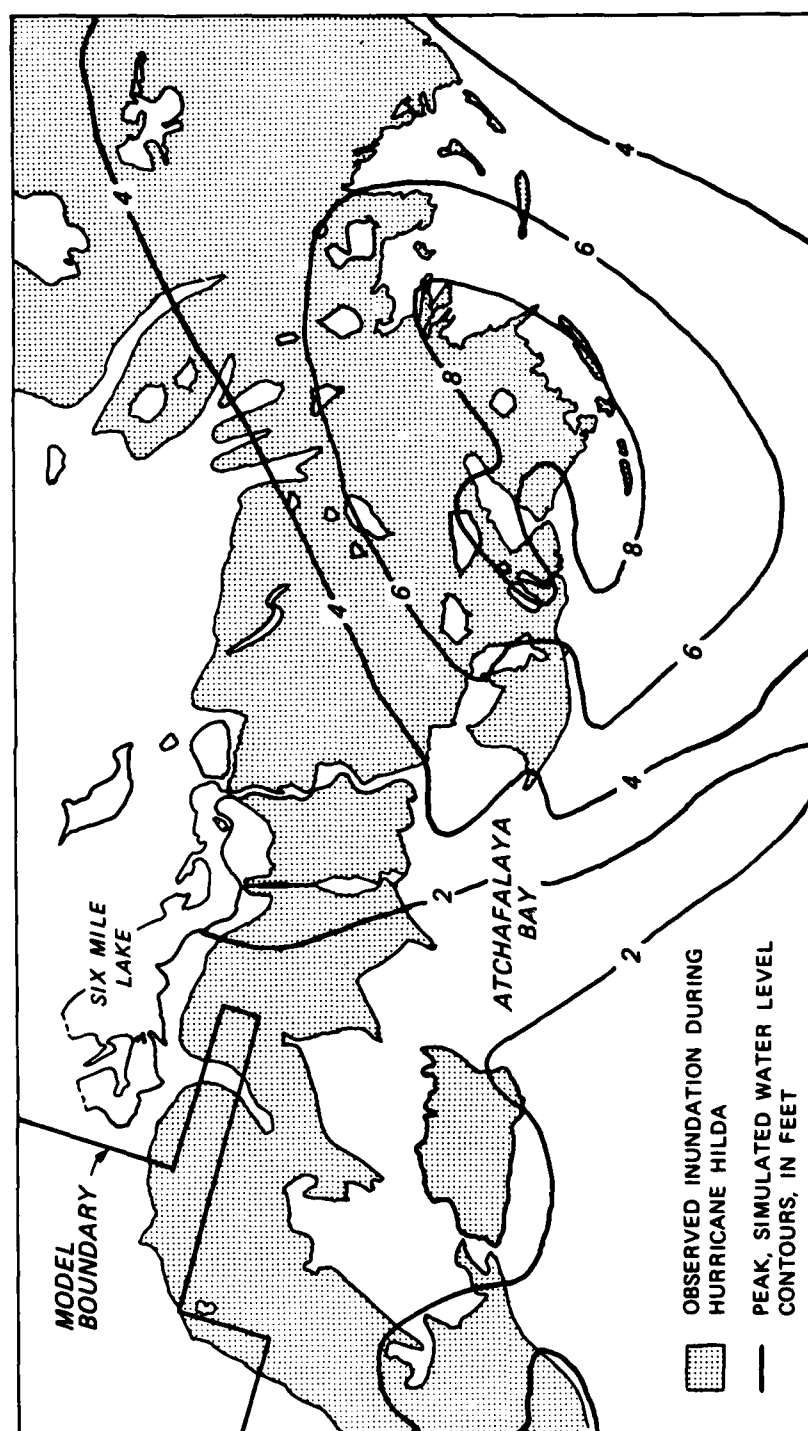


Figure 41. Observed Hilda wind field at hour 48



**Figure 42. Observed inundation and simulated high-water elevations for Hurricane Hilda**

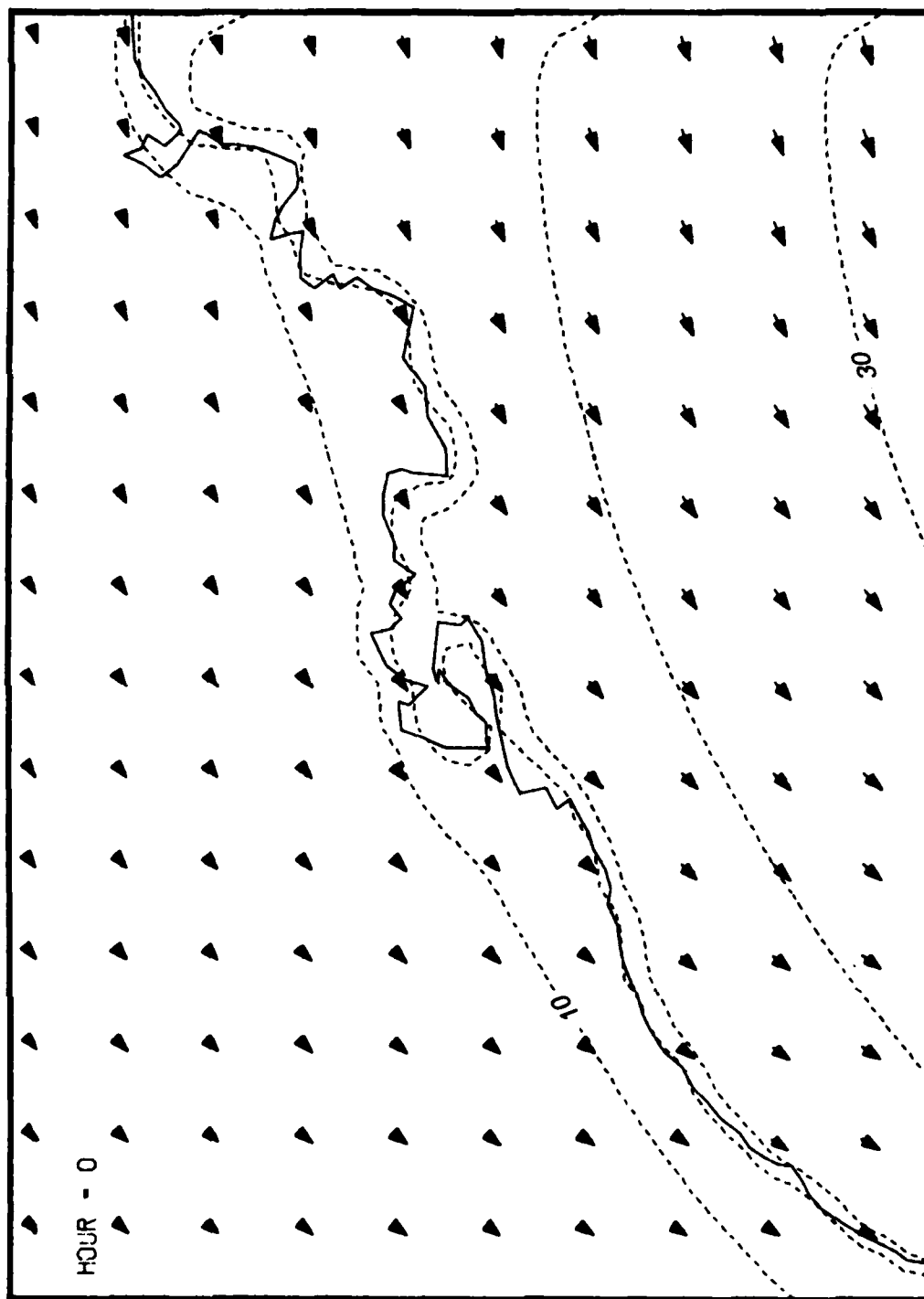


Figure 43. Simulated Audrey wind field at hour 0



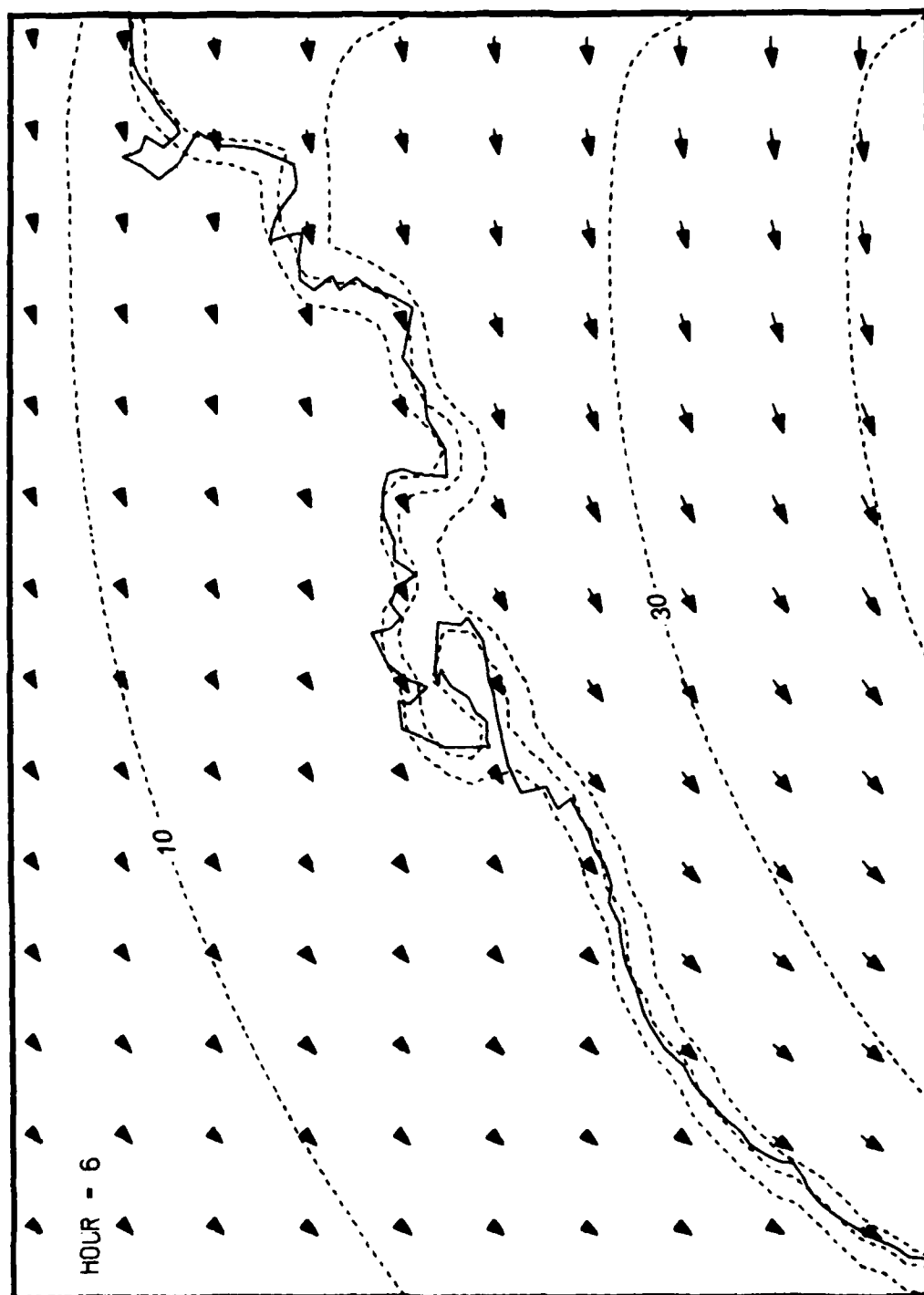


Figure 44. Simulated Audrey wind field at hour 6

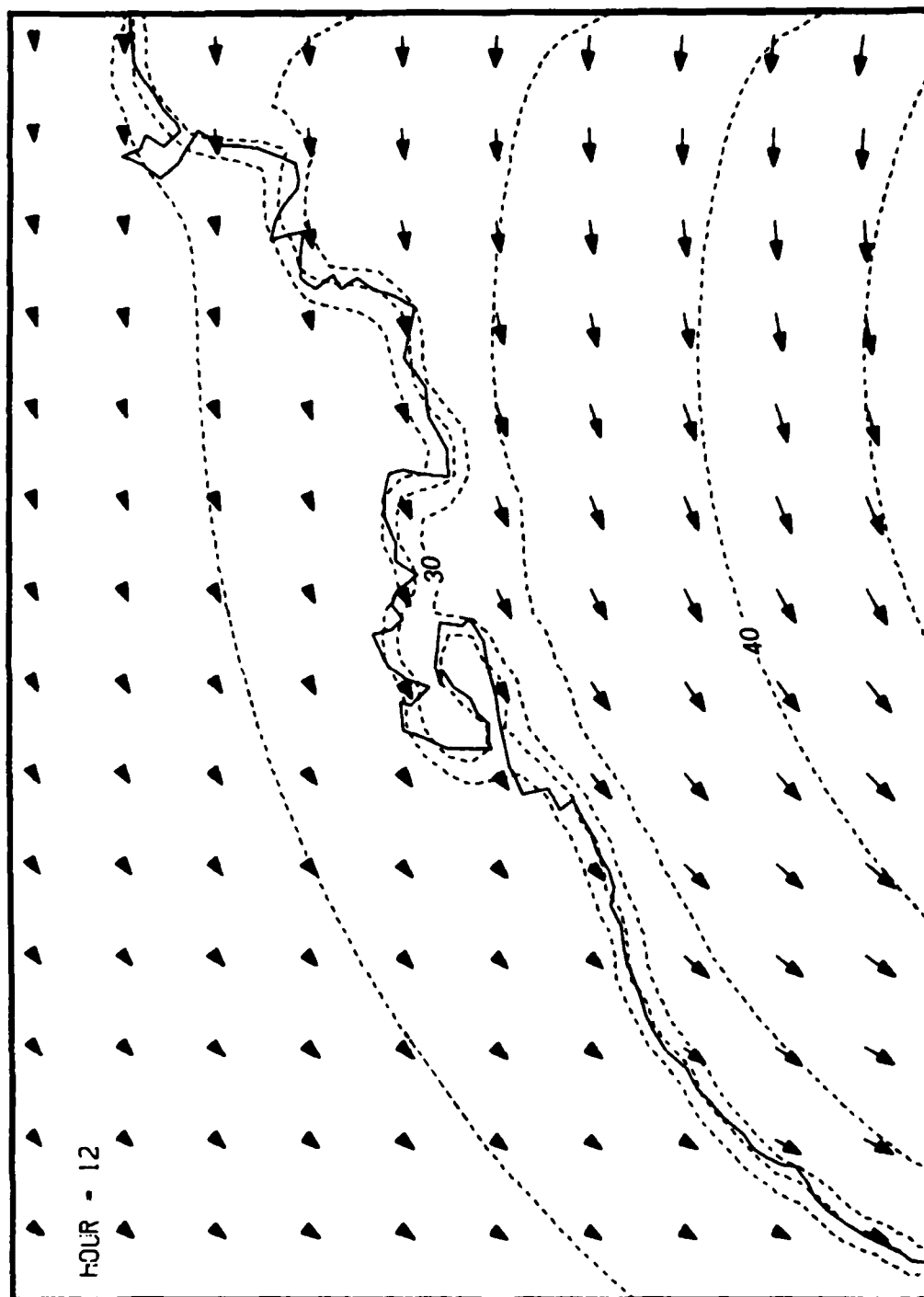


Figure 45. Simulated Audrey wind field at hour 12

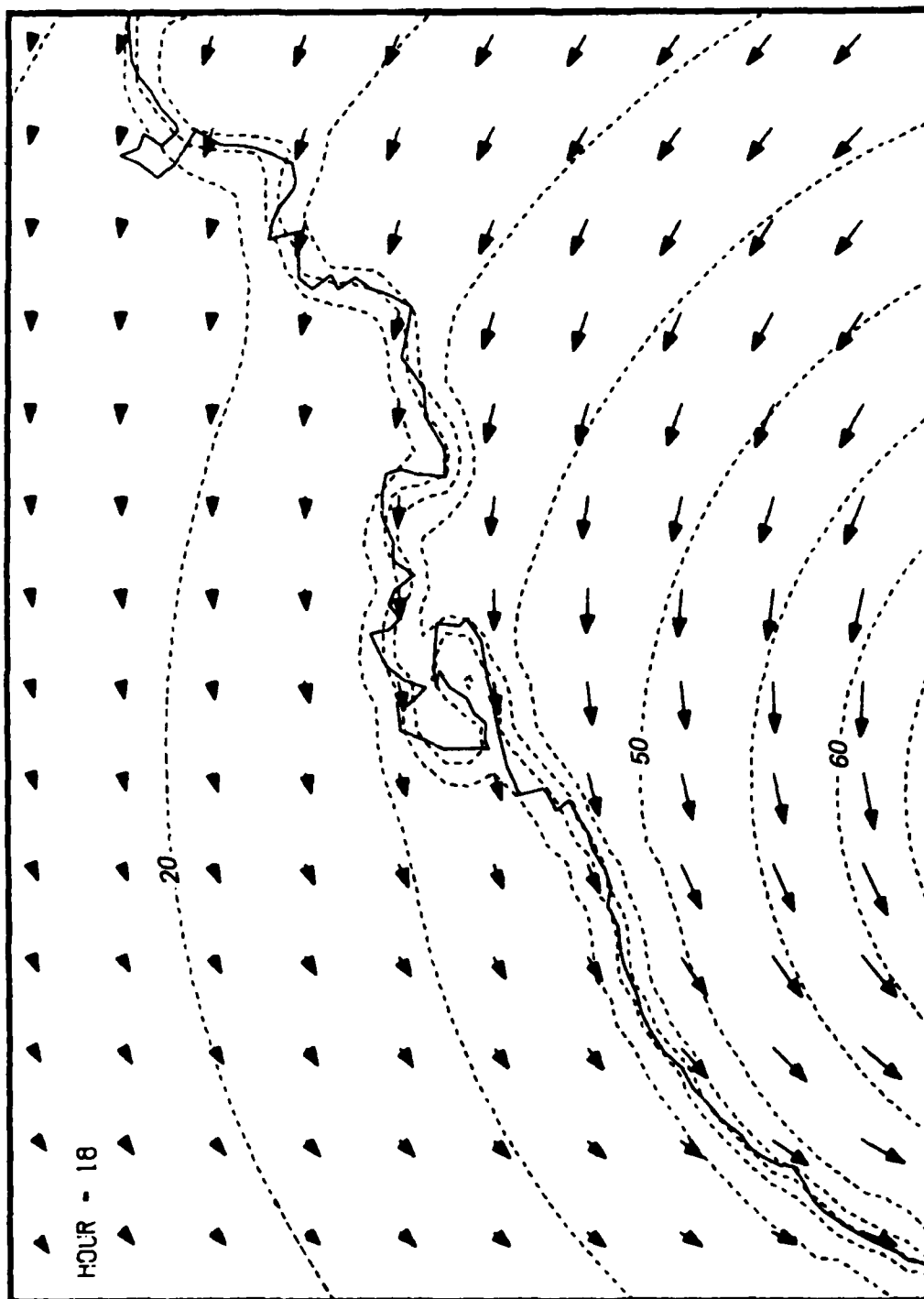


Figure 46. Simulated Audrey wind field at hour 18

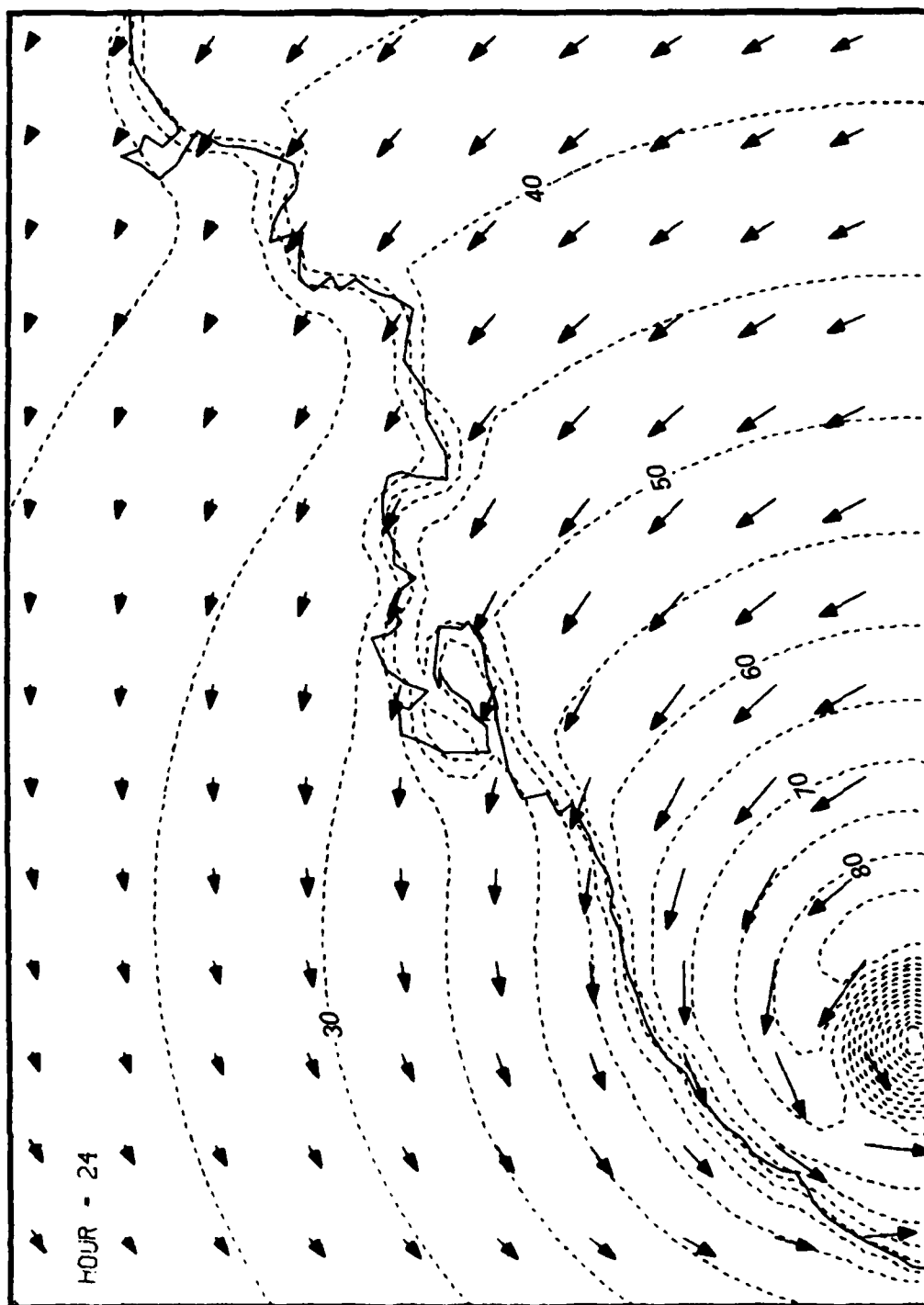


Figure 47. Simulated Audrey wind field at hour 24

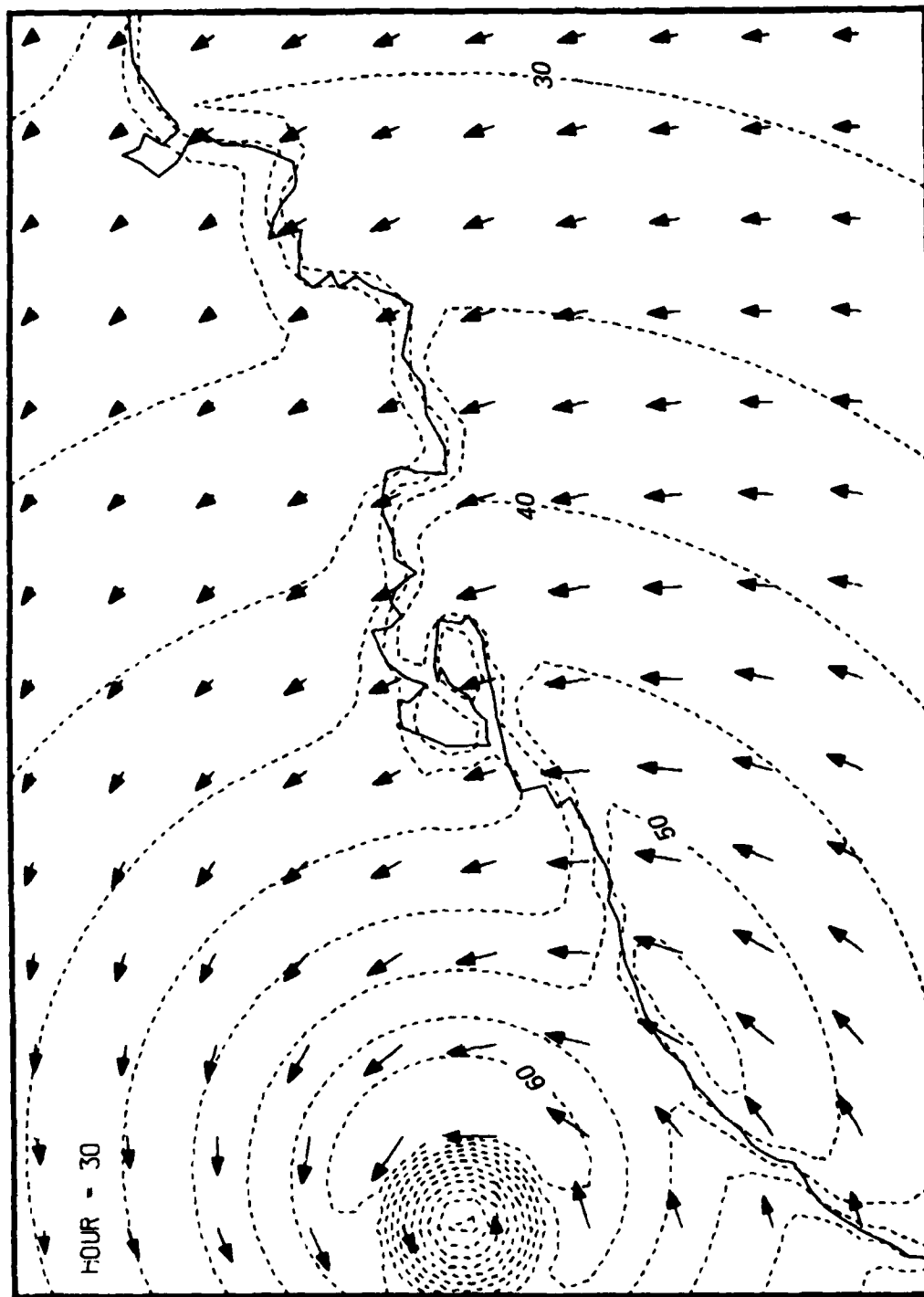


Figure 48. Simulated Audrey wind field at hour 30

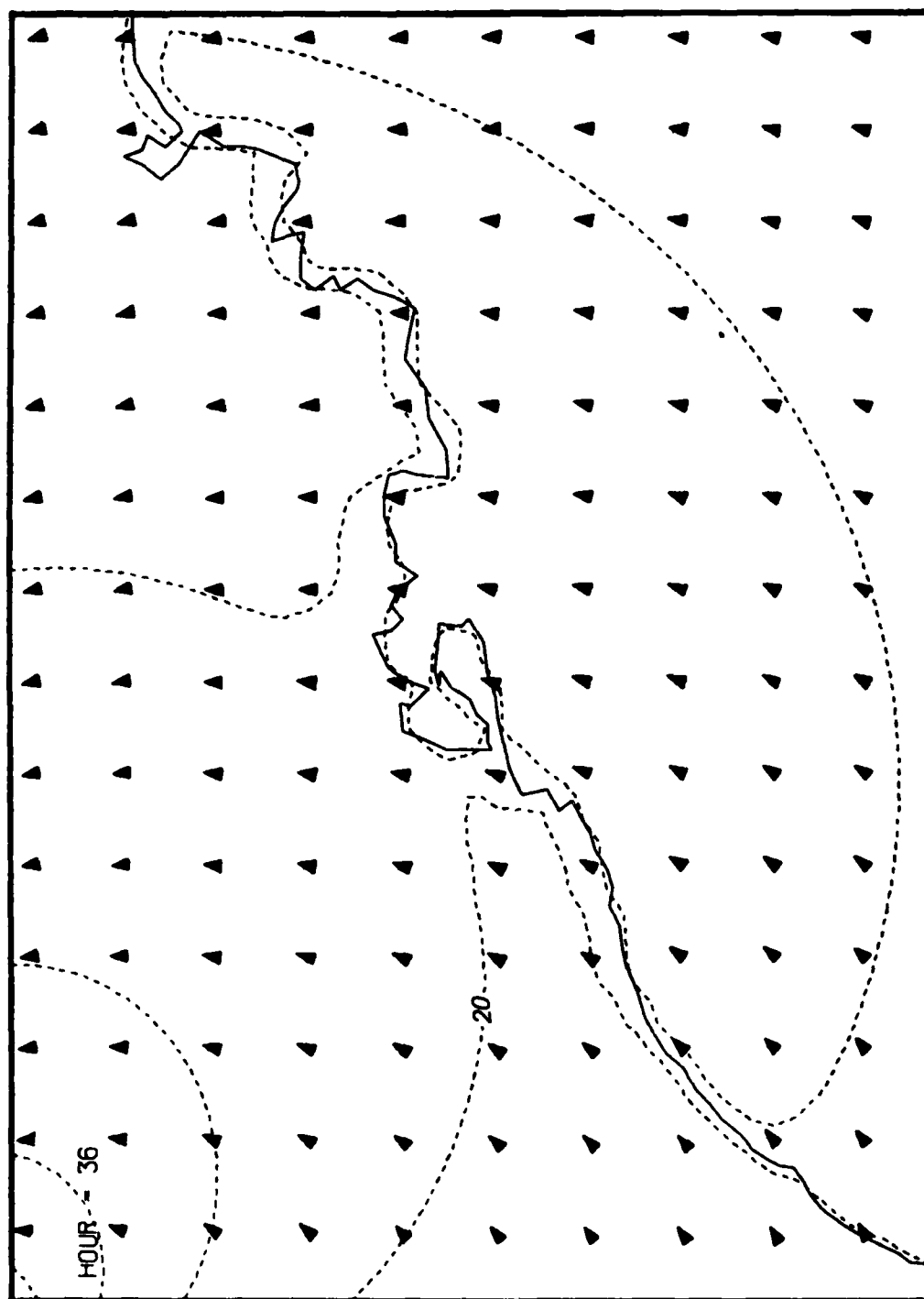


Figure 49. Simulated Audrey wind field at hour 36

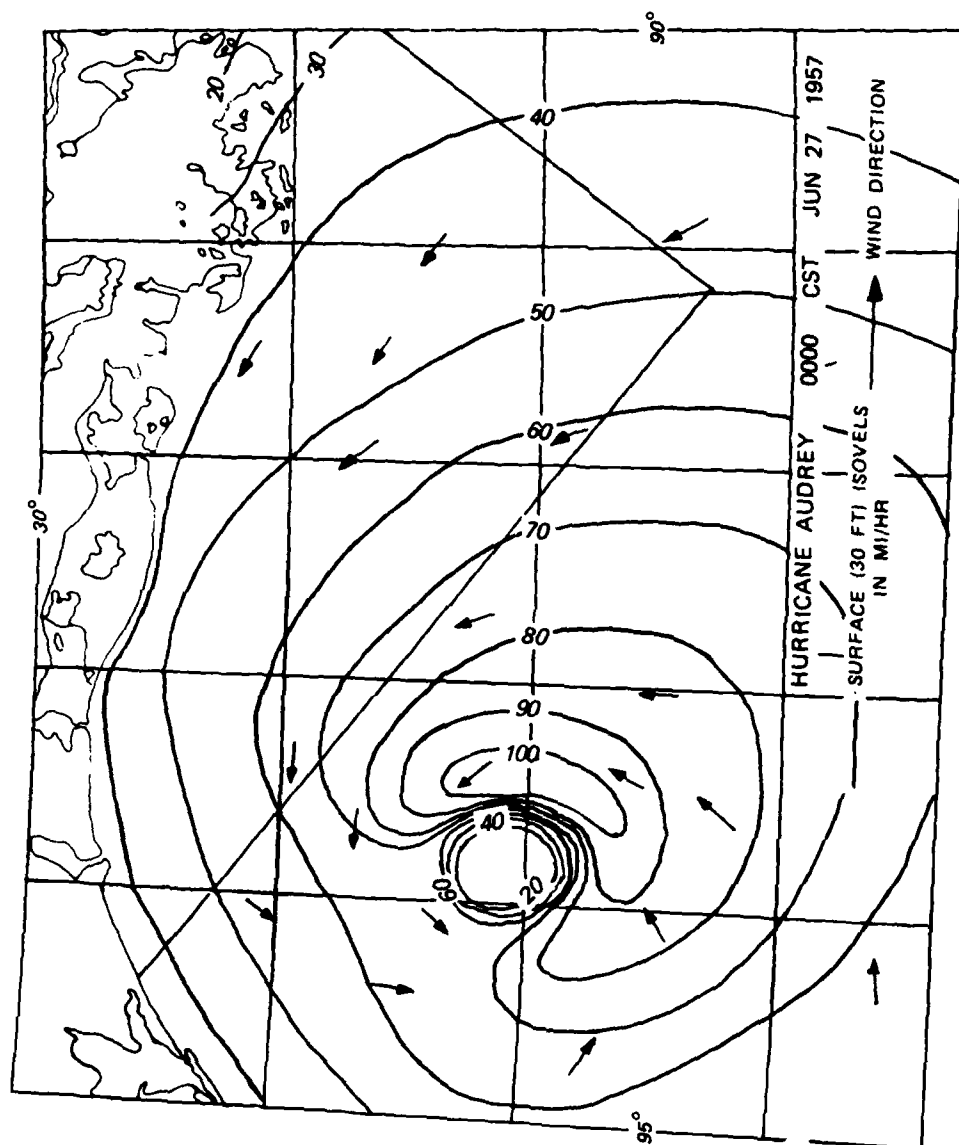


Figure 50. Observed Audrey wind field at hour 18

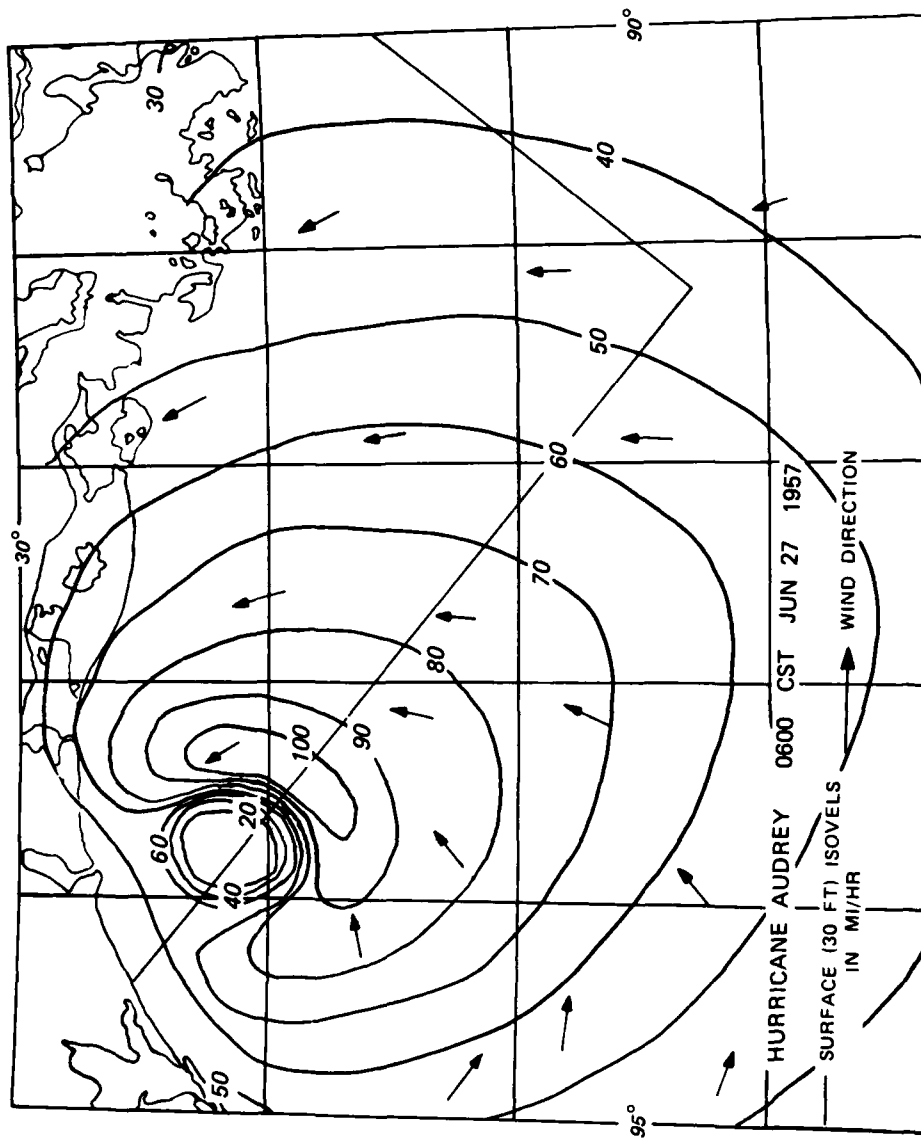


Figure 51. Observed Audrey wind field at hour 24



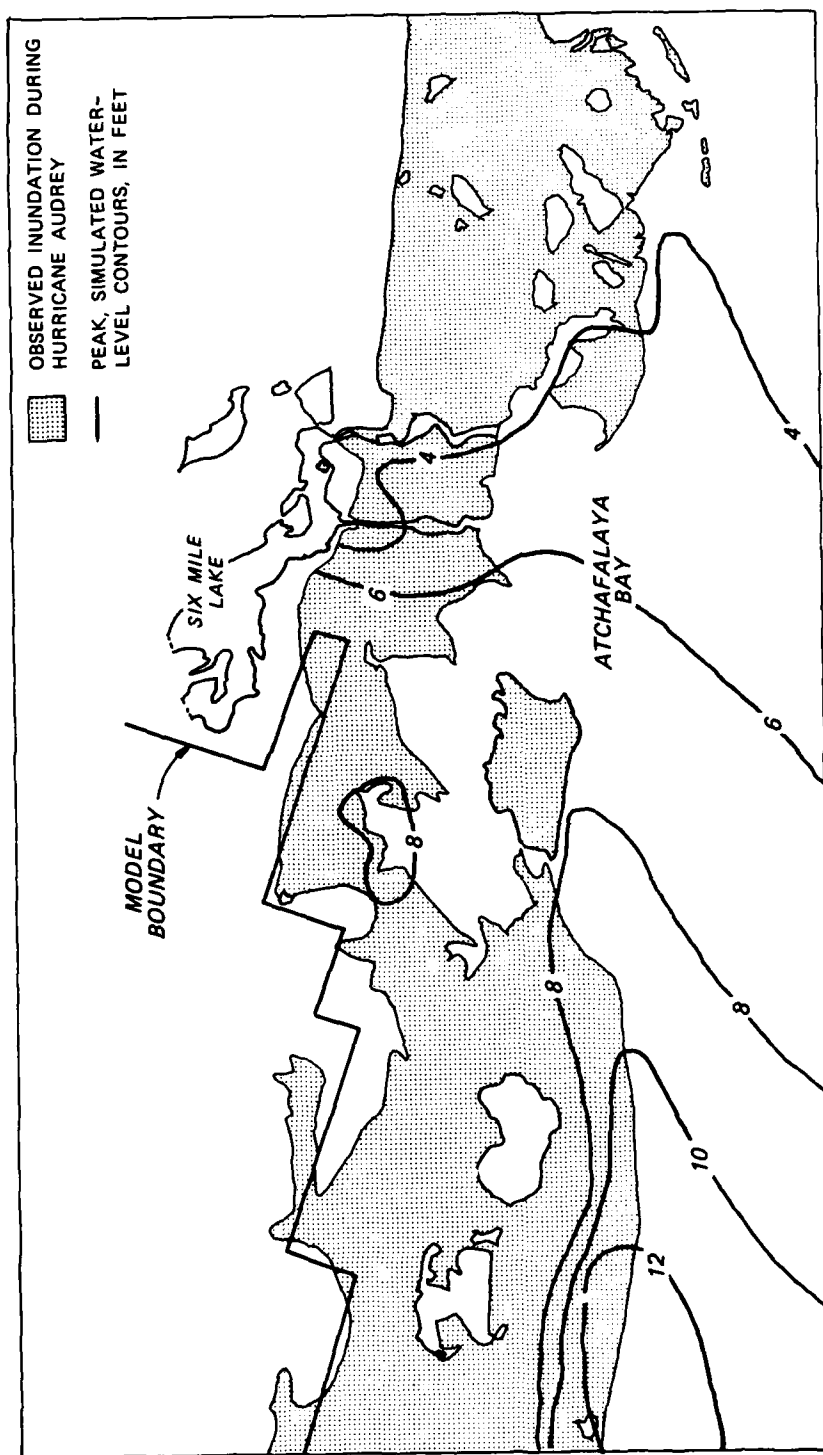


Figure 52. Observed inundation and simulated high-water elevations for Hurricane Audrey

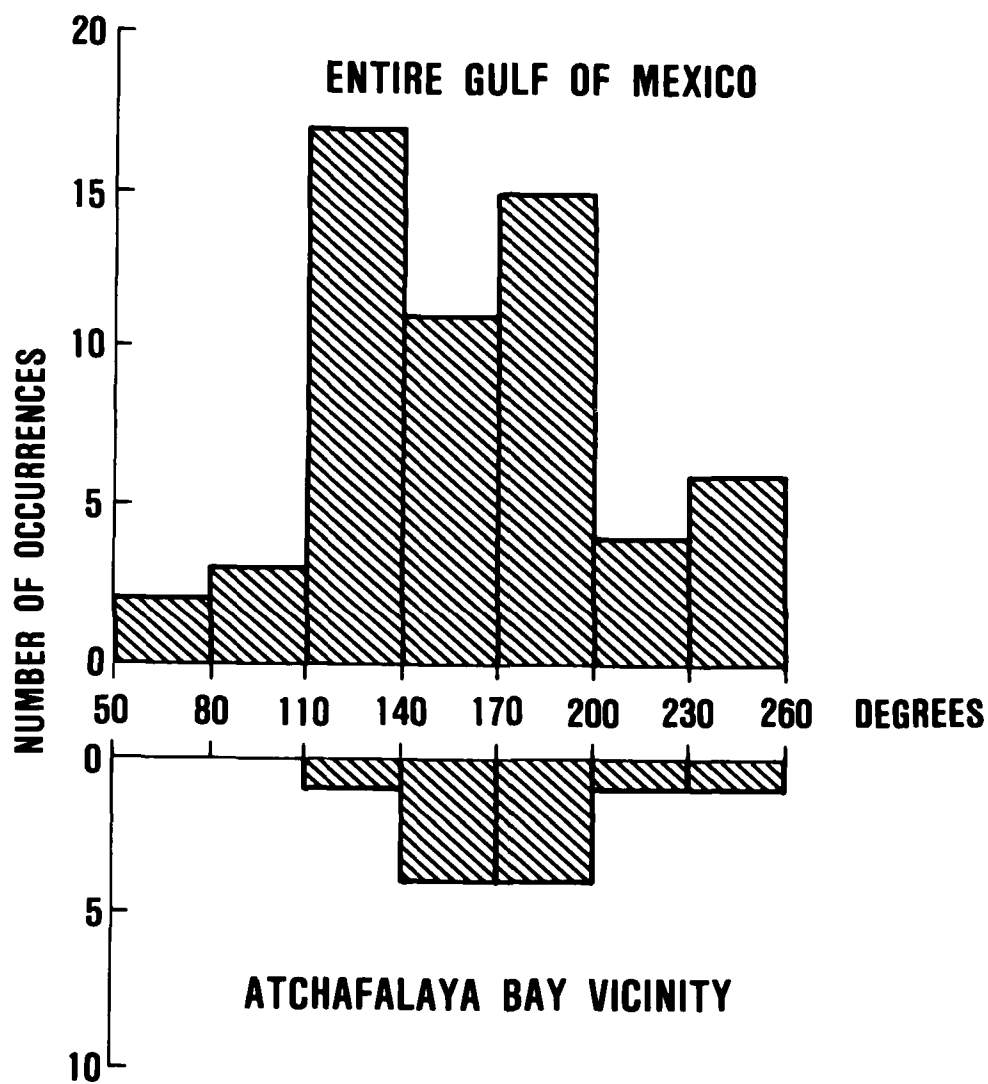


Figure 53. Historical frequency of occurrence for hurricane heading

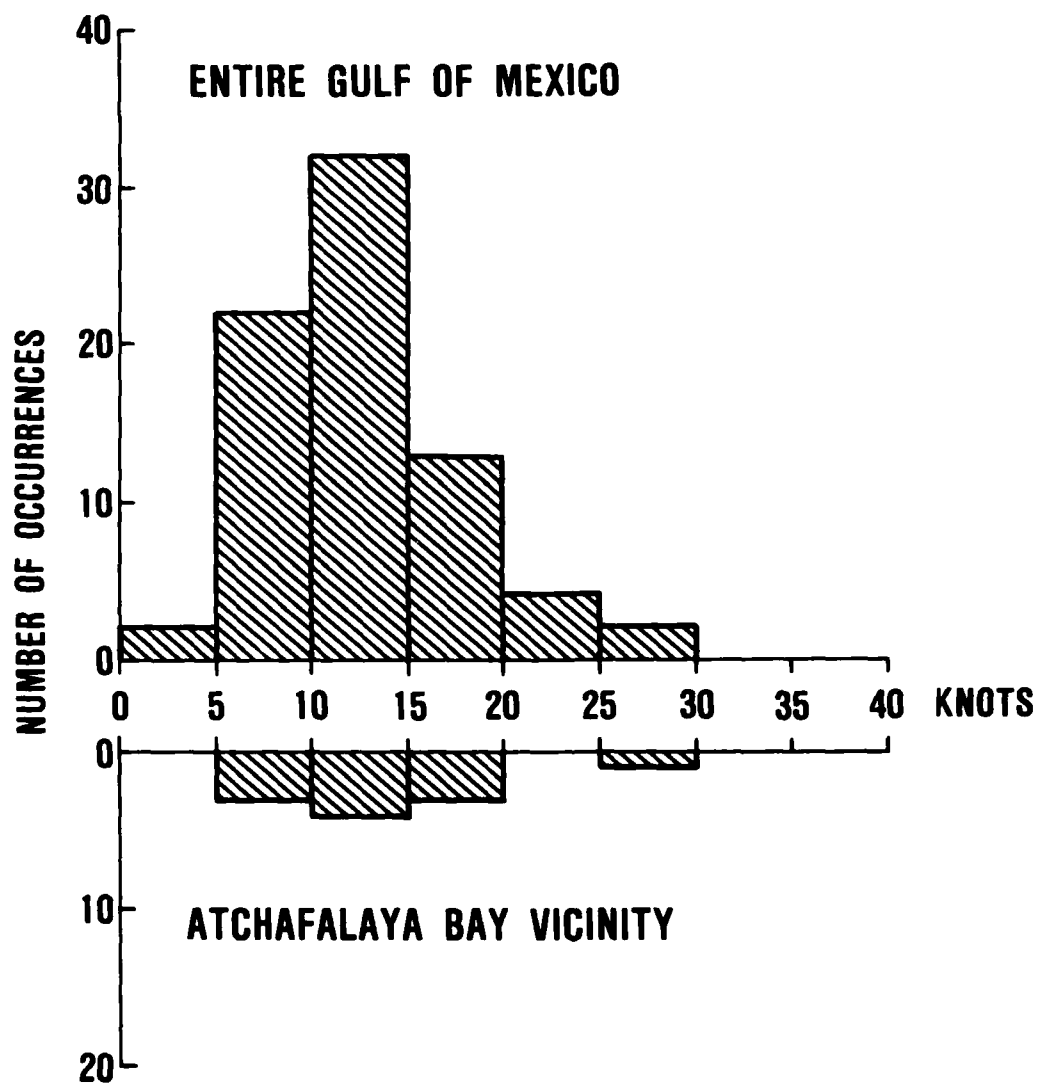


Figure 54. Historical frequency of occurrence  
for hurricane forward speed

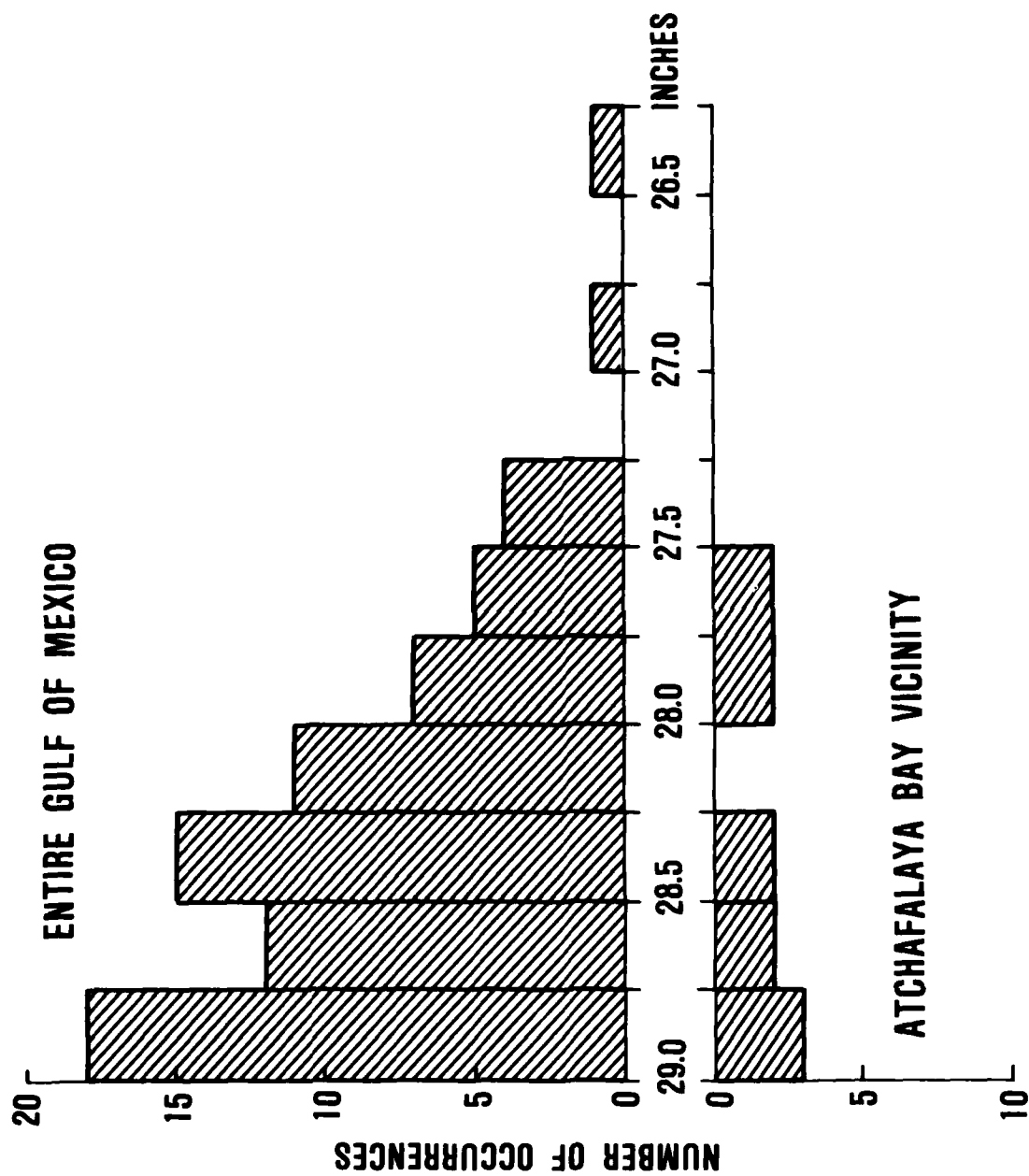


Figure 55. Historical frequency of occurrence for hurricane central pressure.

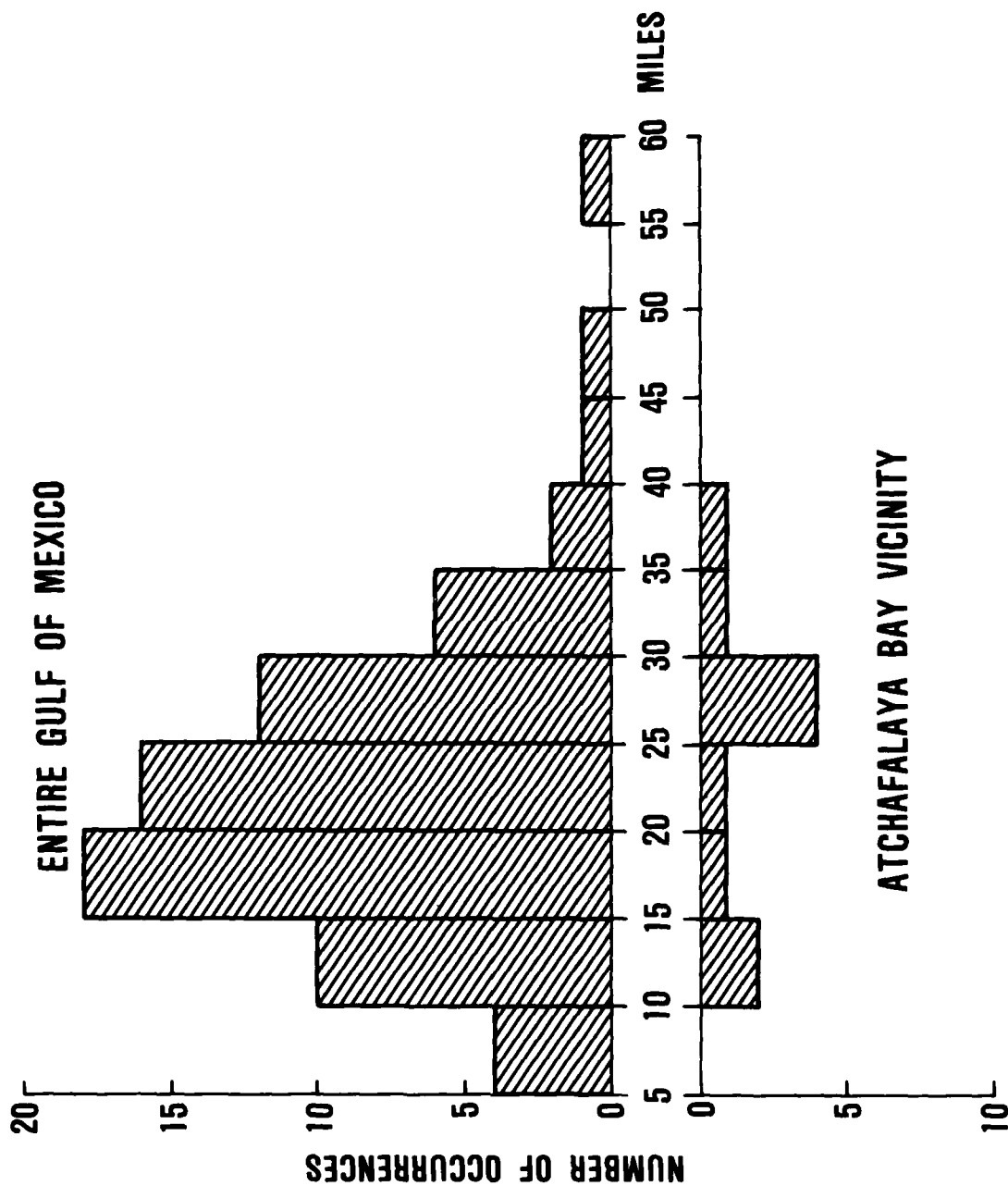
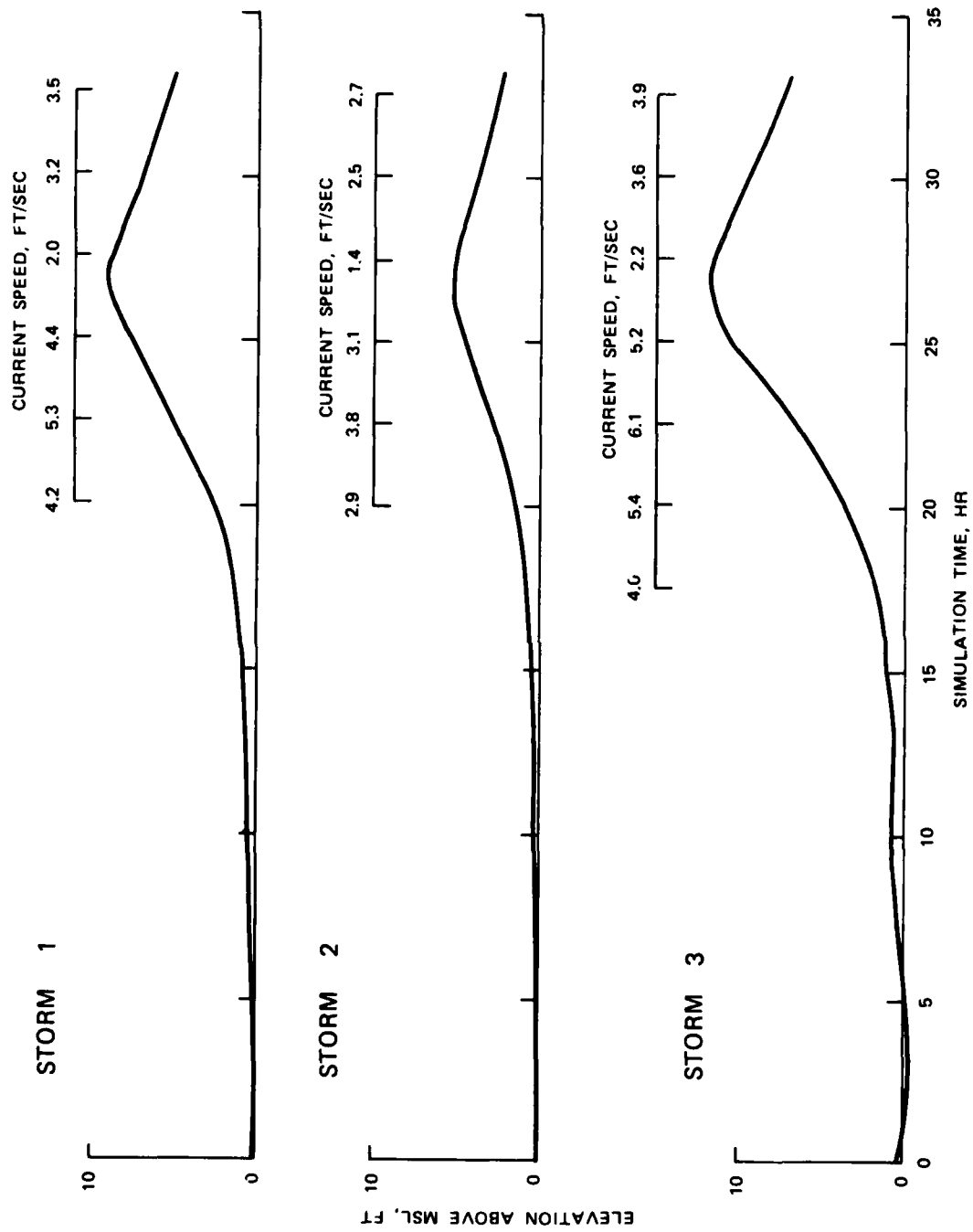
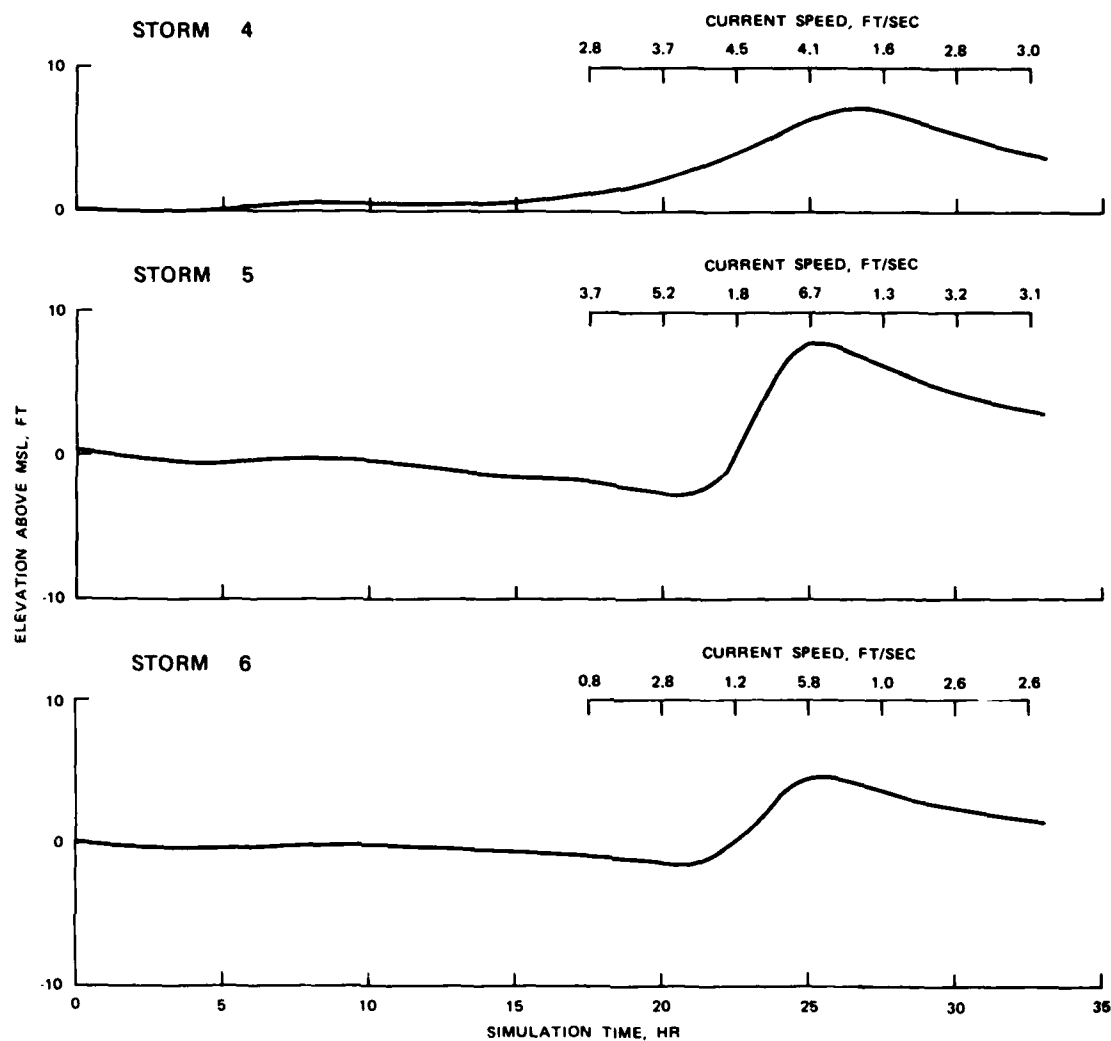


Figure 56. Historical frequency of occurrence for hurricane radius to maximum winds



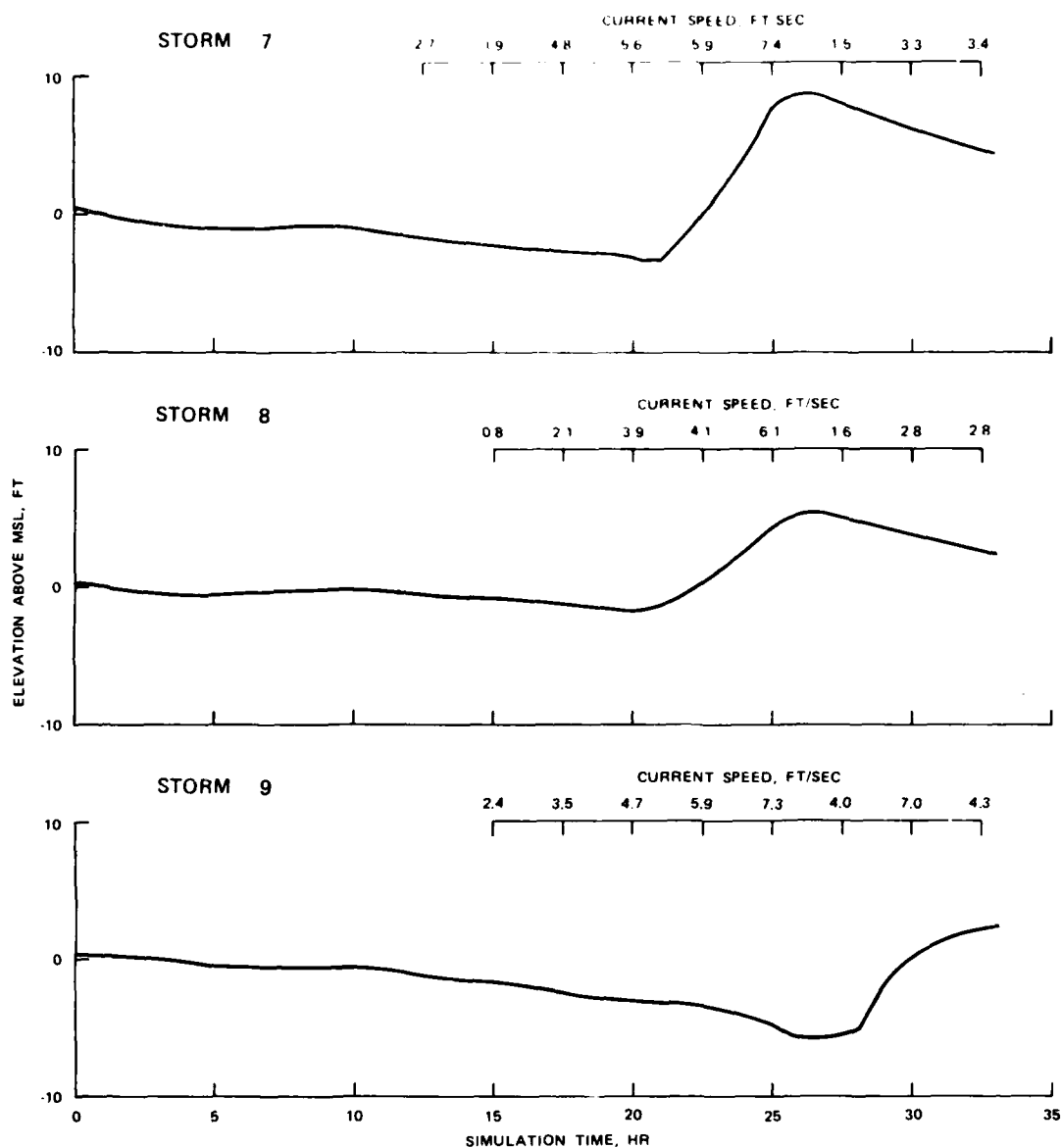
\* COMPUTED VELOCITIES (IN FT/SEC) ARE GIVEN FOR SELECTED TIMES

Figure 57. Simulated water surface and currents at Eugene Island (hypothetical storms 1-3)



\* COMPUTED VELOCITIES (IN FT/SEC) ARE GIVEN FOR SELECTED TIMES

Figure 58. Simulated water surface and currents at Eugene Island (hypothetical storms 4-6)



\* COMPUTED VELOCITIES (IN FT/SEC) ARE GIVEN FOR SELECTED TIMES

Figure 59. Simulated water surface and currents at Eugene Island (hypothetical storms 7-9)



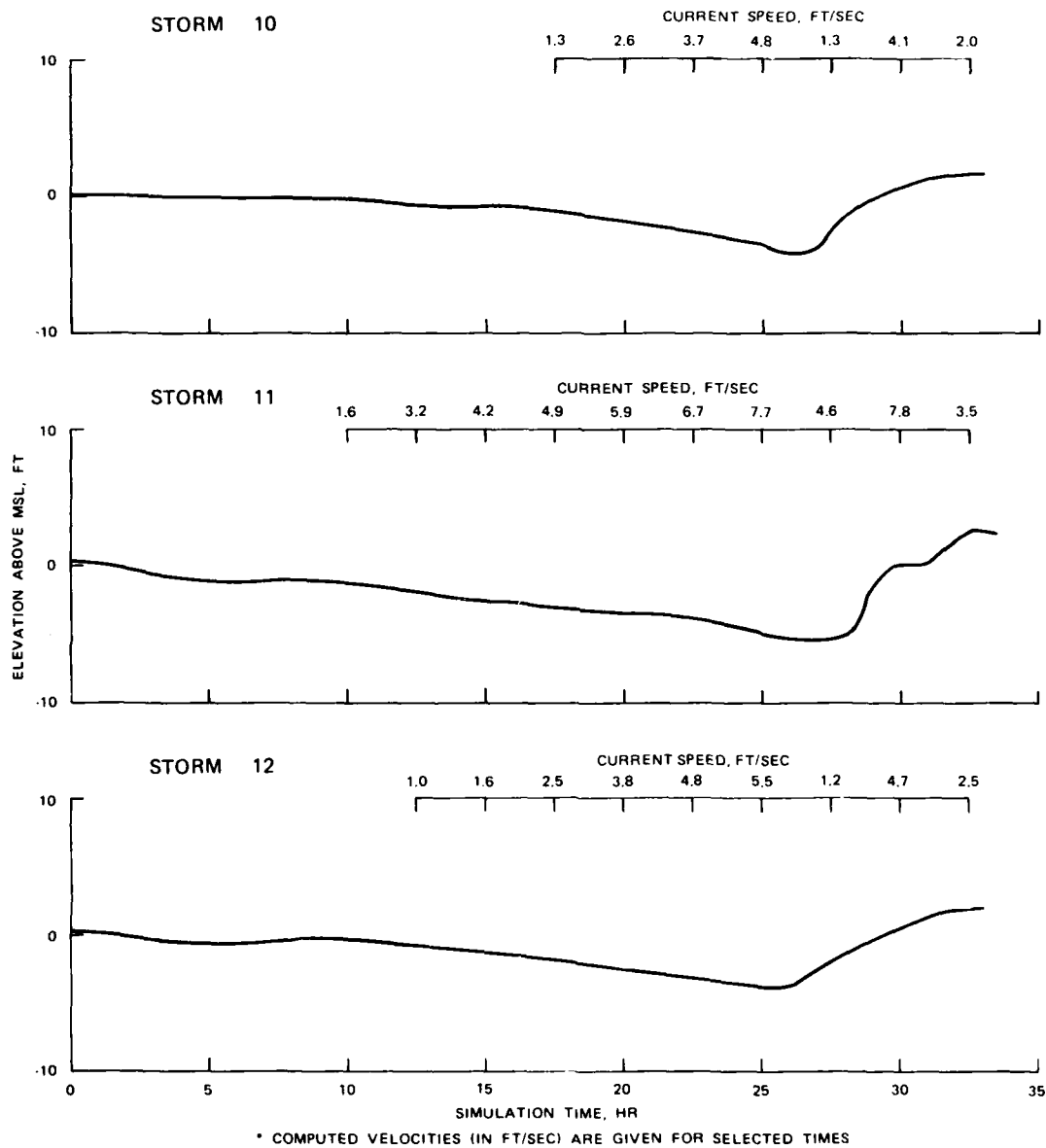


Figure 60. Simulated water surface and currents at Eugene Island (hypothetical storms 10-12)

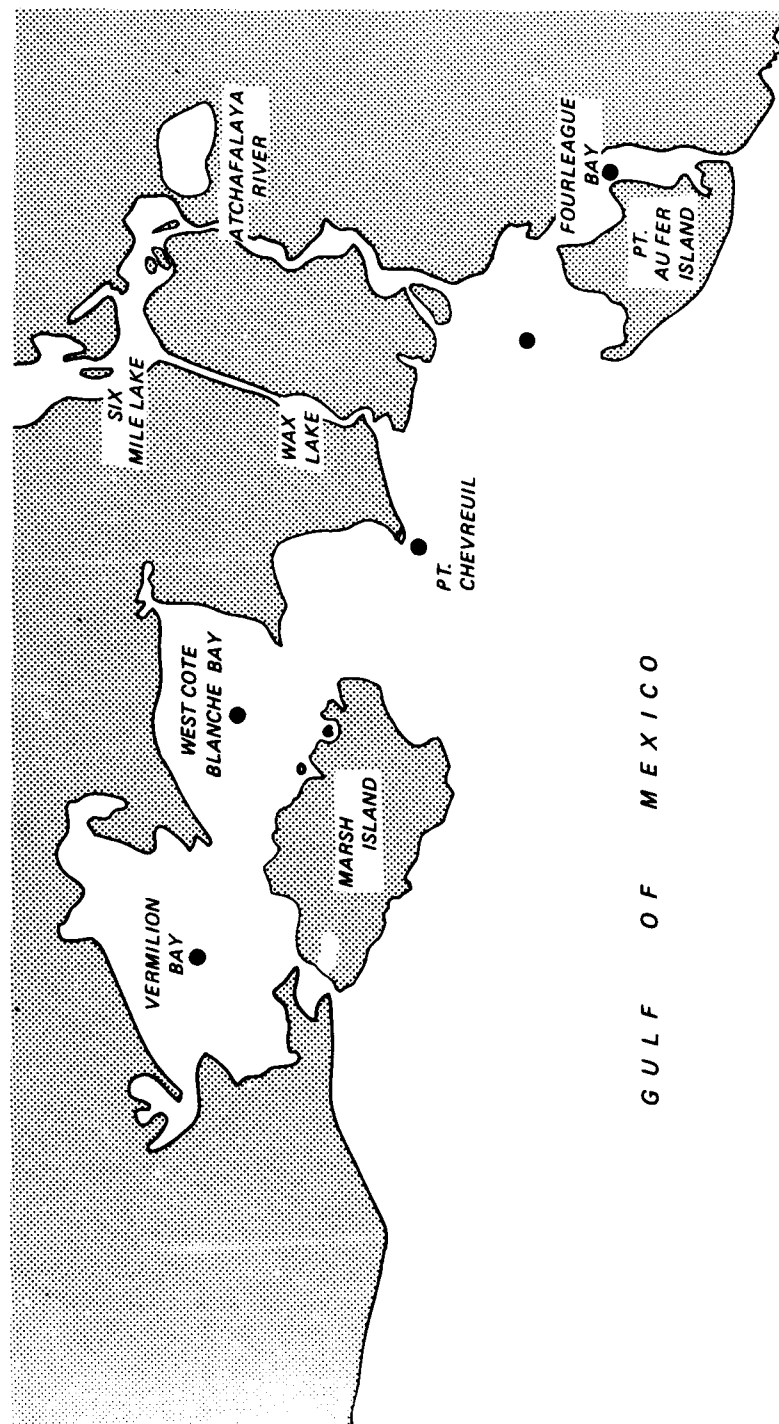


Figure 61. Locations for simulated extreme water-level comparisons during the hypothetical storms